Università
degli Studi
di Napoli
Federico II

Facoltà di
Ingegneria

Stability of delayed systems in structural control applications

Julián Mauricio Londoño Monsalve

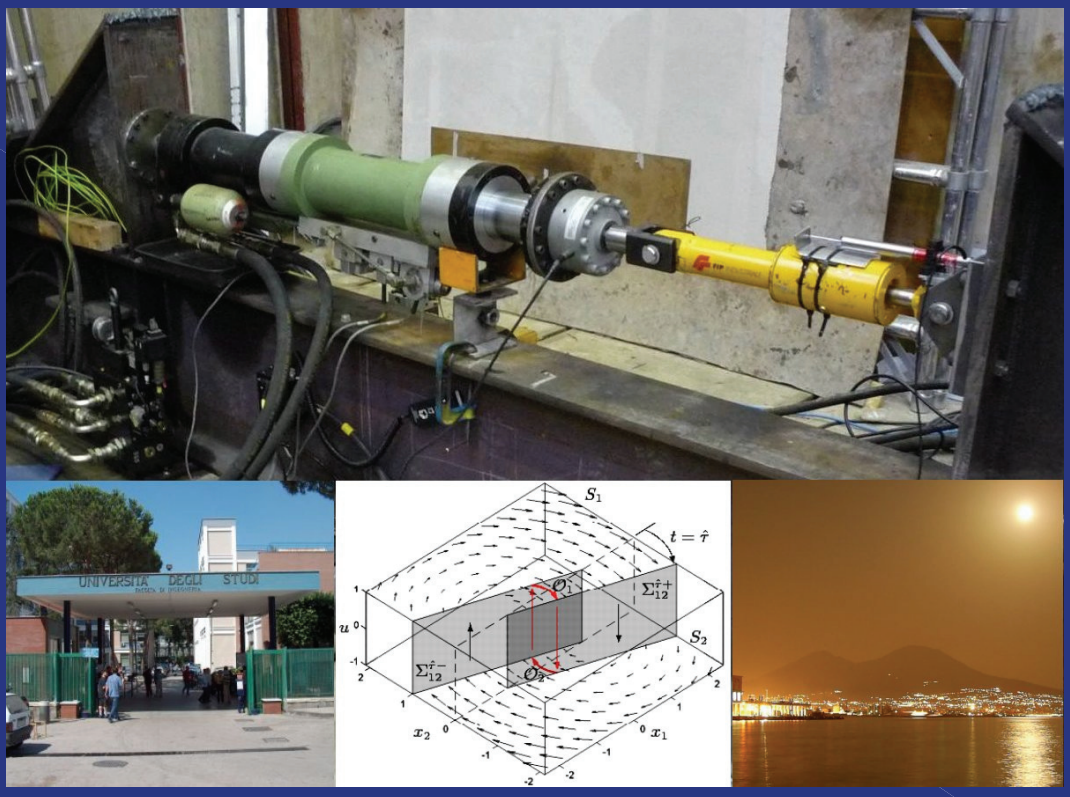

Ph.D. Programme in Construction Engineering

Stability of delayed systems in structural control applications

By
Julián Mauricio Londoño Monsalve

University of Naples "Federico II"
Faculty of Engineering
Department of Structural Engineering
Naples – Italy
2009

Stability of delayed systems in structural control applications

By
Julián Mauricio Londoño Monsalve

Thesis submitted in partial fulfillment of the
requirements for the degree of
Doctor of Philosophy

Supervisor
Prof. Giorgio Serino

University of Naples "Federico II"
Faculty of Engineering
Department of Structural Engineering
Naples – Italy
2009

Printed in Italy.
Naples, November 2009.

Abstract

This thesis analyses the applicability of a quite novel methodology of experimental testing so–called Real–Time Dynamic Substructuring Test (RTDST) in the assessment of protection systems for natural hazards mitigation. RTDST allows testing critical components of the structure at full–scale under realistic extreme loading conditions. Only those components where the non–linearity behavior is concentrated are physically tested, whilst the remainder of the structure is simulated numerically. The main drawback of this technique lies in the unavoidable delays associated to the loop feeding back some experimental measurements to the numerical model. Such delays may cause instability during the test.

This work is focused on testing passive control systems based on large–scale non linear fluid viscous dampers. Throughout a careful explicit stability analysis, we present a complete set of closed–form expressions to describe the dynamics of the main complex delay–induced phenomena exhibited for the delayed system. This analysis is addressed in the context of both classic stability theory for non–linear systems and the qualitative theory of Piecewise Smooth Dynamical Systems. The results obtained are also useful for other kind of mechanical systems where the response of some components is arriving with delay and may cause harmful effects on system behaviour. Semi–active control by MR dampers are examples of such systems.

The theoretical results obtained were confirmed experimentally. When carrying out the experimental campaign, in fact, unexpected self–sustained oscillations were detected. This was caused by delays in the feedback loop, even when they are very small, unavoidably lead the system to self–sustained oscillations at high frequency.

. . . A mis padres Ana Delia y Angel, mis primeros maestros,
quienes con su conducta y amor me enseñaron
lo realmente importante y esencial.

Acknowledgment

I would like to thank the Programme Alβan, the European Union Programme of High Level scholarships for Latin America, for the Scholarship N°E06D101622CO. This financial support is gratefully acknowledged. Alβan made possible this unforgettable and very stimulating life experience.

I have received tremendous help since one year before of starting my PhD from my supervisor Professor Giorgio Serino. I take this opportunity to formally thank for his invaluable guidance, unconditional support, advices and help. This chance of studying in Europe, the research and any of my work would not have been possible without his permanent kindness and patience.

As well, I am very grateful to Prof. David Wagg and Prof. Simon Neild at University of Bristol, not only for taking their time to help me but also for their kindness and for making me feel welcome. Much of the experimental results and theoretical issues presented herein could not have been obtained without their valuable scientific and technical support.

I would like also to express acknowledgment to Prof. Mario di Bernardo at University of Naples Federico II for his time, valuable suggestions and advices in untangling complex but exciting concepts which became decisive for getting what this thesis needed.

I want to express my gratitude to Gustavo Osorio for his warm welcome upon my arrival in Naples, for his friendship when sharing our loneliness and dark days, for the very funny times and the long and relaxing 'chocolaticos' after lunches.

I am grateful to the faculty and all the academic members and colleagues at the Department of Structural Engineering in the University of Naples Federico II, for their financial and intellectual support. Many thanks to Alessandra, Raffaello, Sara, Alberto and Eden for their encouragement and friendship both in and out of the office, and especially to Valeria, Mariacristina and Concetta for their close

friendship and putting up with me along these three years.

Finally, I would like to thanks all my Colombian friends that from all over the world have given me their permanent motivation and friendship. As well, to Naile who shared with me pleasant and significant moments in my life, for her backing and advice in the difficult and busy times. And finally, so many thanks to my family: Mom, Dad, Deysy, Paty, my nieces, aunts, uncles and all my relatives in Colombia for their unconditional encouragement and love. I can be strong because of you all.

Contents

List of Figures

List of Tables

Chapter 1

Introduction

Contents

1.1 Motivation

Earthquake damage has devastating human and economic consequences. The average worldwide repair cost due to earthquake damage has been estimated to be approximately $30bn per year. Reducing this financial cost is a major engineering challenge, which would have significant benefit in reducing human suffering during extreme earthquake events. Such a reduction demands the design of more resistant, reliable and cost–effective both structures and seismic protection systems.

New design procedures in structural engineering as well as in structural control, require better understanding and modelling of nonlinear behavior of structures and components. The response of structural systems under strong dynamic loads, such as earthquake ground motion, is highly unpredictable and then difficult to model. It becomes a troublesome problem, when designing complex infrastructure in regions of high seismic activity. Besides, the application of structural control technologies for protection of civil structures has been a growing interest over the last four decades, not only to reduce the dynamic response under extreme dynamic loads but also to increase the system reliability and for providing human comfort during everyday environmental loads. These protection systems are also difficult to be analysed, due to the strong non–linearities exhibited by the devices commonly used for seismic mitigation.

Different laboratory facilities and experimental methodologies have been developed for years, seeking for better understanding of mechanic and dynamic phenomena in fields relative to earthquake engineering. However, the vast majority of those techniques suffer from technical and physical limitations that restrict their applicability for assessing real scenarios. In fact, large scale engineering structures such as bridges and buildings, present a particular problem in terms of experimental testing. Another experimental challenging issue is connected to the hysteresis and rate–dependent phenomena. That turns into meaningful when testing semiactive and passive control systems, where this dynamic behaviour is introduced into the controlled system by the dissipation devices.

The idea behind this thesis is to evaluate the applicability of a new experimental technique which is radically more effective than traditional approaches. To do this we propose to exploit a state of the art of the dynamic testing technique known as real–time dynamic substructuring. Based on the current knowledge, we intent to find the conditions under which this technique can be employed for testing real scale seismic protection system for buildings. We believe that this technique will enable the engineers to obtain accurate information of the systems in nonlinear range, increasing the understanding of the whole controlled system behaviour, and hence, allowing the improvement of designing structures with added control systems. More efficient control systems imply both cost–effective seismic protection systems and more resistant structure to earthquake excitation. The result will be safer buildings, less human cost in terms of death and injury, and more sustainable infrastructure with increased confidence.

Real–time dynamic substructuring testing (RTDST) is an efficient method for the assessment of dynamic and rate–dependent behavior of systems subjected to dynamic excitation. This new and exciting technique offers the prospect of being able to test prototype adaptive structures in the laboratory under realistic extreme loading conditions, such as those suffered during earthquakes. RTDST provides the capability to isolate and physically test critical components of a controlled structure whilst the remain part of the structure is simulated numerically. These tests can be conduced at real scale and in real time to fully capture any rate dependency, while allowing for hundreds of repeatable tests. This approach overcomes significant limitations of traditional testing methods. For instance, depending on the experimental objectives, RTDST may have several advantages over traditional pseudodynamic tests, where unpredictable rate behavior cannot capture because inertia and damping forces are calculated numerically and applied slowly to the test specimen. Likewise, it may also have many advantages over the dynamic shaking table technique traditionally used, mainly when testing large structures, not only in terms of scale but also cost, geometry and required physical mass of the structural model. An additional benefit is that the mod-

els can simulate experiments in advance. This allows the feasibility of a testing regime to be explored. Simulated results can also give an investigator a degree of confidence that his test has proceeded as intended or otherwise. The apparatus models are complex and must account for the dynamics of all the components, including the controller, servo–valve, actuator and physical test specimen.

Nonetheless, this testing technique suffers from a critical drawback: the delay. Delay in command signals is a serious issue for dynamic system that needs to act in real time. RTDST requires a structural numerical model to be fed back with measurements from the component physically tested. In turn, this component is loaded in the lab according to the outcomes from that numerical model. This information exchange must take place in real time with minimum error between the two parts. But due to the intrinsic dynamics of the laboratory facility which is being used in the test, delay errors in the feedback signal are unavoidable. The success of real time dynamic substructuring testing is then highly dependent on the performance of the actuators which provide the forces (or displacements) to the component physically tested. Their imperfect dynamics can introduce both timing and amplitude errors into the signal, which can affect the accuracy of the performance and may also cause instability. To overcome this, time delay compensation schemes are commonly used to make corrections on the command signal. Even if this compensation works properly, it becomes impossible to reduce such delay error to zero.

Additionally, some systems could be particularly sensitive to the presence of delay, and even a small delay may drastically affect how they behave. Therefore, to make sure that RTDST simulation is accurate and reliable enough, a careful stability analysis of the whole substructured system should be done. The aim of such analysis is to determine the critical delay, beyond which, the test no longer represents the emulated system behaviour, or in other words, to define the confidence interval in terms of delay where the RTDST simulation results can be guaranteed.

In the next section, we shall present details of how this thesis was arranged to face this interesting and promising issue.

1.2 Outline of this thesis

As this thesis combines two worlds which have been usually not connected (structural control and piecewise systems), we consider very unlikely that the reader knows about both. So that, this document covers several areas in an attempt to be comprehensive and easy to read for a wide spectrum of readers. Rather than covering all the issues in deep, the idea is to familiarize the reader with unknown

fundamental definitions. Fundamental in the sense of being useful to understand the work presented here. This thesis is organized as follows.

Chapter 2 is devoted to show some basis of structural control systems. The aim is not to go deep into specific technical, practical or mathematical issues but to highlight the importance and impact of several types of protection systems, the devices employed in each case and the main test methods currently used for their assessment. These information may be useful for readers who are not used to what structural control techniques means in civil engineering.

In Chapter 3 we present the main features, advantages and disadvantages of the testing technique known as real–time dynamic substructuring. Our interest is to show who RTDST can effectively be implemented for testing and designing control systems for seismic protection, and which circumstances are particulary challenging in order to achieve reliable simulations of the emulated structure.

In Chapter 4 we present an overview of the main fundamentals of the classical stability theory for the analysis of linear and non linear systems. The idea is to familiarize the reader with fundamental definitions and properties exhibits for smooths system which are necessary to understand the analysis carried out throughout this thesis. If the reader already knows these mathematical formalisms can skip this chapter.

In Chapter 5 we present an overview of the qualitative theory of smooth and piecewise smooth dynamical systems. Rather than covering all the issues, the purpose is to present the fundamental concepts and definitions, that according to us, are needed in the study. After a brief presentation on smooth dynamical systems, we introduce nonsmooth dynamical systems, namely we present some definitions, invariant sets, stability analysis and numerical analysis emphasizing particularly the major differences with the classical theory of smooth systems.

In Chapter 6 we intend to analyse the close loop behaviour of a RTDST when testing a supplemental energy dissipation system for structural control. We present a stability analysis to highlight the harmful effects caused by delays in dynamic systems when timing errors are considered on the damper's response. Our goal is to assess the constraints on delays, in such a way that the stability and reliability of the closed loop simulation can be guaranteed. This study is addressed in the context of both classic stability theory for linear and non–linear systems and the qualitative theory of Piecewise Smooth Dynamical Systems presented in the previous chapters.

In Chapter 7 we present the description and experimental set–up of a Real–Time Dynamic Substructuring Test of a civil structure provided with a passive seismic protection system. Our interest is to show how this kind of test can be exploited for the assessment and design of current and new protection systems in earthquake engineering. We show that even when a compensation scheme works

properly, the RTDST may become unstable and behave very different from the emulated system.

Finally, Chapter 8 presents the conclusions, remarks and suggested future works derived from this thesis.

Chapter 2

Some Fundamentals on Structural Control

Contents

Structural control had its roots primarily in aerospace industry, principally, in field concerning to flexible space structures. It was rapidly moved into civil engineering. Over the last four decades, there has been a growing interest in the application of control technologies for civil structures in order to reduce their dynamic response and to increase the system reliability, not only for protection against dynamic extreme loads (earthquakes, blasts, crashes, strong winds, extreme waves, etc.) but also for providing human comfort during everyday environmental loads [Housner et al., 1997].

The first real implementations of structural control, were based on base isolation, viscoelastic dampers and tuned liquid dampers in the 1970's. Many years later the active control concept appeared and the first real implementation was

made in the 11-storey Kyobashi Seiwa building in Tokyo–Japan, for reducing the building vibration under strong winds and moderated seismic excitations [Sakamoto et al., 1994]. Recently, the techniques of semiactive and hybrid control were proposed for structural control and their implementations have been made successfully in Japan and USA. Several state–of–the–art reports provide a detailed survey, see e.g. [Spencer and Nagarajaiah, 2003], [Dyke, 2005].

This chapter is devoted to present some basis of structural control systems. The aim is not to go deep into specific technical, practical or mathematical issues but to highlight the importance and impact of various types of protection systems, the devices employed in each case and the main test methods currently used for their assessment.

2.1 Structural control strategies

Different structural control strategies have been developed. Generally speaking, we have three principal groups: (i) *passive control*, where vibratory energy is dissipated by increasing some structural parametric values (like stiffness and damping) without requiring external energy; (ii) *active control*, which adds energy to the structure in opposite direction of the seismic forces to counteract them; and (iii) *semi–active control*, which dissipates energy like passive control, but now device's dissipation capacity can be controlled on–line, so device properties such as stiffness or damping are changed by means of hydraulic, magnetic or electric commands. In what follows, we present a brief description of each strategy and give some examples.

2.1.1 Passive control

Passive energy dissipation systems encompass a large spectrum of materials and devices for adding damping to the structural system (also stiffness and strength are usually increased). They can be used for both natural hazard mitigation and rehabilitation of aging or deficient structures. Passive control systems dissipate energy using the structure's own motion to produce relative movement within the device and develop local control forces. Two principles are used to dissipate energy: conversion of kinetic energy to heat and transference of energy among vibration modes [Skinner et al., 1993], [Constantinou and Symans, 1993]. The devices that pertain to the first class are based on frictional sliding, yielding of metals, deformation of viscoelastic solids or fluids. And those of the second

group are fluid orificing and supplemental oscillators, which act as dynamic vibration absorbers [Cahis et al., 2000].
The added stiffness reduces the dynamic response of the structures by absorbing and dissipating energy, which when combined with the change in initial frequency, helps the structure avoid resonance. Since passive systems involve no external power, they are inherently stable. Passive strategies are characterized by its stability, simplicity, reliability and have a low cost of maintenance and installation. However, its main drawback rely on the fact that they are built carefully tuned for specific operating conditions and cannot adapt to changes and unknown disturbances. Examples of passive systems include among others: base isolation, tuned mass dampers (TMD), tuned liquid dampers (TLD), metallic yield dampers, viscous fluid dampers and friction dampers.

Tuned Mass Dampers. Passive tuned mass damper systems, consist of an auxiliary mass, a spring and a damper, which are attached to a structure in order to reduce its dynamic response (Fig. 2.1). The auxiliary mass limits the motion of the structure when it is subjected to a particular excitation causing the damper to resonate 180° out of phase with the structure motion. The difference in the phase produces energy dissipation by the TMD inertia force acting on the structure.

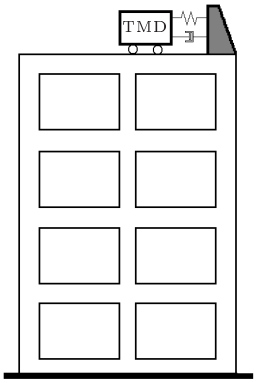

Figure 2.1: Tuned Mass Damper System

Nonetheless, tuned mass dampers are relatively ineffective during earthquakes due to their inability to reach a resonant condition and therefore dissipate energy under random excitation [Kwok and Samali, 1995]. In the last years, tuned mass dampers have been installed in a number of buildings worldwide to reduce building vibration, particularly under wind excitation. A recent example is one of the

world's tallest buildings, the Taipei 101 in Taiwan (See Figure 2.2), which has been successfully equipped with a tuned mass damper to control the excessive sway under large wind. The building hosts a massive pendulum with dampers, an 800–ton sphere 18 feet across swings from the 92^{nd} floor to control wind–induced oscillation.

Figure 2.2: Building Taipei 101 and the 800–ton steel sphere used as TMD.

Base Isolation Systems. A base isolation system consists of a set of flexible support elements, typically rubber bearings, placed at the foundation level as shown in Figure 2.3. These support elements are designed in such a way that the natural period of vibration of the isolated structure is much greater than the dominant period of the expected excitation. Actually, the whole system behaves as a single degree of freedom system due to, under strong dynamic loads, the displacements are absorbed by the supports while the relative structural displacement remains negligible [Kelly, 1996].

Base isolation technology offers a cost–effective and reliable strategy for mitigating seismic damage to structures. It is best implemented in locations of high seismicity for reducing lateral design forces or for existing structures needing to be upgrade in order to satisfy current safety requirements. For cost effectiveness, base isolation needs to be considered in the planning stages of the building project.

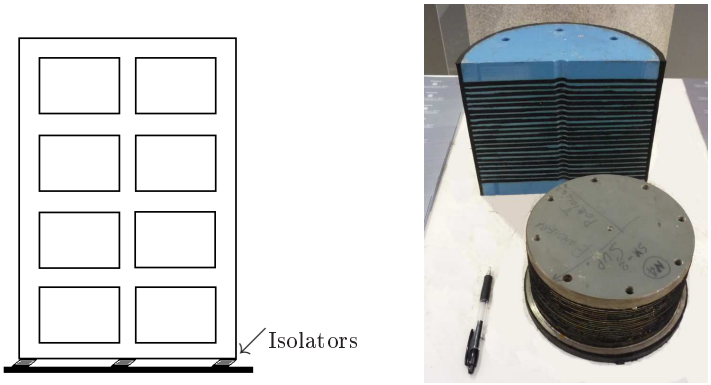

Figure 2.3: Base isolation system and a typical rubber bearing for base isolation.

A lot of examples of real implementations can be found in the literature. Figure 2.4 shows a worship structure seismically isolated in Siracusa (Italy) and the hysteretic isolators installed on it, for further information see [Serino et al., 2008].

Frictional Dampers. Frictional damping dissipates energy due to the heat caused by friction between moving bodies[1] in contact. A frictional damper consists of the friction surface (e.g. steel) clamped together by high strength bolts with slotted holes. Friction dampers are designed to slide over each other during a strong earthquake, the slip force is designed large enough so that no sliding is caused by wind forces. The beneficial approach to passive damping is that because energy is removed, the response cannot become unstable. However, frictional damping looses effectiveness during large seismic excitation [Hanson and Soong, 2001].

Metallic Yielding Dampers. Metallic Yielding Dampers (MYDs) are probably the most familiar to structural engineers, since its concept is the same as typical steel seismic force resistive elements such as steel moment frames and braces. Beam–column connections yield for steel moment frames to absorb the seismic energy. The braces also buckle to absorb the seismic energy. However, the biggest difference between MYDs and typical steel system is the yielding location for MYDs is not in the gravity load carrying elements (Further details in [Hanson and Soong, 2001]).

[1] Moving plates specially treated to increase the friction between them.

Figure 2.4: Worship structure seismically isolated in Siracusa (Italy) and its hysteretic isolators.

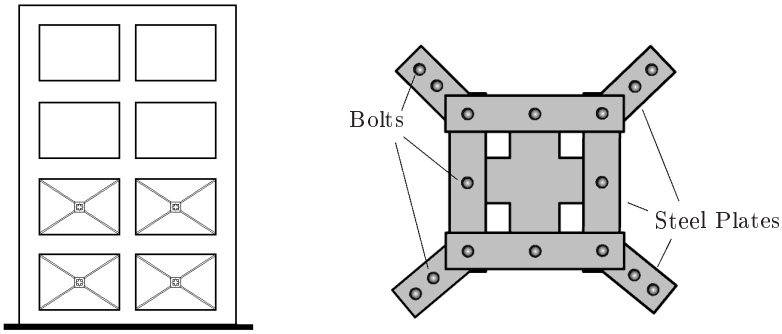

Figure 2.5: Frictional damper system.

Fluid Viscous Dampers. FVDs have been widely used in aerospace and military applications since the early 1900's. After the end of the cold war, its technology became available for civilian usage. They consist of a closed cylinder

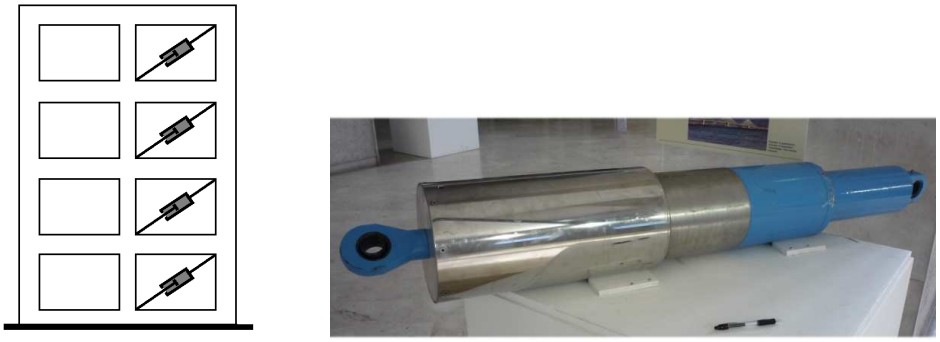

Figure 2.6: Structure equipped with fluid viscous dampers in diagonal brace configuration and typical FV device.

containing a viscous fluid like oil. A piston rod is connected to a piston head with small holes in it. The piston can move in and out of the cylinder. As it does this, the compressible silicon oil is forced to flow through holes in the piston head at high velocity causing friction and generating heat, which is in turn, radiated into the surrounding air. This hydrodynamic process dissipates seismic energy [Miyamoto and Hanson, 2004]. A common example of viscous dampers is a shock absorber in a car or the devices mounted on building doors to prevent the door from slamming shut.
FVDs add viscous damping to the structure and can reduce acceleration and displacement for the most of the frequency range. The dampers are usually installed as part of a building's bracing system using single diagonals. They are the most useful where engineers desire to reduce displacement without increasing the structure's frequency [Constantinou and Symans, 1992].

A real application example is the London Millennium Footbridge shown in Figure 2.7, a pedestrian–only steel suspension bridge crossing the River Thames in London. Unexpected lateral vibration (resonant structural response) caused the bridge to be closed on June 12 2000. After extensive analysis, the problem was fixed by the retrofitting of 37 fluid–viscous dampers to control horizontal movement and 52 tuned mass dampers to control vertical movement (Further information in [Dallard et al., 2001]).

Figure 2.7: London Millennium Footbridge (UK) and fluid viscous damper location.

2.1.2 Active control

Active control systems supply control forces to the structure in order to reduce its own motion. These forces are obtained from an algorithm based on feedback information from sensors that measure the excitation or/and the response of the structure [Soong et al., 1991], [Preumont, 1997]. Typically, an active control system consists of three main components: (i) a monitor, which is the sensors and the data acquisition system; (ii) a controller, a module that decides on the course of action; and (iii) an actuator, a set of physical devices that execute the instructions from the controller. Civil structures require actuator systems (such as hydraulic systems) which are capable of generating large forces. The precise application of such control forces usually demands large power requirements. This conditional becomes particularly critical during seismic events when the main power source to the structure may fail [Soong, 1990].
The merit of the active control systems is that they are effective for transient vibration and also for a wide frequency range. Unlike passive systems, active control is able to adapt to different loading conditions and to control different vibration modes [Spencer et al., 1997a]. However, because external energy is introduced, it may induce instability into the whole structural system by unexpected dynamics changes or erroneous feedback information. In addition, cost and maintenance of such systems is significantly higher than that of passive devices. Active control strategies include active mass damper (AMD), hybrid mass dampers (HMD), active tuned liquid column dampers, active bracing, active base isolation, multiple connected buildings, etc., [Soong and Spencer, 2002], [Nishimura and Shidomaira, 2003].

Active mass damper . An auxiliary mass supported by rollers is attached to a transfer system as shown in Figure 2.8. The idea in that the mass oscillates at the same frequency of the structure but with a phase shift. The transfer system usually consists in a hydraulic actuator or an electric motor. It is used in order to provide a control force to drive the additional mass and counteract or mitigate the motion of the structure [Yoshida et al., 1995], [Ricciardelli et al., 2003].

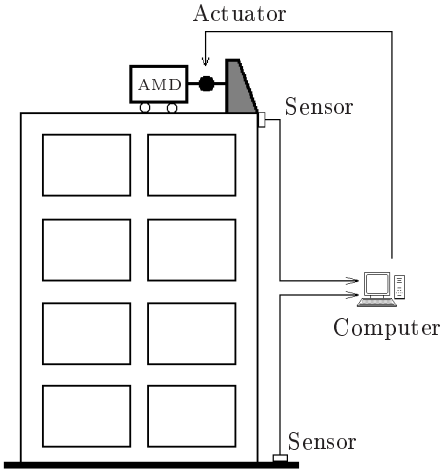

Figure 2.8: Structure equipped with an active mass damper (AMD)

The Kyobashi Seiwa Building in Japan (1989) was the first full–scale application of active control technology. Two active mass drivers were installed on the top floor to reduce the maximum lateral response associated with building vibrations caused by earthquakes and strong winds [Kobori et al., 1991]. Several real applications can be reviewed in [Cao et al., 1998] and [Nishitani and Inoue, 2001]. Besides, Figure 2.9 shows the Herbis Osaka Building in Osaka, Japan. An AMD system installed at the 38th floor level was completed in 1997. Two AMD's, which can move only in one direction, were installed to control both the lateral and torsional direction of the building (Further details in [Yamamoto et al., 2001]).

2.1.3 Semi–active control.

Semi–active control strategies arise as a combination of the positive aspects of both passive and active control systems. They utilize the motion of the structure to develop dissipative control forces but also use feedback measurements to alter the characteristics of the dissipative mechanism in real–time. Semi–active control is particularly promising in protection of civil engineering structures, in

Figure 2.9: Herbis Osaka Building in Osaka, Japan and a prototype of AMD.

the sense that they potentially offer the reliability of passive devices, maintaining the versatility and adaptability of fully active systems at low–power requirements [Casciati et al., 2006]. In the literature, important studies along with experimental results have showed that appropriately implemented semi–active control performs significantly better than passive control and has the potential to achieve the major capabilities of fully active control [Symans and Constantinou, 1999], [Jung and Lee, 2002]. The most common semiactive control devices are: variable–orifice fluid dampers, controllable friction devices and controllable–fluid dampers. In [Housner et al., 1997] and [Marazzi and Magonette, 2001], interesting surveys on semiactive control systems can be found.

Variable–orifice fluid dampers. It behaves as linear viscous dampers with adjustable damping. Its operation principle consists of controlling the damping coefficient by adjusting the opening of the internal valves changing the flow resistance of the hydraulic fluid. Thus, large forces can be achieved with low external power [Kamagata and Kobori, 1994], [Serino and Occhiuzzi, 2003]. Several real applications on high–rise buildings have been accomplished, for instance, these kind of devices have been implemented on a 5–storey office building located in Shizuoka City, Japan [Kurata et al., 2000].

Variable–Friction Damper. It dissipates energy by forces generated on friction surfaces. These forces can be varied by means of electrical signals or gas pressure, which vary the friction coefficient of the device. In [Dowdell and Cherry, 1994] the ability of these devices to reduce the inter–story of a seismically excited structure was investigated. Also, in [Feng et al., 1993], a study of these devices placed in parallel together with a seismic isolation system is presented.

Controllable fluid dampers. In these devices are similar to passive fluid viscous dampers, but in them some properties of their internal fluid can be modified by means of electric or magnetic field, resulting a modification in the quantity of force absorbed. The principal advantage of this type of devices is that the piston is the only moving part; consequently, it can change rapidly from a state to another (e.g. from viscous to a semi–solid in milliseconds) when exposed to an electric/magnetic field. Semiactive controllable fluid dampers can be: (i) Electrorheological (ER), if the smart fluid changes rheological properties[2] in presence of an electric field; and (ii) Magnetorheological (MR), if the smart fluid properties change under different magnetic fields. Several ER dampers have been developed and adapted to civil engineering structures. Important developments can be reviewed in [Masri et al., 1994], [Gavin, 2001] and [Leitmann and Reithmeier, 2002] among others.
MR dampers have become as an alternative of ER damper. When the external signal is applied (a magnetic field), the inside fluid becomes from semisolid to viscous state and it exhibits a viscoplastic behavior. MR devices typically have very low power requirements with voltage between 12–24V and current demand of around 1–3 amps[3], offering highly reliable operation at modest costs [Poynor, 2001], [Gravatt, 2003]. Many numerical simulations and laboratory tests have been accomplished to demonstrate the effectiveness of MR devices for seismic response reduction. Some interesting documents are [Dyke et al., 1997a], [Dyke et al., 1997b] and [Renzi and Serino, 2004] among others.

Double–ended MR dampers are generally used for semiactive control applications in civil structures (See Figure 2.10). Due to the presence of nonlinearities, in particular the hysteresis phenomenon, the modelling of these devices is quite challenging being lot of literature devoted to this topic [Spencer et al., 1997b], [Yang et al., 2004], [Ikhouane and Rodellar, 2007], [Aguirre et al., 2008] and more. An example of real application is the Dongting Lake Bridge (Fig. 2.11), a cable–stayed bridge crossing the Dongting Lake in southern central China. The world's

[2]Rheology is the study of the flow of matter, mainly liquids but also soft solids or solids which, under particular conditions, flow rather than deform elastically.
[3]Note that common car batteries can supply this power.

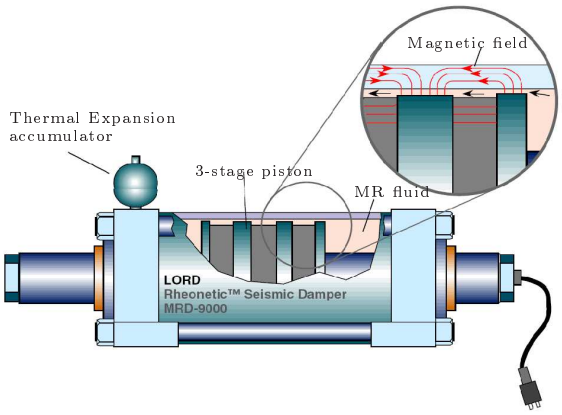

Figure 2.10: Schematic of a full scale MR damper

first application of MR dampers on cable–stayed bridge to suppress the rain–wind–induced cable vibration. For further details see [Chen et al., 2003].

Figure 2.11: Dongting lake bridge in Hunan, China and MR dampers attached to the stay cables.

2.2 Structural control algorithms

During the last two decades, various types of structural control strategies have been applied to the control of civil engineering structures. High–quality control systems require the design of the feedback controller with specific control objectives in mind, related to meaningful structural performance measures, while at

the same time addressing device (or actuator) and system nonlinearities and the uncertainties in the system and excitation models. Depending on the available information for each controlled structure, the mathematical model associated, types of measurements, actuators and disturbances, each control solution can be suitable only for one specific type of structure and not for all kinds [Soong, 1990]. Due to this thesis is not focused in control theory, in what follows we shall limit to mention some strategies commonly used in civil engineering fields.

Most of the research efforts on control law design for civil engineering applications have been done on extending linear control methodologies, primarily some variant of H_2 control [Kucera, 2007], to structural control problems, see for instance [Spencer and Nagarajaiah, 2003], [Miyamoto and Hanson, 2004] and [Ang et al., 2005]. At the controller design stage, potential nonlinearities regarding to the structural and excitation models are either: (i) neglected, for example in the context of the well known clipped–optimal control design for semi–active systems [Dyke et al., 1996]; or (ii) approximated considering linearization techniques [Erkus and Johnson, 2006]. To consider the nonlinearities arising from the limitations of the actuators, heuristic feedback controller design techniques have been suggested; methods such as hysteretic, dissipation–based, and energy–based approaches, e.g., [Gavin, 2001], [Jansen and Dyke, 2000].

One of the most prolific field on literature has been devoted to semiactive control. The most relevant works deal with strategies such as: Lyapunov based control, e.g [Jansen and Dyke, 2000]; H_∞ control, e.g. [Yang et al., 2002]; sliding mode control, e.g. [Moon et al., 2003]; QFT control, e.g. [Sanz, 2005] and backstepping control, e.g. [Zapateiro et al., 2009].

Note that most aforementioned methodologies primarily focus on the mean square structural response and do not explicitly account for uncertainties in the system and excitation models. Thus, some researcher found that the optimal strategy in structural control design with uncertainties should be that which maximizes the reliability. Theoretical reliability–related control methods, such as μ–synthesis and the many offshoots of these, have become the standard tools in the design of feedback controllers that are robust to model uncertainty, where a compact set of possible models for the system is chosen [Dullerud and Paganini, 1999], [Yoshida et al., 1995].

2.3 Testing of seismic protection system

In structural control, similar to other application fields, the main objective is to develop integrated control methodologies that are robust, effective, implementable, reliable and with the minimum control effort. However, sometimes it is difficult due to some problems such like nonlinearities, uncertainties, dynamic coupling and measurement limitation. To assess structural resistance and seismic protection system behavior under dynamic loads, a test method that emulates the full dynamics of the system is needed. This section gives a brief overview of several well–established testing methods that are currently the most widely used testing methods in seismic engineering research.

2.3.1 Shaking table method

The most natural experimental technique used for earthquake engineering is shaking table testing. A specimen representing the structure (usually scaled down for practical reasons) is fixed on top of a rigid platform (table), which is connected to one or more hydraulic actuators that control the movement of the platform in one or more degrees of freedom and vibrates to replicate ground motions.
Effective shaking–table testing of structural models started to be carried out in the late 1960's and early 1970's. This came as a result of the advances in electro–hydraulic servo equipment, as well as improvements in computer hardware and instrumentation, for control and acquisition of data [Aristizabal and Clark, 1980]. Such work was mainly initiated in the US with the set–up of dynamic testing facilities at the University of Illinois at Urbana–Champaign [Sozen et al., 1969] and the University of California at Berkeley [Bouwkamp et al., 1971]. Since then, shaking table testing has been widely adopted in earthquake engineering research centres worldwide. Differences in shaking tables generally relate to the number and types of degrees of freedom that can be controlled during testing, the mass that can be supported and the actuators' movement limits. For instance, the shaking table system in the laboratory of the Department of Structural Engineering at University of Naples "Federico II" is shown in Figures 2.12 and 2.13. Two square tables (3m side) can be moved asynchronously in order to reproduce the seismic effects on structures with long spans. For each, the maximum load is 200kN with a frequency range of 0–50Hz, peak velocity of 1m/sec and total displacement of 500mm. The hydraulic system has 12 motor pumps groups with a maximum total capacity of 2500lit/min.

Shaking table testing better represents live earthquake experience inside a laboratory. Even though the shake table test might be considered the most ad-

Figure 2.12: Asynchronous shaking table system at University of Naples "Federico II".

Figure 2.13: Hydraulic system which supplies oil pressure to shaking tables at University of Naples "Federico II".

vanced form of seismic testing, it is also the most expensive, as it requires that several skilled personnel and costly equipment. Note as well that, in shaking table testing only base vibration is introduced and loads due to wind for exam-

ple cannot be modelled. Additionally, the limited power of the actuators that drive the table imposes the use of reduced scale specimens, what in turn, introduces difficulties and uncertainty in the interpretation of experimental results [Williams and Blakeborough, 2001]. Consequently, considerable effort and funding has been placed over the past 40 years in the construction of continuously larger and more powerful shaking table facilities around the world. As an example, on July 14 2009, Colorado State University and Simpson Strong–Tie along with other partners successfully led the world's largest earthquake shake table test. A ground motion equivalent to a 2500–year earthquake (similar to a 7.5 Richter magnitude) was applied on a seven–story, 40–foot by 60–foot condominium tower with 23 living units. The test took place on the nowadays world's largest shake table (known as E–Defense) in Miki City, near Kobe, in Japan (Further details in www.strongtie.com/about/research/capstone.html).

2.3.2 Pseudo–dynamic (PsD) method

The pseudo–dynamic test method is a computer controlled testing technique that enables dynamic testing of structures into the non–linear range while using the same loading equipment that is used for static or quasi–static testing[4]. The structure to be analyzed is spatially discretised according to a lumped mass approximation and actuators are located at these points to provide the loading. This experimental concept originated in Japan as early as 1969 following failed attempts to realize real–time hybrid tests. [Takanashi and Nakashima, 1987] provide general overviews of the method and historic development.

The PsD method can be considered a hybrid testing method as it combines online computer simulation of the dynamic behaviour of a structure with information measured directly from the structure. The test structure is physically attached through the actuators against an very stiff reaction wall. A computer calculates the structural response by a time–stepping integration method considering the idealised lumped–mass model of the structure subject to the input earthquake motion . While the inertial and viscous damping forces are modelled analytically, the solution of the equations of motion provides the displacements to be applied to the structure at each time step. These displacements are physically applied by actuators in a quasi–static manner[5] as long as the reacting forces are measured experimentally to be used in the equations of motion for the next time step [Mahin et al., 1989], [Shing et al., 1996a]. The actual size of the reac-

[4] In quasi–static testing loads are applied a very slow rate.

[5] Slow loading of the structure is important so as not to excite its inertial and damping properties, which are already accounted.

tion wall is also important to accommodate large scale structures. For instance, Figure 2.14 shows the reaction wall at the European Laboratory for Structural Assessment (ELSA) with 16m high, 20m long and 4m thick [Donea et al., 1996].

Figure 2.14: Pseudo–dynamic test set–up using the reaction wall at the European Laboratory for Structural Assessment (ELSA).

Positive attributes of the PsD method are that large massive structures can be tested at full scale using simple devices and low hydraulic power. As the conventional test is performed relatively slowly, arbitrarily large ground excitations can be used, and there is good opportunity for detailed observation of the structural behaviour and failures throughout the test [Shing et al., 1996b]. However you cannot examine rate–dependent behaviours, e.g., the effectiveness of fluid viscous dampers added to the structure could not be assess.

2.3.3 Effective force testing (EFT)

EFT is a dynamic testing procedure to apply real–time earthquake loads to large–scale structures that can be simplified as lumped mass systems. The test setup is very similar to that of the PsD method. The test structure is anchored to a fixed base, and dynamic forces are applied by hydraulic actuators to the center of each story mass of the structure. The force to be imposed (effective force) is the product of the each lumped mass and the ground acceleration record, and thus is

independent of the structural properties such as stiffness and damping, and their changes during the test. Unlike in a PsD test, the loading can be determined in advance of the test and no numerical integration is needed [Shield et al., 2001], [Dimig et al., 1999].

Motions measured relative to the ground are equivalent to the response that a structure can develop relative to a moving base as in a shake table test or an earthquake event. But, as for PsD testing, the EFT method is is only suitable for structures that can be represented as a series of lumped mass systems. The major limitation of EFT lies in the inability of hydraulic actuators to produce accurately a force at the natural frequency of a lightly damped structure, which was attributed to the interaction between the actuator piston velocity and the actuator control [Zhao et al., 2003].

2.3.4 PsD with substructuring

A special set-up procedure for the pseudo-dynamic test, known as "sub–structuring", enables portions of a structure to be tested. The idea is to apply physically quasi–static loading on a sensitive part of the structure while the remaining part is numerically simulated on a host computer together with the inertial and damping characteristics of the sensitive part. Sub–structuring method allows relatively inexpensive dynamic testing of large multi–degree of freedom (MDOF) structures and also makes possible focusing on important elements of a structure such as isolation bearings [Pegon and Pinto, 2000].

The technique generally provides an efficient way to gain valuable information on the performance of different parts of a structure. The major advantage is that only the part of main interest is physically tested, providing infinite repeatability of the remainder. Despite this, some disadvantages comes: first, the failure mechanism for the structure must be assumed beforehand, and second, the creation of the substructure interface makes the experiment more difficult to be implemented and controlled [Pinto et al., 2004].

2.3.5 Real–time substructure testing

Real–time substructure testing (RTST) may be considered a derivative of sub–structured pseudo–dynamic testing [Nakashima et al., 1992]. An RTST is a hybrid method involving a physically tested part and a numerically modelled part; the two substructures are complementary to form the complete emulated struc-

ture. During the RTST, the physical substructure interacts, by means of a feedback loop, with a computational model of the structure (numerical substructure); both substructures send and receive data from each other, because they need to know the state of the other part to work out their own. This interaction most take place in real–time to achieve reliable results, however, because of the mechanical characteristics of the transfer system in between the numerical and physical substructures, the presence of delays is unavoidable [Darby et al., 2002], [Wallace et al., 2005a].

As PsD with substructuring testing, RTST allows one to concentrate on the behaviour of a specific part of the structure, while having the rest of the structure modelled separately with infinite repeatability. When such a real–time experiment is conducted, the damping and inertial properties of the specimen are no longer computed but are fully accounted for through the measured force feedback. This method removes the uncertainty in modelling complex structural parts as these may be tested physically being especially convenient to study the behaviour of structures that contain highly non–linear and/or rate–dependent parts within them [Sivaselvan et al., 2004].

Due to this thesis is mainly devoted to the stability analysis of a rate–dependent device for seismic protection which is suppose to be tested in lab by means of a real–time substructuring test, this testing method shall be widely discussed in the next chapter.

Chapter 3

Real–Time Dynamic Substructuring Test

Contents

Rate–dependent effects are often significant when testing concrete structures (to a lesser extent for steel structures) but of great value when evaluating the behaviour of energy dissipation devices as part of seismic protection systems, like viscous dampers added to a structure. Throughout the last decades, shaking tables have been traditionally used to provide real–time loading, allowing the engineer to measure and evaluate the dynamic behaviour of nonlinear and velocity–dependent structural systems. However, as it was pointed out before, this testing method presents serious drawbacks concerning size and power limits, what generally imposes the use of reduced scale specimens.

Real–time dynamic substructuring test (RTDST) is a promising dynamical testing method in earthquake engineering as it allows, theoretically, the assessment of dynamic behavior of structural systems in nonlinear range under realistic extreme loading conditions, even when considering large structures at full–scale.

In this chapter, we present the main features, advantages and disadvantages of this method. Our interest is to show how RTDST can effectively be implemented for testing and designing control systems for seismic protection, and which circumstances are particulary challenging in order to achieve reliable simulations of the emulated structure.

3.1 An overview of RTDST

Real–time dynamic substructuring, also called real–time hybrid simulation or real–time pseudodynamic testing, is a relatively new method for testing in earthquake engineering; it has being growing in acceptance as a consequence of advances in computing power, digital signal processing and hydraulic control. Real–time substructure testing is essentially, a fast version of the substructure approach to PsD testing described earlier in §2.3.2. It is useful when testing large scale civil engineering structures under dynamic loads, because critical components can be tested at full–scale[1] even if they exhibit rate–dependent behaviour. As before, the system is split up into two principal subsections: the physical (experimental) and numerical (analytical) substructures, keeping as the physical substructure those components of the structure that are critical due to their complexity, containing typically, unknown or non–modelled behaviour with strong non–linearities. The challenging issue is to ensure that the physical and the numerical substructures together behave in the same way as the whole real system [Neild et al., 2005], i.e., the emulated structure.
Figure 3.1 shows a conceptual view of real–time substructuring test considering a building with a tuned mass damper (TMD) at the top floor. Two different settings up are sketched: the first one extracting only the TMD from the system and using reaction wall facilities for the test; and the second one, extracting the upper floor with the TMD and using shaking tables facilities. In a typical displacement–controlled simulation, the displacements computed by the numerical substructure are applied to the physical specimen, and the resisting force is measured and fed back into the numerical substructure. Whilst in a PsD test only the static restoring force is fed back, in a real–time test the fed back force will also include damping and inertia components (therefore they do not need to be

[1] This avoids scaling effects problems for material such as reinforced concrete [Abrams, 1996].

included in the numerical substructure). For earthquake loads, this means that each cycle through the loop in the figure, must be completed in a time–scale of a few milliseconds. Consequently, this feedback loop needs very rapid computation and efficient communication between the two substructures, as well as robust control [Gawthrop et al., 2007].

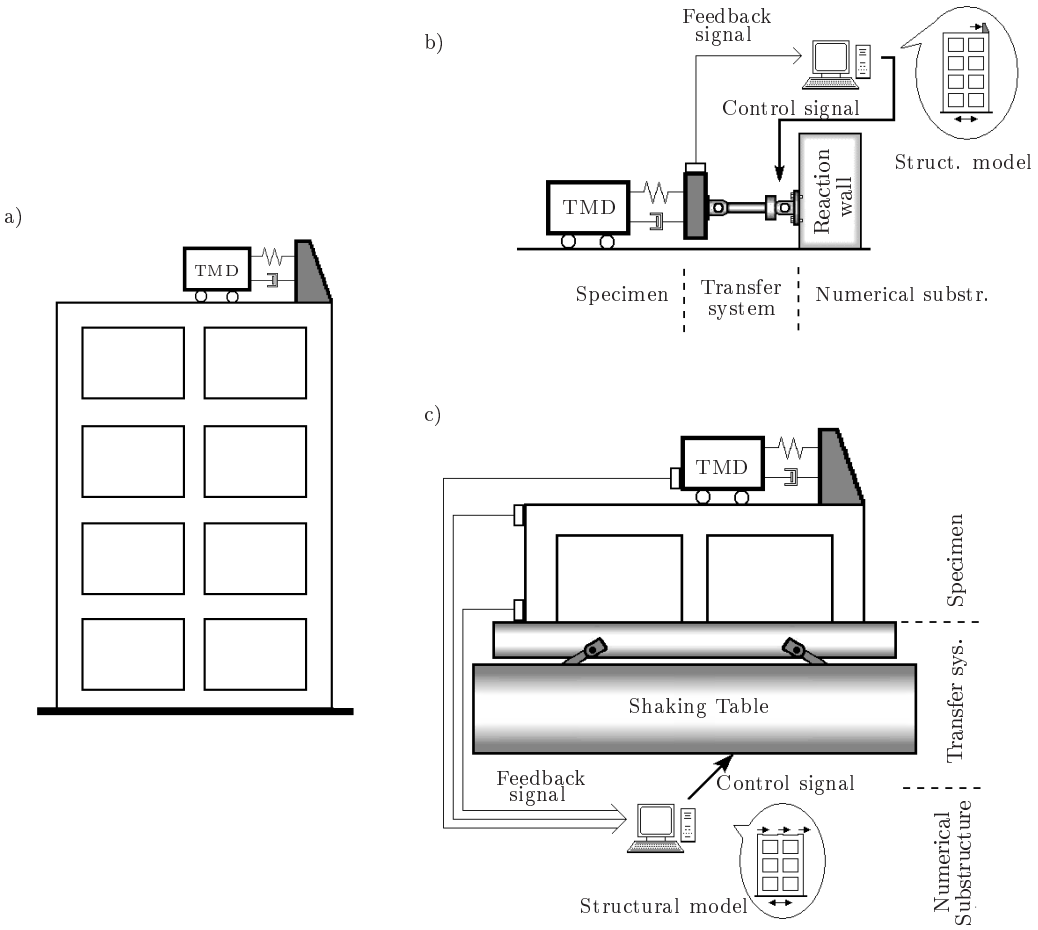

Figure 3.1: Conceptual view of a RTST test. (a) The emulated structure. (b) RTST by using an actuator. (c) RTST by using a shaking table.

RTST has its origins in a kind of component testing so–called *hardware–in–the–loop* (HIL) which has been used in a variety of electronic and mechanical engineering applications. Originally, the hardware component (an electronic control unit or a real engine) and the software models (which simulate the behaviour

of the rest of the system) can communicate with each other via electrical signals [Faithfull et al., 2001]. In extending the HIL to test mechanical component, instead of electrical signals, forces and velocities are required to be transferred to the specimen (typically by means of a set of actuators), therefore an additional dynamic transfer system must be included in the loop [Wagg and Stoten, 2001]. A extensive review of HIL is given by [Bacic, 2006].

The first reported RTST was performed on a viscous damper located at the base of a multi–storey building [Nakashima et al., 1992]. In that work, only the damper was tested physically while the building was modelled as a linear single degree of freedom (SDOF) system, so that the computations involved were very simple. [Darby et al., 1999] have also performed real–time tests using a linear SDOF numerical substructure, with the physical test specimen being a stiffness, damping or inertia element. As it shall be explain later, RTST requires to compensate for delay, the signal to be applied on the test specimen. In this direction, [Horiuchi et al., 1999] investigated the use of simple polynomial curve fits and found that, by using a third–order function, stable and accurate results could be achieved. As well, [Nakashima and Masaoka, 1999] demonstrated the effectiveness of the extrapolation and interpolation procedures, through a series of real–time tests applied to a multi degree of freedom (MDOF) structure treated as SDOF models.

The concept of pseudodynamic testing was successfully extended to real–time scales for testing nonlinear structures as in [Shing et al., 1996b]; and also extended for testing velocity–dependent components as in [Magonette et al., 1998] and [Jung and Shing, 2006]. The integration scheme is an important part of a RTST test as it relates the unknown values for a given time step to the known values at one or more previous time steps. [Jung et al., 2006] presented the implementation details of a real–time PsD test system that adopts an implicit time integration scheme along with a theoretical system model which incorporates the dynamics and nonlinearity of the test structure and also actuator compensation for delays.

Some test have been also done using shaking table facilities as the transfer system for RTST experiments. For instance, [Neild et al., 2005] separated the large structural mass of the single DOF system into two parts and selected the smaller one as the experimental substructure and the larger one (with attached spring and dashpot) as the numerical substructure to conduct a shaking table test. Similarly, a RTST for the shaking table test is proposed in [Lee et al., 2007] where the upper part of a structure is chosen as the experimental substructure

and the lower part is considered as the numerical one. The validity and accuracy of the proposed technique is proven by obtaining good agreement between experimental and numerical results. As well, [Ji et al., 2009] performed a substructure shaking table test to reproduce large floor responses of high–rise buildings at full–scale. Due to various certain capacity limitations, a rubber–and–mass system was proposed to amplify the table motion in order to reproduce such a large responses.

Additionally, real–time substructuring test has been recently used for testing semi–active control devices, [Christenson et al., 2008] conduced a test for three large–scale MR fluid dampers simulating the seismic response of a three–storey steel frame structure and presents a technique called virtual coupling which is used to ensure an appropriate tradeoff between performance and stability. Real–time simulations have been also used in automotive industry for testing novel suspension systems and in relative areas to Mechanical Engineering. For instance, in [Wallace et al., 2007] a real–time dynamic substructuring test of a helicopter rotor blade coupled with a lag damper from the EH101 helicopter is presented; the results revealed how the inclusion of a real damper produces a more realistic representation of the dynamic characteristics of the overall blade system involving the hysteretic dynamic profile due to the nonlinear behaviour of the dampers.

3.2 How RTDST works

To carry out a real–time dynamic substructuring test, the component of interest is identified as the physical substructure, extracted from the system and fixed into an experimental rig. Those important parts are tested experimentally while the remainder of the structure is modelled numerically (See Fig. 3.1). To link the test specimen to the numerical model, a set of systems should be connected all together as shown in Figure 3.2, where through a block diagram of a substructuring test, the systems comprising each substructure are sketched.

Roughly speaking, we can identify the next main systems. A *numerical model* which includes the mathematical model of the structure and the time integration scheme used to solve it. A *compensator* which allows the signal to be corrected and compensated for delay errors. A *transfer system* which makes possible the physical transfer of force and velocity from the numerical model to the specimen; it comprises both hardware (e.g. an actuator) and software (e.g. a control law) components. The *specimen* which is the physical part of the emulated structure to be actually tested in the lab. And finally, a *measurement system* which is required to get back information from the specimen response, it comprises trans-

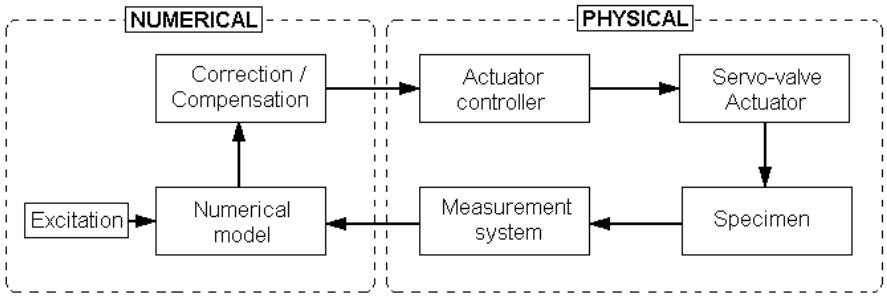

Figure 3.2: Block diagram of a substructured system.

ducers, signal conditioners, data acquisition system and software (e.g. a digital filter).

Considering the external excitation and the current state of the system, the displacements along the degrees of freedom of interest are calculated solving the numerical model by time–stepping integration. The numerical model is often assumed to behave linearly in essence, but more complete models may include nonlinearities which must be attended when adopting the numerical time integration technique. Once calculated, this displacement is passed into the delay compensator. The corrected/compensated signal is then passed to the actuator controller which in turn, generates the signals to drive the actuator[2]. Now, these displacement are imposed on the specimen while the forces required to impose them are measured and passed back to the numerical model. Thus, the next integration step can be solved by updating the excitation and the system's states.

To accurately represent the whole structure, the entire aforementioned process must take place in real–time and both, the physical and numerical substructures, must operate in parallel with minimal errors at the interfaces between them. Therefore, it is crucial that the error between the displacements calculated from the numerical model and those imposed by the actuators on the physical substructure are minimized. In what follows this issue shall be discussed comprehensively.

[2]Note that the transfer system is typically a single (electric or hydraulic) actuator with its controller, but it may also be a more complex test facility like multiple actuators (for multiple DOF control) or shaking table.

3.3 Saturation, delay and instability

Like for some techniques in structural control, real–time substructuring test requires performance of all the computations, application of displacements (or forces) and acquisition of the measured responses, within a very small time frame. However, in consequence of the complexity in solving the numerical model and mainly due to the mechanical characteristics of the transfer system used, the presence of delay errors on command signals are unavoidable. In real–time testing, there is a delay between a command signal being sent to an actuator and its moving to the desired position, what becomes more critical when operating hydraulic actuators[3] where the response time is larger. The force fed back from the experiment to the numerical model is therefore incorrect, since it is measured before the actuator has reached its target position.
In some cases, this delay error may be small and can be neglected, but it is normally large enough to affect the overall dynamics and may cause instability [Wagg and Stoten, 2001]. For a linear system, [Horiuchi et al., 1999] have shown that this error introduces additional energy into the system, being equivalent to negative damping. This can distort the simulation results and, if the negative damping exceeds the inherent structural damping, cause the test to become unstable. As well, [Wallace et al., 2005a] showed how if the delay in the transfer system is less than a critical delay, the substructured system is stable; nevertheless, they also pointed out that typically, the delay of the transfer system is larger than the critical one, and then, oscillations which increase exponentially in amplitude are developed in the simulation. As a matter of fact, let us consider a single degree of freedom oscillator with constant delay τ in the stiffness element. Figure 3.3 shows the collection of maximum oscillator's displacements in free vibration varying τ, the larger the delay the larger the response.

Hence, it is essential for the stability, accuracy and reliability of the simulation, to make corrections and compensation on the signals being transmitted between numerical and experimental substructures [Wallace et al., 2005b], as otherwise, the errors may cumulate during the iterations and significantly alter the simulation outcome.

To avoid wrong feedbacks when setting up a RTST simulation, some physical saturation effects must be also considered, since the overall accuracy and realism of the test may decrease as realistic loading are no longer achieved. Four saturation effects can occur within a test constraining the range of application: (i) the maximum imposed displacement is limited on account of the finite strokes of the

[3] Hydraulic actuators are required for large structures when large loads are needed.

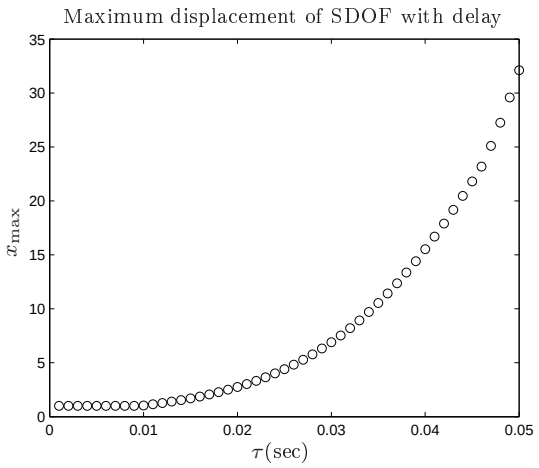

Figure 3.3: Maximum displacement of the oscillator $\ddot{x}(t) + a\dot{x}(t) + bx(t-\tau) = 0$ when τ is varying; $a = 4(0.03)\pi,\ b = 4\pi^2$ and $t_{max} = 5$sec.

actuator; (ii) the velocity of the actuator is constrained due to the limited power of the pumps and the flow ratings of the controlling servo–valves; (iii) frequency range is required to be evaluated too, particulary for the deleterious effect of oil column resonance common to shaking tables [Neild et al., 2005]; and finally, (iv) the force that can be applied to an actuator is limited to the available supply pressure. Thus, in assessing the feasibility of a particular real–time substructure test, it is essential to consider saturation effects in both test design and actuator's control strategies [Gökçek et al., 2000].

3.3.1 Delay compensation

As explained above, the dynamics of the transfer system must be compensated in order to impose fast and accurate displacements (or force and velocity) on the physical component. The development of compensation algorithms and the study of their effect on system performance requires a detailed knowledge of the equipment behaviour. Simultaneously, in light of the current computing capabilities, there is a limit on the number of degrees of freedom that can be included in the numerical model, since a large model will require a long computation time. Therefore, when seeking for more realistic RTST simulations, longer time to accomplish each iteration arise from increasing size and complexity in both substructures. With such a long delay, it becomes increasingly difficult to ensure that the RTST simulation remains stable.

The importance of experimental errors, especially systematic errors such as time delay, was recognized early on [Shing and Mahin, 1983] in the extension of pseudodynamic test to fast and real–time application. Many literature on fast hybrid simulation is devoted to the development of actuator delay compensation and signal correction procedures [Horiuchi et al., 1999, Wallace et al., 2005b]. Delay compensation is a well known technique with the most common strategy being delay compensation by extrapolation [Sivaselvan et al., 2004]. Polynomial extrapolation has been used extensively due to its simplicity and efficiency, it uses only a few recent command data to predict a compensated signal in advance [Bonnet et al., 2007]. However, those extrapolation suffer from significant limitations which restrict its usefulness in experimental implementation. [Ahmadizadeh et al., 2008] used a different prediction algorithm by assuming a linear variation of acceleration, which also provides a third order displacement variation, demonstrating the improved accuracy in the simulations. As well, [Nakata et al., 2006] proposed a model–based response prediction method which incorporates known information about the system and the excitation, allowing larger prediction horizons as more accurate prediction of the system response could be achieved. Several procedures which take advantage of state equations of the system have been also suggested to eliminate the delay effect in the control system as in [Wallace et al., 2005a] and [Kyrychko et al., 2007]. In addition, some adaptive procedures has been developed to compensate variations of the actuator time delay along a hybrid simulation (particularly as the stiffness of the experimental specimen changes) as presented in [Darby et al., 2002]. Finally, schemes for delay compensation have been also carefully studied by researchers in fields relative to active and semi-active control of structures as in [Rodellar et al., 1987] and [Serino and Georgakis, 1999]. For further information, a review of the most common compensation methods is presented by [Bonnet et al., 2007].

3.4 Compensator based on neural networks

In this thesis, we propose an novel approach for real–time systems in which time delay compensation is implemented using a model based on adaptive prediction by means of artificial neural networks. The aim is carried out a forward prediction of the command signal, to compensate it for time delay and thus enable the experiments to be run nearby to real–time.

It is common to approximate the behavior of a delayed system by including a constant time delay between the receiving a command signal. Although this

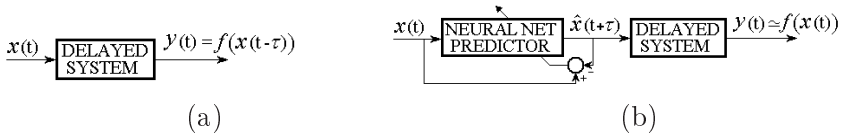

(a) (b)

Figure 3.4: (a) Delayed system. (b) Compensated system.

is not strictly correct since delays may be altered with the signal frequency, at the relatively low frequencies normally encountered in civil engineering dynamics, this is often considered to be a reasonable approximation [Bonnet et al., 2007]. Thus, in the proposed method, the compensated command signal is predicted forward a time equals to the delay τ. The prediction is generated through an artificial neural network which is self–adapted each time–step by using the available data (See Fig. 3.4). In presence of noisy signals, this method has shown to provide not only a robust criterion larger than other common methods, but also, a smoother signal avoiding the slight discontinuities which can be found in other schemes.

3.4.1 Forward prediction scheme

Delay compensation by extrapolation is not a new concept, single time–step prediction techniques have already been proposed as presented before. Here a neural network is trained on–line to predicting forward at each iteration the new reference signal to feed the delayed system. We consider a constant delay τ[4] along all the prediction.

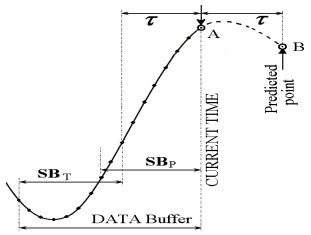

Figure 3.5: Forward prediction scheme.

For this approach a data buffer is required. It should be equal to the delay τ plus the sub–buffer length necessary[5] to achieve a suitable network's behavior. The prediction procedure may be summarized as follow with reference to fig. 3.5.

[4]The delay error must be known and accurate.

[5]Enough points to give sufficient information about the signal to the network.

At each time step, the data within the training sub-buffer SB_T are used as the train input vector $\mathbf{X}$ to the network and the last point in the main buffer ($\mathbf{A}$) is used as the desiderated output. This input-output sample is used to adjust the network's parameters. Once the network is updated, the predicted point ($\mathbf{B}$) is estimated by feeding forward the second sub-buffer SB_P to the network. After that, the buffer is updated with the new available data and the process is applied again in the next time step.

The above process enables the neural network for working in on–line prediction. For completeness, the next section presents some fundamentals and how the neural networks can be employed.

3.4.2 Artificial neural networks

During the 1940's, researchers desiring to duplicate the function of the human brain, have developed simple hardware models of biological neurons. McCulloch and Pitts [McCulloch and Pitts, 1943] published the first systematic study of the artificial neural network. The primary factors for the recent resurgence of interest in the area of neural networks are the extension of Rosenblatt, Widrow and Hoff's works dealing with learning in a complex [Rosenblatt, 1961], multi-layer network, Hopfield mathematical foundation, as well as much faster computers than those of 50's and 60's. The general objective of *training* the neural network is to modify the connection weights (and bias) to reduce the errors between the actual output values and the target output values to a satisfactory level[6]. This process is carried out through the minimization (optimization) of the defined error function using an approach usually based on gradient descent methods [Jang et al., 1997].

Elements of neural networks

An artificial neuron is the basic element of a neural network (see fig.3.6(a)). It consists of three basic components. The weight factors w_i are associated with each node to determine the strength of input row vector $\mathbf{X}$. The internal threshold θ is the magnitude offset that affects the activation of the node output. The activation function $f(.)$ performs a mathematical operation on the signal output.

$$a = f(s) = f\left(\sum_{i=1}^{N} w_i \cdot x_i + \theta\right) \tag{3.1}$$

A comprehensive review on activation functions, training methods and more

[6]Note that some networks never learn. This could be because the input data do not contain the specific information from which the desired output is derived or the network's architecture is not enough suitable (complexity) to solve the problem.

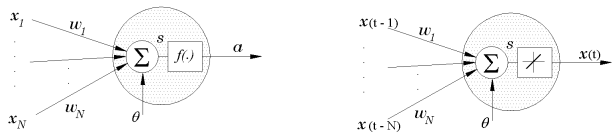

Figure 3.6: (a)Artificial neuron. (b)Adaptive filter by adaptive network.

topics concerning to neural networks architectures can be found in [Looney, 1997].

Adaptive filters

Adaptive filters adjust their own characteristics according to an optimizing algorithm in proportion to the signals encountered, in this way they will match as closely as possible the response of an unknown system from samples. Adaptive filtering is one of its major application areas for ADAptive LINear Element (ADALINE). You can create one by combining an input delayed layer within a neuron in which the activation function $f(.)$ is restricted to be linear and by using an iterative learning process in which data are presented to the network one at a time and the weights are adjusted each time[7]. Now, the input vector will be $\mathbf{X} = [x(t-1), x(t-2), \ldots, x(t-n)]^T$ and the output will be $a \triangleq y = x(t)$. Accepting that the signal is not quickly varying over time, the adaptive filter presented in figure 3.6(b) must predict the future values of the desired signal based on past values.

It is just this model of NNEt what we used along this thesis for delay compensation.

3.4.3 Numerical results.

To show the efficacy of the neural networks in prediction, we execute some numerical simulation[8] considering different system command signal to be predicted. Three different methodologies purposed by other authors has been applied too in order to compare and evaluate the network behavior: (1) The exact polynomial extrapolation (EPE), in which a polynomial is fit to the last few data points of the signal; a third–order polynomial has been widely adopted in literature and will be used here [Bonnet et al., 2007]. (2) The 4-point sine-fit prediction method (SFPM), which allows to predict the amplitude and frequency of the half period sine wave which best fits the actual signal segment [Serino and Georgakis, 1999]. And (3) the least-squares polynomial extrapolation (LSPE), which takes into account a larger number of points and uses a least-squares approximation rather

[7] Here delta rule is used to train adaptive linear networks.
[8] All numerical tests have been done in PC Pentium(R)D 3.4GHz.

than an exact fit [Wallace et al., 2005b]; a fourth–order polynomial was used here for LSPE method. Although the last approach considers some additional adaptive delay compensators, only the extrapolation scheme is considered here.

Sine sweep tests

A sine sweep excitation which speeds up from 3Hz to 10Hz in 5 sec and then back to 3Hz in 5 sec, is considered as the signal to be predicted forward an amount of time τ equals to 5ms. As the time step was used 1ms. A training buffer of 10 points was considered for both the neural network and LSPE method.

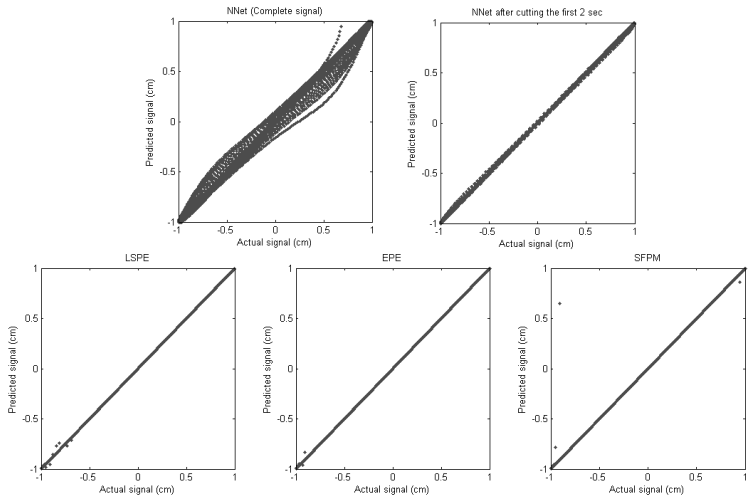

Figure 3.7: Subspace plots for sine sweep test.

Method	Nnet	LSPE	EPE	SFPM
Time (sec)	0.587	1.406	0.170	0.185
RMS error(%)	0.22	0.15	0.12	0.15

Table 3.1: Sine sweep test. Error and sequential time for 9982 steps.

Figure 3.7 shows the so–called subspace plots, in which the predicted signal is plotted versus the actual one. The more dispersion from the line $y = x$, the less accurate prediction was done. More dispersion means less synchronization.
Here the network exhibits the worst behavior, nevertheless, it is interesting to note the improvement getting by the network as long as the time pass. Table 3.1 presents the sequential execution time employed by each scheme for doing prediction through 9982 time steps in the simulation. The fastest one is the EPE

method while the highest computational cost was spent for the LSPE method. As statistical measure of the prediction, the root mean square of error is included in the table too[9].

Sine sweep with noise added (SNR=50dB)

The same sine sweep excitation was considered but here a low white gaussian noise was added to the signal. The signal to noise ratio (SNR) is equal to 50dB and as before ΔT=1ms and τ=5ms. A prediction buffer of 15 points has been used for both the neural network and the LSPE method.

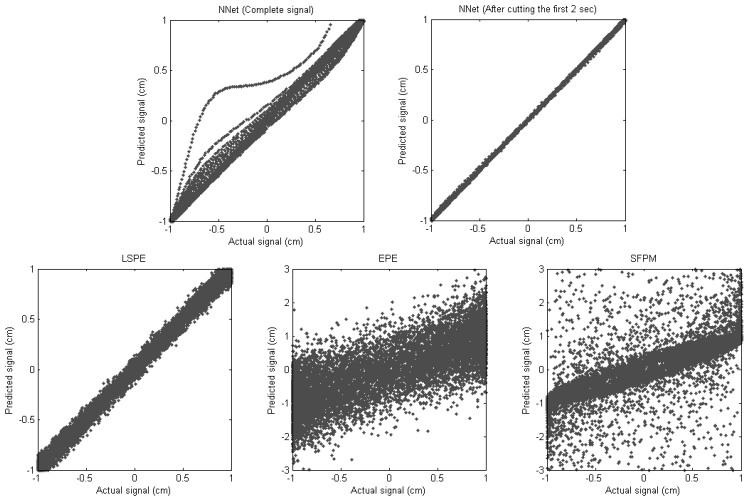

Figure 3.8: Subspace plots for sine sweep with noise test.

Method	Nnet	LSPE	EPE	SFPM
Time (sec)	0.687	1.592	0.187	0.265
RMS error(%)	0.63	5.55	61.84	72.50

Table 3.2: Sine sweep with noise test. Error and sequential time for 9982 steps.

Figure 3.8 shows the subspace plots for each prediction scheme. Similarly, Table 3.2 presents the sequential execution time employed by each scheme when predicting a whole signal through 9982 time steps.
Considering both computational costs and synchronization capabilities, the neural networks presents the best characteristics when signal becomes noisy.

[9]For neural networks, the RMS value doesn't include the errors in the fist two seconds of the simulation.

Predicting noisy signals, the neural network demonstrates much more capacity and robustness than the other methods, this advantageous behavior is due to the inherent generalization capacity of neural networks and their high tolerance to noisy data. Besides, neural network provides a smoother signal when moving from one time step to the next one, so, slight discontinuities in the predicted command signal are avoided. Because of the adaptive training, the network shown behavior improvements as long as the simulation time pass.
Once the training process becomes well–balanced (about 2sec in the examples), this linear network was able to adapt quickly to the change in the target signal. The scheme is well suitable for being used within systems whose properties do not change abruptly and is able to smooth out the effects from noise when acquiring a signal.

Further information can be found in [Londoño and Serino, 2008].

3.5 Theoretical formulation of RTDST

The aim of the substructuring process is to model the dynamical behaviour of the overall system using a numerical part and an experimental part. The dynamics of the structure (overall system) are governed by a general system of differential equations equations, as:

$$\dot{x}(t) = h(x,t) \tag{3.2}$$

where x is the state vector of the overall system, $h(\cdot)$ denotes an arbitrary function and an overdot represents differentiation with respect to time t. Typically, we wish to characterize the dynamic response of the overall system subject to some excitation signal $r(t)$; such as an earthquake. In general, the form of $h(\cdot)$ is not known explicitly, but we assume that it can be split into linear and non-linear parts, so that

$$\dot{x}(t) = Hx(t) + Gr(t) + \hat{h}(x,t) \tag{3.3}$$

where G is a gain matrix, H is a matrix representing the linear part of h, and $\hat{h}$ the non-linear (i.e. the difficult to model) part. To formulate the substructured model we separate the overall system dynamics, equation (3.3), in such a way that the linear dynamics are modelled numerically, and the non–linear dynamics are modelled using a physical test specimen. To separate the two parts of the model, we divide the coordinates x into a subset associated with the physical substructure, $x_c \subset x$; and those which represent the numerical model, z where $z \cup x_c = x$. Thus x_c represents the state of the critical elements of the system.

Now equation (3.3) can be expressed as [Wagg and Stoten, 2001]:

$$\begin{bmatrix} \dot{z} \\ \dot{x}_c \end{bmatrix} = \begin{bmatrix} H_1 & H_2 \\ H_3 & H_4 \end{bmatrix} \begin{bmatrix} z \\ x_c \end{bmatrix} + \begin{bmatrix} G_1 \\ G_2 \end{bmatrix} r(t) + \begin{bmatrix} \hat{h}_1(z, x_c, t) \\ \hat{h}_2(z, x_c, t) \end{bmatrix} \tag{3.4}$$

If the dynamics of the numerical model are considered to be strictly linear, then $\hat{h}_1(z, x_c, t) = 0$. The dynamics represented by $H_2 x_c$ map to a series of experimental measurements $H_2 x_c \mapsto Rf(t)$; where $f(t)$ is a vector of experimental measurements, and R is a transformation matrix. If the excitation is restricted to the numerical model, we can also assume that G_2 is a null matrix. Thus, the numerical model can now be written as:

$$\dot{z}(t) = H_1 z(t) + G_1 r(t) + Rf(t) \tag{3.5}$$

Due to the fact that we are assuming that the non–linearity defined by $\hat{h}_2$ is unknown, the dynamics of x_c is not expressed mathematically but are included in model through the experimental measurements $f(t)$ from the physical substructure under the current states (z, x_c). Thus, equation (3.5) becomes the substructured model of the system.

3.6 Integration scheme

Three factors are essential in the implementation of a real–time substructuring test: the loading operation of the experimental substructure; the measurement of the interface force between two substructures; and the calculation of the numerical substructure by using a numerical time integration technique, which solves the temporally and spatially discretised equations of motion, for the structural system being investigated. It is quite likely that yielding will occur in several locations under a large earthquake load, being therefore desirable to be able to perform tests in which nonlinearities are permitted in both the physical and numerical substructures. Thus, integration schemes able to solve non–linear differential equations are required. Nevertheless, as with MDOF systems, nonlinear analysis requires long computation times so that considerable compensation for delay error may be necessary [Nakashima and Masaoka, 1999].

RTST simulation generally makes use of explicit numerical integration methods such as the central difference method (CDM), for which the computations are very simple and quick as well. They are also conditionally stable for time integration schemes [Shing, 2006] but may become prone to numerical instability as showing in [Pegon, 2001]. Implicit methods use the equilibrium condition to

determine the solution for the required time step and have advantages of being stable irrespective of the time step used. Although they were traditionally abandoned due to implementation difficulties, implicit methods are successfully being used in RTS test. A comprehensive valuation of implicit methods can be found in [Bursi and Shing, 1996]. A more complex algorithm based on a first–order hold approximation was used in [Darby et al., 1999], it appears to offer improved accuracy and stability. Besides, [Combescure and Pegon, 1997] investigated a non–iterative step-by-step implicit time integration scheme named α–operator splitting (α–OS) for PsD testing. They showed that it provides unconditional stability even when the number of degree of freedom is large while preserving simplicity. In a similar way, [Pinto et al., 2004] applied the α–OS technique to solve the spatially discrete equations of motion and compared it to the α–Newmark scheme which is in essence an implicit method. As well, [Magonette et al., 1998] have developed a high–speed continuous substructuring test method using a staggered implicit–explicit integration technique, in which the equations of motion for the experimental substructure are solved with an explicit scheme, while those for the analytical substructure with an implicit method; however, this has only partially addressed the stability issue. Additionally, [Bayer et al., 2005] have implemented an implicit integration scheme based on the Newmark time domain solution of the equation of motion[10]. The proposed procedure employs sub–stepping instead of iteration to reach equilibrium within each time step and was proposed suitable for real–time performance of the PsD test.

Before formalising two explicit methods typically used in RTST simulations, some key concepts shall be presented.
Direct step by step integration schemes are general methods that reduce differential equations into an algebraic form using a finite difference approach. In this way the response quantities at the end of a time step can be related to previously known response quantities. These methods are by far the most widely used methods of solution of non–linear problems [Butcher, 2003].
A general multiple degree of freedom system with substructuring can be represented through a set of differential equations of motion:

$$M\ddot{x} + C\dot{x} + Kx = E + F \tag{3.6}$$

where M, C and K are respectively the mass, damping and stiffness matrices; $\ddot{x}$, $\dot{x}$ and x are respectively the vectors of nodal accelerations, velocities and displacements for the degrees of freedom; E is the external excitation and F is the vectors of substructure forces.

[10] The Newmark method is a numerical integration scheme used to solve differential equations [Newmark, 1959]. It is often used in finite element analysis to model dynamic systems.

As the response of the numerical substructure depends on the physical substructure outcomes over time (which is not known inadvance) the problem cannot be solved analytically. Instead, time is discretised and the integration of the equation of motion is done numerically, assuming idealised properties over small time steps. M, C, K and F are known entities at the beginning. Note however that K and C may change during the analysis while M is usually regarded as a constant, assuming mass conservation even during failures. The solution at each time–step, depending on the scheme considered, are obtained through difference equations which can be written either as:

$$x_{n+1} = h\left(x_n, \dot{x}_n, \ddot{x}_n, x_{n-1}, \dot{x}_{n-1}, \ddot{x}_{n-1}, \ldots\right) \tag{3.7a}$$

$$x_{n+1} = h\left(\dot{x}_{n+1}, \ddot{x}_{n+1}, x_n, \dot{x}_n, \ddot{x}_n, x_{n-1}, \dot{x}_{n-1}, \ddot{x}_{n-1}, \ldots\right) \tag{3.7b}$$

where n is the current integration time–step. Thus, the numerical schemes can be classified as: *explicit scheme*, if the solution at the time–step $(n+1)$ can be obtained based exclusively on past values of the system as in equation (3.7a); or *implicit scheme*, if the solution at $(n+1)$ also exhibits dependency on one or several values from step $(n+1)$ itself, as in equation (3.7b). An implicit scheme involves more complex implementation, comprising often an iterative process.
For simplicity and fastness, explicit numerical integration methods have been extensively used in RTST simulations, in what follows, two popular scheme shall be presented.

3.6.1 Central Differential Method

The central difference method (CDM) is probably the most popular time integration scheme for PsD and RTST testing [Nakashima et al., 1992, Shing et al., 1996a, Horiuchi et al., 1999, Nakashima and Masaoka, 1999]. It can be mathematically described as in equations (3.8) where η is the integration time step chosen.

$$\begin{aligned} M\ddot{x}_n + C\dot{x}_n + Kx_n &= E_n + F_n \\ \ddot{x}_n &= \frac{1}{\eta^2}\left(x_{n+1} - 2x_n + x_{n-1}\right) \\ \dot{x}_n &= \frac{1}{2\eta}\left(x_{n+1} - x_{n-1}\right) \end{aligned} \tag{3.8}$$

The CDM is an explicit method. By substituting the acceleration and velocity terms from the difference equations into the equation of motion, the next step displacement vector x_{n+1} can be isolated and expressed as a function of terms known from the two previous time steps.
This scheme allows the easy introduction of a non–linear stiffness. Indeed, with the displacement being worked out from previous steps only, the stiffness matrix

can be updated accordingly for the next calculation to take the non–linearity into account. Non–linear damping can also be introduced, but because the velocity is only determined with a one step delay, only a fairly simple non–linear damping behaviour could be accommodated without an iterative process. Although CDM generates no amplitude error, it produces a periodicity error (period shortening) increasing with the time step. This method is only conditionally stable, the required time step for a stable solution might not be realized in the experiment depending on the fundamental frequencies of the specimen. Specifically, for a structure with a maximum natural frequency ω_{max}, the time step η must satisfy the condition: $\eta\omega_{max} < 2$, [Bathe and Wilson, 1976].

3.6.2 Runge–Kutta Method

The methods most commonly employed by scientists to integrate ordinary differential equations (ODEs) were first developed by the German mathematicians C.D.T. Runge and M.W. Kutta in the latter half of the nineteenth century [Press et al., 1992]. They are an important family of implicit and explicit iterative methods for the numerical approximation of solutions for ODEs. The basic reasoning behind the so–called Runge–Kutta (RK) methods is the use of Taylor's expansion of a smooth function[11] and the use of trial steps at the midpoint of each interval to cancel out lower-order error terms. The power of this method is that there are different orders according to the Taylor's expansion length taken. An arbitrarily large–ordered RK method can be derived, attaining an arbitrarily error.
The most often used method of the Runge–Kutta family is the Fourth–Order one. It uses a sampling of slopes through an interval and takes a weighted average to determine the right end point. A fourth–order Runge–Kutta integration method (RK4) represents an appropriate compromise between the competing requirements of both a low truncation error and a low computational cost per step, being one of the most powerful predictor–corrector algorithms. Thus, most computer packages designed to find numerical solutions for ODEs use it by default.
The standard RK4 method approximates the solution of an initial value problem of the form (3.2) assuming $h(x, 0) = x_0$. Here we use the first four terms of the Taylor series to describe the behavior of $h(x, t)$ near the midpoint $(x_{n+1/2}, t_{n+1/2})$. It requires four gradient or k terms to calculate x_{n+1} as follow, where η indicates

[11] Derivatives exist and are continuous up to certain desired order.

the integration step:

$$\begin{aligned} k_1 &= \eta h(x_n, t_n) \\ k_2 &= \eta h(x_n + \eta/2, t_n + k_1/2) \\ k_3 &= \eta h(x_n + \eta/2, t_n + k_2/2) \\ k_4 &= \eta h(x_n + \eta, t_n + k_3) \\ x_{n+1} &= x_n + \tfrac{\eta}{6}\left(k_1 + 2k_2 + 2k_3 + k_4\right) + O\left(\eta^5\right) \end{aligned} \tag{3.9}$$

Thus, the next value x_{n+1} is determined by the present value x_n plus the product of the size of the interval η and an estimated slope (a weighted average). The error per step of RK4 methods is on the order of η^5, while the total accumulated error has order η^4.
Several variation have been introduced, adaptive RK methods were designed to produce an estimation of the local truncation error of a single Runge–Kutta step, as well, implicit versions have been developed due to they are more general than the explicit ones and due to their high (possibly unconditional) stability.$\diamond$

Finally, considering the time–integration schemes for non–linear substructuring, explicit schemes are suitable when a small number of DOFs is involved, whereas implicit schemes depend strongly on the local nature of the problem and could result in significant local deviations from the medium time–step duration [Pinto et al., 2004]. In other words, an explicit scheme will need a time step short enough to ensure the stability of the scheme, while the stability of an implicit scheme will not depend on the time step chosen because it is partially based on a term from the end of the step considered.

Chapter 4

Stability Analysis Theory

Contents

Stability is the main goal in control engineering. For linear systems, the concept of stability is very well–defined and there exist many easy–to–use criteria for addressing its analysis. On the other hand, the stability analysis for nonlinear systems can become quite involved since not only there exists several definitions of stability, but also most of the known criteria provide sufficient but not necessary conditions when determining stability. In this chapter, we present some fundamentals and important definitions in stability analysis fields. Our aim is to supply a comprehensive background to facilitate later discussions on stability issues. First, the most important stability criteria using the characteristic polynomial for linear systems are introduced. Then, a graphical method for studying the qualitative behaviour of second–order systems is presented. We also examine the salient results of Lyapunov's stability theory; it is attractive for mechanical

systems, because of its exceptional physical meaning and its wide ranging applicability, specially for the analysis of nonlinear systems.
The following material shall be restricted to time–invariant systems (autonomous systems), but most of the concepts can be extended to time–varying systems. Most of the concepts are stated without a rigorous mathematical demonstration and focussed on vibrating mechanical systems; however, a deeper discussion of them can be found in the cited references within.

4.1 Stability of linear systems

A system is called linear if the principle of superposition applies. The principle of superposition states that the response produced by the simultaneous application of two different forcing functions is the sum of the two individual responses. A system is called *linear time–invariant systems* (or linear constant–coefficient) if the coefficients of the differential equation of the system are constants or functions only of the independent variable. Systems that are represented by differential equations whose coefficients are functions of time are called *linear time–varying systems*. An example of a time–varying control system is a aircraft control system (The mass of a aircraft changes due to fuel consumption).

Definition 4.1. A system is said to be *externally stable* if every Bounded Input produces a Bounded Output. This is also called *BIBO* stability.

Let us consider the second–order linear time–invariant system described by:

$$\ddot{x} + a\dot{x} + bx = 0 \tag{4.1}$$

These equations can be solved in the frequency domain by using Laplace transforms for continuous time systems and Z–transforms for discrete time systems. This approach is limited to linear systems. Since we are eventually interested in nonlinear systems, we will perform the analysis in the time domain solving for the time history. A common procedure is to assume a solution of the form $x(t) = ke^{\lambda t}$. By substituting the supposed solution, the characteristic equation of (4.1) can be written as:

$$\lambda^2 + a\lambda + b = 0 \tag{4.2}$$

We can then find the roots of the characteristic equation as:

$$\lambda_1 = \frac{1}{2}\left(-a + \sqrt{a^2 - 4b}\right); \qquad \lambda_2 = \frac{1}{2}\left(-a - \sqrt{a^2 - 4b}\right)$$

Thus, the solution of the system can be expressed by formula (4.3) where k_1 and k_2 depends on the initial conditions $\mathbf{x}_0 = (x(0), \dot{x}(0))$.

$$x(t) = k_1 e^{\lambda_1 t} + k_2 e^{\lambda_2 t} \tag{4.3}$$

Definition 4.2. For any linear time–invariant system:

- The system is called *asymptotically stable*, if for all $\mathbf{x}_0$ we have

$$\lim_{t \to \infty} x(t) \to 0$$

- The system is (critically) *stable* if for all $\mathbf{x}_0$ there exists C such that

$$\|x(t)\| \leq C \qquad \forall t$$

  In this statement, $\| \cdot \|$ stands for a norm, measuring the distance to the origin; the Euclidian norm is defined as $\|x\| = (x^T x)^{1/2}$.

- The system is *unstable* if it is neither stable nor asymptotically stable.

To facilitate later discussions, let us transform the scalar second–order differential equation in (4.1) into an equivalent system of two first–order differential equations by substituting $x_1 = x$ and $x_2 = \dot{x}$. Now, the system can be described in terms of the *equations of state* as follows, where x_1 and x_2 are the so–called *state variables* of the system.

$$\dot{x}_1 = x_2 \tag{4.4a}$$
$$\dot{x}_2 = -bx_1 - ax_2 \tag{4.4b}$$

The state variables of a dynamic system are the variables making up the smallest set of variables x_i that, for any time, completely describe the behavior of the system (which is also called *state* of the system). The n–dimensional space whose coordinate axes consist of the x_1–axis, x_2–axis, ..., x_n–axis is called the *state space*. Any *state* can be represented by a point in the state space.

We can also rewrite the equation (4.4) in vectorial form as:

$$\dot{\mathbf{x}} = \mathbf{A}\mathbf{x} \tag{4.5}$$

where $\mathbf{x} = (x_1, x_2)$ and

$$\mathbf{A} = \begin{bmatrix} 0 & 1 \\ -b & -a \end{bmatrix}$$

Finally, the solution of the system can be also written as in formula (4.6), where $\mathbf{x}_0$ represents the initial conditions.

$$x(t) = e^{\mathbf{A}t}\mathbf{x}_0 \tag{4.6}$$

It is worth to note that the roots of the characteristic equation in (4.2) are exactly the same as the eigenvalues of the matrix $\mathbf{A}$ in the state space model. Depending on the roots of the characteristic equation, the following necessary and sufficient stability conditions can be formulated.

Lemma 4.1.

- A linear system is *asymptotically stable*, if all the roots of its characteristic equation (or eigenvalues) satisfy $\Re\{\lambda_i\} < 0,\ \forall i$
- A linear system is (critically) *stable*, if all the roots of its characteristic equation (or eigenvalues) satisfy $\Re\{\lambda_i\} \leq 0,\ \forall i$ and if at least one root λ_i satisfy $\Re\{\lambda_i\} = 0$.
- A linear system is *unstable*, if at least one root λ_i of its characteristic equation (or eigenvalue) lies in the right–half of the complex plane ($\Re\{\lambda_i\} > 0$).

Hence, if it can be ascertained that a linear system has none of the roots of the characteristic equation (or eigenvalues) lying on the right–half of the complex plane, the BIBO stability is assured (i.e. when the system is stable or asymptotically stable) [Vidyasagar, 1992]. That is why, most of the techniques for determination of stability for linear systems essentially try to find the location of λ_i. Note that for stability scope, there is often no need to know these root with high precision but fundamentally its sign.

In what follows, we present two algebraic stability criteria based on the characteristic equation. They contain algebraic conditions which are only valid if all of the roots lie in the left–half complex plane. More sophisticated methods to be applied in the stability analysis of linear systems such as: root–locus method, Bode diagrams, Nyquist stability criterion and frequency response analysis, can be examined in [Ogata, 1990] where they are widely described.

4.1.1 The Hurwitz stability criterion

Let us consider the polynomial:

$$P(\lambda) = a_n\lambda^n + \cdots + a_1\lambda + a_0 \tag{4.7}$$

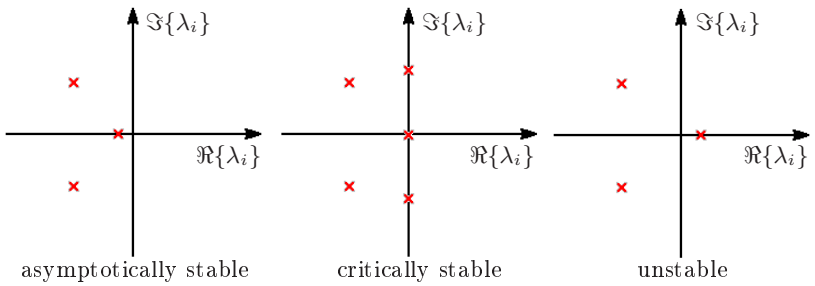

Figure 4.1: Stability of linear systems according to the root locus in the complex plane

For the polynomial to have all roots with negative real parts it is necessary that

$$\text{sign}(a_0) = \text{sign}(a_1) = \ldots = \text{sign}(a_n) \tag{4.8}$$

Formula (4.8) is the so-called *Stodola criterion* [Slotine and Li, 1991]. These conditions are also sufficient for $n = 1$ and $n = 2$ as can be easily verified by calculating the roots. However, for $n \geq 3$ this is no longer the case.
A polynomial for which all roots λ_i have negative real parts is called *Hurwitzian*. A polynomial $P(\lambda)$ is Hurwitzian, if and only if for $a_n > 0$ all determinants $D_1, D_2, \ldots, D_n$ are positive, where:

$$\begin{aligned}
D_1 &= a_{n-1} \\
D_2 &= \begin{vmatrix} a_{n-1} & a_n \\ a_{n-3} & a_{n-2} \end{vmatrix} \\
D_{n-1} &= \begin{vmatrix} a_{n-1} & a_n & \cdots & 0 \\ a_{n-3} & a_{n-2} & \cdots & \cdot \\ \cdot & \cdot & \cdots & \cdot \\ \cdot & \cdot & \cdots & \cdot \\ 0 & 0 & \cdots & a_{n-1} \end{vmatrix} \\
D_n &= a_0 D_{n-1}
\end{aligned} \tag{4.9}$$

Therefore, according to the stability conditions introduced in definition 4.1, a linear system is only asymptotically stable if its characteristic polynomial is Hurwitzian.

4.1.2 Routh's stability criterion

Routh's stability criterion enables us to determine whether or not there are unstable roots[1] in a polynomial equation without actually solving for them. To apply the Routh criterion, you need to form the so–called *Routh Array* from the polynomial coefficients in (4.7). Then, after some computations, the criterium determines the number of characteristic roots within the right–half plane
The Routh array contains $n+1$ rows:

$$\begin{array}{c|cccccc} n & a_n & a_{n-2} & a_{n-4} & a_{n-6} & \cdots & 0 \\ n-1 & a_{n-1} & a_{n-3} & a_{n-5} & a_{n-7} & \cdots & 0 \\ n-2 & b_{n-1} & b_{n-2} & b_{n-3} & b_{n-4} & \cdots & 0 \\ n-2 & c_{n-1} & c_{n-2} & c_{n-3} & c_{n-4} & \cdots & 0 \\ \vdots & \vdots & \vdots & & & & \\ 3 & d_{n-1} & d_{n-2} & 0 & \cdots & & \\ 2 & e_{n-1} & e_{n-2} & 0 & \cdots & & \\ 1 & f_{n-1} & & & & \cdots & \\ 0 & g_{n-1} & & & & & \end{array} \tag{4.10}$$

The coefficients b in the third row are the results from cross multiplication the first two rows according to:

$$\begin{aligned} b_{n-1} &= \frac{a_{n-1}a_{n-2} - a_n a_{n-3}}{a_{n-1}} \\ b_{n-2} &= \frac{a_{n-1}a_{n-4} - a_n a_{n-5}}{a_{n-1}} \\ b_{n-3} &= \frac{a_{n-1}a_{n-6} - a_n a_{n-7}}{a_{n-1}} \\ &\vdots \end{aligned} \tag{4.11}$$

The calculation of these coefficients must be continued until all remaining elements become zero. The calculation of the coefficients c are performed accordingly from the two rows above as follows:

$$\begin{aligned} c_{n-1} &= \frac{b_{n-1}a_{n-3} - a_{n-1}b_{n-2}}{b_{n-1}} \\ c_{n-2} &= \frac{b_{n-1}a_{n-5} - a_{n-1}b_{n-3}}{b_{n-1}} \\ c_{n-3} &= \frac{b_{n-1}a_{n-7} - a_{n-1}b_{n-4}}{b_{n-1}} \\ &\vdots \end{aligned} \tag{4.12}$$

[1] Roots that lie in the right–half complex plane.

From these new rows further rows will be built in the same way. Finally, the last two rows are:

$$\begin{aligned} f_{n-1} &= \frac{e_{n-1}d_{n-2} - d_{n-1}e_{n-2}}{e_{n-1}} \\ g_{n-1} &= e_{n-2} \end{aligned} \tag{4.13}$$

Now, the Routh criterion establishes that a polynomial $P(\lambda)$ is Hurwitzian, if and only if the following conditions are valid:

- All coefficients a_1 are positive.
- All coefficients $b_{n-1}, c_{n-1}, \cdots$ in the first column of the Routh array are positive.

An interesting property of the Routh array is that the number of roots with positive real parts is equal to the number of changes of sign of the values in the first column.

Some limitations of Routh–Hurwitz criterions are: (i) it gives only information about absolute stability of the system, i.e., the degree of stability (critical, asymptotic, exponential, etc) of a stable system cannot be obtained. (ii) The criterion can be applied only if the characteristic equation has constant coefficients and cannot be applied if they are not real or contain exponential terms as in the case of systems with dead time.

4.2 Phase Plane Analysis

Phase plane analysis is a graphical method for studying the *qualitative behaviour* of second–order systems (linear or not), which was introduced well before the turn of the century by mathematicians such as Henri Poincare. Its basic idea is to solve a second–order differential equation graphically, instead of seeking an analytical solution. Essentially, the method generates a family of system motion trajectories corresponding to various initial conditions on a two-dimensional plane and then examines the qualitative features of these trajectories. In that way, information concerning to stability and other motion patterns of the system can be obtained. Phase plane analysis has a number of important advantages. First, as a graphical method, it allows us to visualize what goes on in a system, even if it is nonlinear, starting from various initial conditions, it is frequently used to provide intuitive insights about nonlinear effects. Second, it is not restricted to small or smooth nonlinearities, but applies equally well to strong nonlinearities and to hard nonlinearities. Finally, some practical mechanical systems can indeed be adequately

approximated as second–order systems, and the phase plane method can be used easily for their analysis. Conversely, of course the fundamental disadvantage of the method is that it is restricted to systems which can be well approximated by a second-order dynamics, because the graphical study of higher-order systems is computationally and geometrically complex.

4.2.1 Key definitions

A second–order time invariant system can be represented by two scalar differential equations:

$$\dot{x}_1 = f_1(x_1, x_2) \tag{4.14a}$$
$$\dot{x}_2 = f_2(x_1, x_2) \tag{4.14b}$$

where x_1 and x_2 are the states of the system and, f_1 and f_2, are nonlinear functions of the states. Geometrically, the state space of this system is a plane having x_1 and x_2 as coordinates. This plane (x_1–x_2) is called the *phase plane*.
Let $\mathbf{x}(t) = (x_1(t), x_2(t))$ be the solution of (4.14) given a set of initial conditions $\mathbf{x}(0) = \mathbf{x}_0 = (x_{10}, x_{20})$. The locus in the plane (x_1–x_2) of $\mathbf{x}(t)$ for all $t \geq 0$ represents geometrically a curve that passes through the point $\mathbf{x}_0$. Such a curve is called a *trajectory* or *orbit*. A family of trajectories corresponding to various initial conditions is called the *phase portrait* of the system (See Figure 4.2(b)).
The right-hand side of the system in (4.14) expresses the tangent vector $\dot{\mathbf{x}}(t)$ to the curve.

$$\dot{\mathbf{x}} = \mathbf{f}(\mathbf{x}) \tag{4.15}$$

where $\dot{\mathbf{x}}(t) = (\dot{x_1}(t), \dot{x_2}(t))$ and $\mathbf{f}(\mathbf{x})$ is a *vector field* $(f_1(\mathbf{x}), f_2(\mathbf{x}))$ on the state plane, which means that to each point $\mathbf{x}$ in the plane, we assign a vector $\mathbf{f}(\mathbf{x})$ (See Figure 4.2(a)).

Singular points

A singular point or *equilibrium point* in the phase plane is defined as a point where the system states can stay forever, this implies that $\dot{x} = 0$, that is:

$$f_1(x_1, x_2) = f_2(x_1, x_2) = 0 \tag{4.16}$$

Singular points are very important features in the phase plane. Examination of the singular points can reveal a great deal of information about the properties of a system. In fact, the stability of linear systems is uniquely characterized by the nature of their singular points. There is usually only one singular point (or a

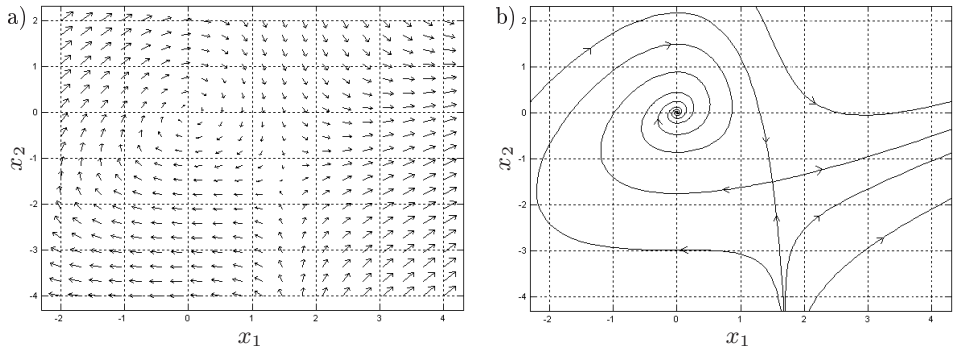

Figure 4.2: Examples of (a) vector field and (b) phase portrait

continuous set of singular points) for linear systems. However, a nonlinear system often has more than one isolated singular point, additionally there may be more complex features, such as limit cycles and chaos. The stability of an equilibrium point is related to the behaviour of the trajectories in its vicinity. For instance, we can always define a domain $\mathcal{D}$ containing an equilibrium point. If we can find trajectories starting within this domain which remain arbitrary close to the point, this equilibrium point is said to be stable; if any trajectory starting in the domain eventually converge towards the point, the equilibrium point is said to be asymptotically stable. These definitions will be formalized later.

4.2.2 Phase portraits of linear systems

To illustrate the above concepts, let us consider a second–order linear system with the characteristic equation in (4.2). Different behaviours can be observed in accord with the root locus as follows.

Stable or unstable node. When λ_1 and λ_2 are both real and have the same sign, the origin corresponds to a node. If the roots are negative, the origin is called a stable node because both $\dot{x}(t)$ and $x(t)$ converge to zero exponentially as $t \to \infty$. If both roots are positive, the point is called an unstable node, because both $\dot{x}(t)$ and $x(t)$ diverge from zero exponentially. Since the eigenvalues are real, there is no oscillation in the trajectories. See Figure 4.3(a)–(b).

Saddle point. When λ_1 and λ_2 are both real and have opposite signs, the origin corresponds to a saddle point. Because of the unstable root (the positive one), almost all of the system trajectories diverge to infinity. There exist a

converging straight line corresponds to initial conditions which make equal zero the coefficient k_i associated with the negative root. See Figure 4.3(f).

Stable or unstable focus. When λ_1 and λ_2 are complex conjugate with non-zero real parts, the origin corresponds to a focus. A stable focus occurs when the real part of the roots is negative, which implies that $\dot{x}(t)$ and $x(t)$ converge to zero as $t \to \infty$. The trajectories encircle the origin one or more times before converging to it, unlike the situation for a stable node. If the real part of the roots is positive, then $\dot{x}(t)$ and $x(t)$ both diverge to infinity, and the point is called an unstable focus. See Figure 4.3(c)–(d).

Center point. When λ_1 and λ_2 are are complex conjugates with real parts equal to zero, the origin corresponds to a center point. The name comes from the fact that all trajectories are ellipses and the origin is the center of these ellipses. See Figure 4.3(e).

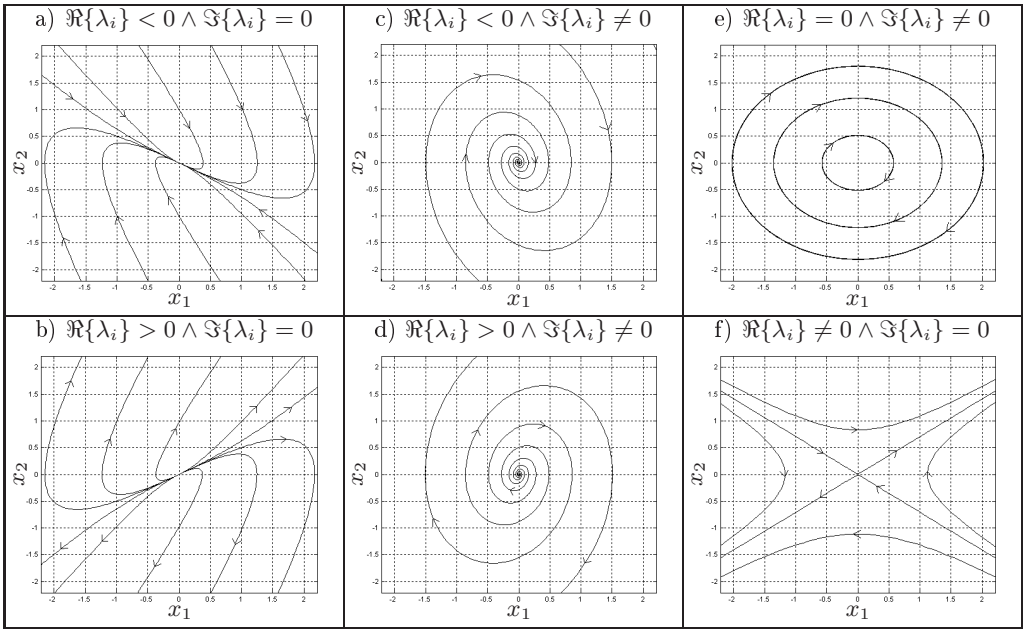

Figure 4.3: Phase portraits of linear systems

4.2.3 Nonlinear systems

The dynamic of nonlinear systems are much richer than the dynamics of linear systems, there are essentially nonlinear phenomena that can take place only in

presence of nonlinearities and cannot be described by a linear model. Thus, let us discuss some common nonlinear system phenomena in order to provide a useful background for our study in the rest of this document. A wider and more complete discussion on these and others nonlinear behaviour can be reviewed in [Slotine and Li, 1991].

Multiple equilibrium points. Nonlinear systems frequently have more that one isolated equilibrium point. The state may converge to one of several steady–state points, depending on the initial state of the system. See Figure 4.4(a).

Limit cycles. Nonlinear systems can display oscillations of fixed amplitude and fixed period without external excitation. These oscillations are called limit cycles, or self–excited oscillations. Of course, sustained oscillations can also be found in linear systems (center point) or in the response to sinusoidal inputs. However, limit cycles in nonlinear systems are different. First, the amplitude of the self–sustained excitation is independent of the initial condition, as seen in Figure 4.4(b). Second, the of self-sustained oscillations in linear systems are very sensitive to changes in system parameters, while limit cycles are not easily affected by parameter changes. Limit cycles represent an important phenomenon in nonlinear systems. They can be found in many areas of engineering and nature. Aircraft wing fluttering, a limit cycle caused by the interaction of aerodynamic forces and structural vibrations, is frequently encountered and is sometimes dangerous. Limit cycles can be undesirable in some cases, but desirable in other cases.

Bifurcations. As the parameters of nonlinear dynamic systems are changed, the stability of the equilibrium point can change (as it does in linear systems) and also the number of equilibrium points. Values of these parameters at which the qualitative nature of the system's motion changes are known as critical or bifurcation values. The phenomenon of bifurcation occurs when quantitative change of parameters leading to qualitative change of system properties. A very interesting case of bifurcation involves the emergence of limit cycles as parameters are changed. In this case, a pair of complex conjugate eigenvalues cross from the left–half plane into the right–half plane, and the response of the unstable system diverges to a limit cycle. This type of bifurcation is called a *Hopf bifurcation*.

Chaos. For stable linear systems, small differences in initial conditions can only cause small differences in output. In nonlinear systems however, the system output is extremely sensitive to initial conditions. The essential feature of

chaos is the unpredictability of the system output. Chaos must be distinguished from random motion. In random motion, the system model or input contain uncertainty and, as a result, the time variation of the output cannot be predicted exactly (only statistical measures are available). In chaotic motion, on the other hand, the involved problem is deterministic, and there is little uncertainty in system model, input, or initial conditions. Some mechanical and electrical systems known to exhibit chaotic vibrations include buckled elastic structures, mechanical systems with play or backlash, systems with aeroelastic dynamics, wheelrail dynamics in railway systems and feedback control devices.

Other behaviors. Other interesting types of behavior, such as jump resonance, subharmonic generation, asynchronous quenching, and frequency–amplitude dependence of free vibrations, can also occur and become important in some particular system.

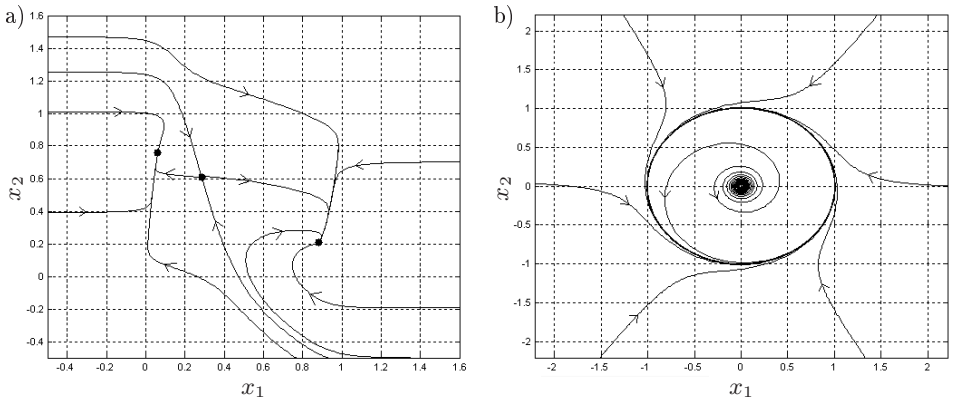

Figure 4.4: Examples of (a) multiple equilibrium points (tunnel–diodo circuit) and (b) Stable limit cycle for the system: $\dot{x}_1 = x_1(0.1+x_1^2+x_2^2-(x_1^2+x_2^2)^2)-x_2$; $\dot{x}_2 = x_2(0.1+x_1^2+x_2^2-(x_1^2+x_2^2)^2)+x_1$

4.3 Existence of periodic orbits

In this section, we present three simple classical theorems to predict the existence of limit cycles for second–order systems. Since all of the proofs are mathematically complex (actually, a family of such proofs led to the development of algebraic topology) they were omitted because fall outside the scope of this thesis. Nevertheless, the demonstrations and some interesting application examples can be

studied in [Khalil, 2000] and [Vidyasagar, 1992].

The first theorem reveals a simple relationship between the existence of a limit cycle and the number of singular points that it encloses. This theorem is sometimes called the *index theorem*. In this statement, N represents the number of nodes, centers, and foci enclosed by a limit cycle, and S the number of enclosed saddle points.

Theorem 4.1 (Poincare)**.** *If a limit cycle exists in the second–order autonomous system* (4.14)*, then* $N = S + 1$.

The second theorem is concerned with the asymptotic properties of the trajectories of second–order systems. It establish that bounded trajectories in the plane shall have to approach periodic orbits or equilibrium points as time tends to infinity.

Theorem 4.2 (Poincare–Bendixson)**.** *If a trajectory of the second–order autonomous system* (4.14) *remains in a finite region* $\mathcal{M}$*, then one of the following is true:*

- *The trajectory goes to an equilibrium point.*
- *The trajectory tends to an asymptotically stable limit cycle.*
- *The trajectory is itself a limit cycle.*

The third theorem provides a sufficient condition for the non–existence of limit cycles. This theorem is sometimes called the *Bendixson Criterion*.

Theorem 4.3 (Bendixson)**.** *For the nonlinear system* (4.14)*, no limit cycle can exist in a region* $\mathcal{M}$ *of the phase plane in which* $\partial f_1/\partial x_1 + \partial f_2/\partial x_2$ *does not vanish and does not change sign.*

The above theorems are easy to understand and apply. Even if they represent very powerful results, have no equivalent in higher–order systems where exotic asymptotic behaviors (other than equilibrium points and limit cycles) can occur.

4.4 Lyapunov stability

In 1892, the Russian mathematician Alexander Mikhailovitch Lyapunov introduced his famous stability theory for nonlinear and linear systems. A complete English translation of Lyapunov's doctoral dissertation was published in 1992 for its centenary [Lyapunov, 1992].
Basic Lyapunov theory comprises two methods, the indirect and the direct method. The indirect method, or l*inearization method*, states that the stability properties of a nonlinear system in the close vicinity of an equilibrium point are essentially the same as those of its linearized approximation. The direct method is a powerful tool for nonlinear system analysis, and therefore the so–called *Lyapunov analysis* often actually refers to the direct method. The direct method is a generalization of the energy concepts associated with a mechanical system: the motion of a mechanical system is stable if its total mechanical energy decreases all the time. Lyapunov stability theorems give sufficient conditions for stability, asymptotic stability and so on, but they do not say whether the given condition are also necessary. The power of this method comes from its generality; it is applicable to all kinds of control systems, be they time–varying or time–invariant, finite dimensional or infinite dimensional. Conversely, the limitation of the method lies in the fact that it is often difficult to find a Lyapunov function for a given system as it shall be shown.

Seeking for completeness, some definitions of stability which are necessary for later theorems are included here. For all definitions and theorems from now on, let us consider a time–invariant system, linear o not, as the one shown in formula (4.15) such that $\mathbf{f}(0) = 0$, i.e. $\mathbf{x} = 0$ (the origin) is an equilibrium state.

Definition 4.3. The equilibrium state $\mathbf{x} = 0$ is (locally) *stable in the sense of lyapunov* if, for every $\varepsilon > 0$ there exist some $\delta > 0$ (depending on ε) such that, if $\|\mathbf{x}(0)\| < \delta$, then $\|\mathbf{x}(t)\| < \varepsilon$ for all $t > t_0$.

Definition 4.4. The equilibrium state $\mathbf{x} = 0$ is *asymptotically stable in the sense of Lyapunov* if it is (locally) stable in the sense of Lyapunov and if, there exist some $\delta > 0$ such that, if $\|\mathbf{x}(0)\| < \delta$, then $\mathbf{x}(t) \to 0$ as $t \to \infty$.

Thus, the asymptotic stability is more restrictive than the definition 4.3 as definition 4.4 imposes that the trajectories converge to the equilibrium state. Note that for a mechanical system, asymptotic stability implies some damping, unlike

Lyapunov stability. Besides, for a linear time–invariant system asymptotic stability is always global, while nonlinear systems exhibit more complicated behaviour.

Definition 4.5. The equilibrium state $\mathbf{x} = 0$ is (locally) *exponentially stable in the sense of Lyapunov* if, there exist positive constants α, β and δ such that, if $\|\mathbf{x}(0)\| < \delta$, then $\|\mathbf{x}(t)\| \leq \alpha\|\mathbf{x}(0)\|e^{-\beta t}$ for all $t > t_0$.

State which are not stable in the sense of Lyapunov are *unstable*. Besides, exponentially stability implies asymptotically stability, but the opposite is not true. Stability, as it was defined before, is a local property since ε and δ can be chosen arbitrarily small. But if stability is independent of the size of the initial perturbation $\mathbf{x}(0)$, i.e., if $\mathbf{x}(0)$ can be chosen on a domain $\mathcal{D}$, such that $\mathcal{D} \in \mathbb{R}^n$, the stability is said to be *global*.

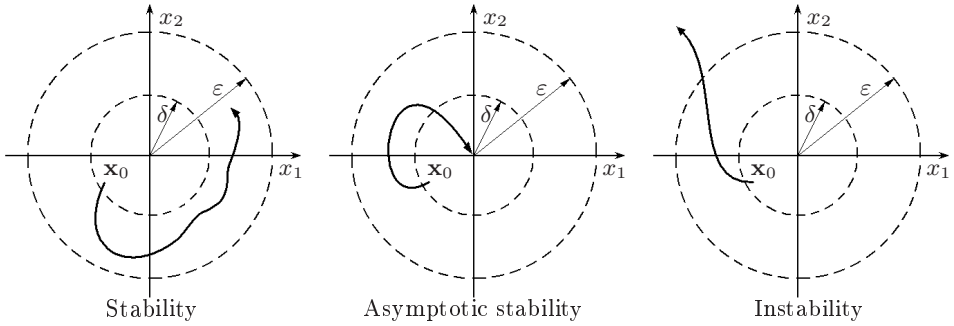

Figure 4.5: Concepts of stability

4.4.1 Lyapunov's direct method

The basic philosophy of Lyapunov's direct method is the mathematical extension of a fundamental physical observation: if the total energy of a mechanical (or electrical) system is continuously dissipated, then the system, whether linear or nonlinear, must eventually settle down to an equilibrium point.

Definition 4.6. A scalar continuous function $V(\mathbf{x}) : \mathbb{R}^n \to \mathbb{R}$ is said to be *locally positive definite* if:

$$V(0) = 0 \quad \text{and} \quad V(\mathbf{x}) > 0, \quad \forall \mathbf{x} \in \mathcal{D} - \{0\} \tag{4.17}$$

where $\mathcal{D}$ is a certain domain containing the origin. If the above property holds over the whole state space, i.e. $\mathcal{D} \in \mathbb{R}^n$, then $V(\mathbf{x})$ is said to be *globally positive definite.*

Other few related concepts can be defined similarly, as in local as in global sense. A function $V(\mathbf{x})$ is negative definite if $-V(\mathbf{x})$ is positive definite; $V(\mathbf{x})$ is positive semi–definite if $V(0) = 0$ and $V(\mathbf{x}) \geq 0$ for $\mathbf{x} \neq 0$; $V(\mathbf{x})$ is negative semi–definite if $-V(\mathbf{x})$ is positive semi–definite. The prefix "semi" is used to reflect the possibility of V being equal to zero for $\mathbf{x} \neq 0$.

Definition 4.7. If, in a certain domain $\mathcal{D}$ containing the origin, the function $V(\mathbf{x}) : \mathbb{R}^n \to \mathbb{R}$ is positive definite and has continuous partial derivatives, and if its time derivative along any state trajectory of system (4.15) is negative semi–definite, i.e.,

$$\dot{V}(\mathbf{x}) = \frac{dV(\mathbf{x})}{dt} = \frac{\partial V}{\partial \mathbf{x}}\dot{\mathbf{x}} = \frac{\partial V}{\partial \mathbf{x}}\mathbf{f}(\mathbf{x}) \leq 0 \tag{4.18}$$

then $V(\mathbf{x})$ is said to be a *Lyapunov function* for the system (4.15).

A complete description of the geometrical meaning of positive definite functions and the graphical interpretation of the above concepts, including several examples, can be studied in [Slotine and Li, 1991] and [Preumont, 1997].

In using the direct method to analyze the stability of a nonlinear system, the idea is to construct a scalar energy–like function (a Lyapunov function) for the system, and to see whether it decreases. The relations between Lyapunov functions and the stability of systems are made precise in a number of theorems in Lyapunov's direct method.

Theorem 4.4 (Local Stability)**.** *Consider the system in* (4.15)*, the equilibrium point* $\mathbf{x} = 0$ *is stable, if in a certain domain* $\mathcal{D}$ *containing the origin, there exists a scalar function* $V(\mathbf{x}) : \mathbb{R}^n \to \mathbb{R}$ *with continuous first partial derivatives such that:*

- $V(\mathbf{x})$ *is positive definite (locally in* $\mathcal{D}$*)*
- $\dot{V}(\mathbf{x})$ *is negative semi–definite (locally in* $\mathcal{D}$*)*

If, actually, the derivative $\dot{V}(\mathbf{x})$ *is locally negative definite in* $\mathcal{D}$*, then the stability is asymptotic.*

In applying the above theorem for analysis of a nonlinear system, one goes through the two steps: choosing a positive definite function, and then determining its derivative along the path of the nonlinear systems.

In order to assert global asymptotic stability of a system, one might naturally expect that the domain $\mathcal{D}$ in the above local theorem has to be expanded to be the whole state space. Nevertheless, an additional condition on the Lyapunov function has to be satisfied: $V(\mathbf{x})$ must be *radially unbounded*, i.e., $\mathbf{x}$ can tend to infinity in any direction. The reason of that is to assure that the contour curves of $V(\mathbf{x}) = v_\alpha$ correspond to closed curves (See Figure 4.6). If the contour curves are not closed, the trajectories might drift away from the equilibrium point. Now, the following powerful result, known as Barbashin–Krasovskii theorem, can be established.

Theorem 4.5 (Global Stability)**.** *Consider the system in* (4.15)*, the equilibrium at the origin is globally asymptotically stable, if there exists a scalar function* $V(\mathbf{x}) : \mathbb{R}^n \to \mathbb{R}$ *with continuous first order derivatives such that:*

- $V(\mathbf{x})$ *is positive definite*
- $\dot{V}(\mathbf{x})$ *is negative definite*
- $V(\mathbf{x}) \to \infty$ *as* $\|\mathbf{x}\| \to \infty$

The above theorems provide *sufficient conditions* (but not necessary) to determine the stability of a system; the fact that no Lyapunov function can be found to satisfy theorems 4.4 and 4.5 does not mean that the system is not stable; just one cannot draw any conclusions on the stability or instability of the system. Actually, this is the main weakness of the Lyapunov's method, as there is no general procedure for constructing Lyapunov function for a given system. However, there are some methods for particular systems which provided Lyapunov function candidates to be tested. Most of them require solving partial differential equations or trial and error procedures as the Variable Gradient method and Krasovskii's method [Krasovskii, 1959]. Further general information and examples on this subject can be found in the literature e.g. [Khalil, 2000] and [Slotine and Li, 1991].

4.4.2 Invariant Set Theorems

Lyapunov's stability theorems studied above are often difficult to apply to establish asymptotic stability, as it often happens that $\dot{V}$ is only negative semi–definite.

Even in this situation, with the help of the invariant set theorems, it is still possible to draw conclusions on asymptotic stability. The central concept in these theorems is the generalization of the idea of equilibrium point to the invariant set.

Definition 4.8. A set $\mathcal{M}$ is an *invariant set* for the dynamic system in (4.15) if every trajectory $x(t)$ which starts from a point in $\mathcal{M}$ remains in $\mathcal{M}$ for all time (future and past), i.e.,

$$x(0) \in \mathcal{M} \Rightarrow x(t) \in \mathcal{M}, \ \forall t \in \mathbb{R} \tag{4.19}$$

Definition 4.9. A set $\mathcal{M}$ is an *positively invariant set* for the dynamic system in (4.15) if every trajectory $x(t)$ which starts from a point in $\mathcal{M}$ remains in $\mathcal{M}$ for all future time, i.e.,

$$x(0) \in \mathcal{M} \Rightarrow x(t) \in \mathcal{M}, \ \forall t \geq 0 \tag{4.20}$$

Thus, any equilibrium point is an invariant set, but the domain of attraction of an equilibrium point is also an invariant set.

Theorem 4.6 (Local invariant set theorem)**.** *Consider an autonomous system of the form* (4.15)*, with* $\mathbf{f}$ *continuous and let* $V(\mathbf{x}) : \mathbb{R}^n \to \mathbb{R}$ *be a scalar function with continuous first partial derivatives. Assume that*

- *for some* $l > 0$*, the set* Ω_l *defined by* $V(\mathbf{x}) \leq l$ *is bounded.*
- $\dot{V}(\mathbf{x}) \leq 0$ *for all* $\mathbf{x}$ *in* Ω_l*.*

Let $\mathcal{R}$ *be the set of all points within* Ω_l *where* $\dot{V}(\mathbf{x}) = 0$ *and* $\mathcal{M}$ *be the largest invariant set in* $\mathcal{R}$*. Then, every solution* $\mathbf{x}(t)$ *originating in* Ω_l *tends to* $\mathcal{M}$ *as* $t \to \infty$*.*

In the above theorem, "largest" is understood in the sense of set theory, so $\mathcal{M}$ is the union of all invariant sets within $\mathcal{R}$. The geometrical meaning of the theorem is illustrated in Figure 4.6, where a trajectory starting from within the bounded region Ω_l, is seen to converge to the largest invariant set $\mathcal{M}$.

The local invariant set theorem can be simply extended to a global result, by requiring the radial unboundedness of the scalar function V rather than the existence of a bounded Ω_l.

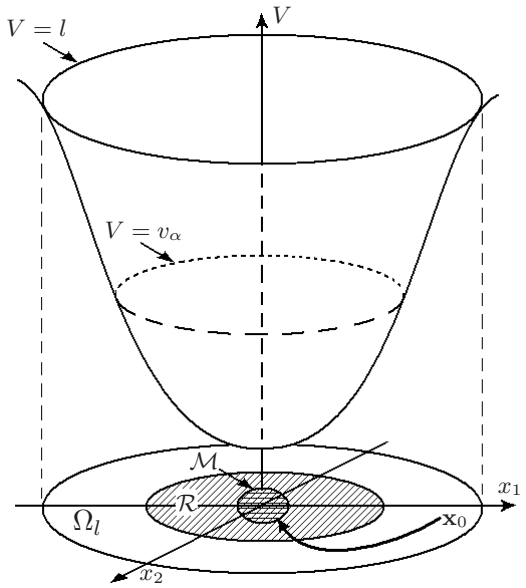

Figure 4.6: Convergence to the largest invariant set $\mathcal{M}$. Adapted from [Slotine and Li, 1991].

Theorem 4.7 (Global invariant set theorem)**.** *Consider an autonomous system of the form* (4.15)*, with* $\mathbf{f}$ *continuous and let* $V(\mathbf{x}) : \mathbb{R}^n \to \mathbb{R}$ *be a scalar function with continuous first partial derivatives. Assume that*

- $V(\mathbf{x}) \to \infty$ *as* $\|\mathbf{x}\| \to \infty$..
- $\dot{V}(\mathbf{x}) \leq 0$ *for all* $\mathbf{x}$ *in* $\mathbb{R}^n$.

Let $\mathcal{R}$ *be the set of all points where* $\dot{V}(\mathbf{x}) = 0$ *and* $\mathcal{M}$ *be the largest invariant set in* $\mathcal{R}$*. Then, all solutions converge to* $\mathcal{M}$ *as* $t \to \infty$*.*

No only the foregoing theorems relax the negative definiteness requirement of Lyapunov's theorem, but also extends it in two different directions: (i) the above theorems can be used when the system has an equilibrium set (e.g.a limit cycle) rather than an isolated equilibrium point; (ii) the function $V(x)$ does no have to be positive definite although often still referred to as a Lyapunov function.

When our interest is to showing that $\mathbf{x}(0) \to 0$ as $t \to \infty$, we need to establish the the largest invariant set in $\mathcal{R}$ is the origin. This is doing by showing that no solution can be stay in $\mathcal{R}$, other than the trivial solution $\mathbf{x}(t) \equiv 0$. Specializing

theorem 4.6. to this case and taking $V(\mathbf{x})$ positive definite, we obtain the following theorem which is attributed to LaSalle.

Theorem 4.8 (LaSalle)**.** *Let $V(\mathbf{x}) : \mathbb{R}^n \to \mathbb{R}$ be a scalar function with continuous first partial derivatives such that on $\Omega_l = \{\mathbf{x} \in \mathbb{R}^n : V(\mathbf{x}) \leq l\}$ we have $\dot{V}(\mathbf{x}) \leq 0$. Define $\mathcal{R} = \{\mathbf{x} \in \mathbb{R}^n : \dot{V}(\mathbf{x}) = 0\}$. Then, if $\mathcal{R}$ contains no other trajectories other than the trivial solution $\mathbf{x}(t) \equiv 0$, then the origin is asymptotically stable.*

The proofs of the above theorems are omitted here due to they involve a number of concepts in topology and real analysis which are outside of the topics of this thesis, however if the reader is interested, they are addressed (or at least sketched) in [Khalil, 2000] and [Vidyasagar, 1992].

Chapter 5

Piecewise Smooth Dynamical Systems

Contents

The aim of this chapter is to present an overview of the qualitative theory of piecewise smooth dynamical systems. Rather than covering all the issues, we will focus on basic definitions and fundamental concepts that, according to us, are needed through this thesis. Qualitative theory of dynamical systems comprises methods for analyzing differential equations and iterated mappings. Specifically, nonlinear dynamics is concerned with the study of the stability of fixed points and

periodic orbits, stable and unstable manifolds. Most of the material presented in this chapter is inspired from [Osorio, 2007] and [di Bernardo et al., 2007] and some references therein.

5.1 Smooth dynamical systems

A *smooth dynamical systems* or simply a dynamical system is a rule for the time evolution of a set of possible states. The time t takes values in an index set $\mathcal{T}$ which we usually consider to be either discrete (the set of integers $\mathbb{Z}$), or continuous (the set of real numbers $\mathbb{R}$). The possible states belonging to state space X, is a discrete or continuous collection of coordinates that gives a complete description of the system. Given the current state of the system $x_0 \in X$, the evolution rule or flow φ, predicts the state or vector $x(t)$ as:

$$\varphi : X \times \mathcal{T} \to X \tag{5.1}$$

assuming $x(t) \triangleq \varphi(x_0, t)$, with $x(0) = x_0$.
We say that (5.1), together with X and $\mathcal{T}$, defines a dynamical system if following conditions are satisfied:

$$\varphi(x, 0) = x, \qquad \text{for all } x \in X, \qquad \text{(Identity)} \tag{5.2a}$$

$$\varphi(x, t+s) = \varphi(\varphi(x,t), s), \quad \text{for all } x \in X, \text{and} t, s \in \mathcal{T}. \quad \text{(Group)} \tag{5.2b}$$

The identity condition in (5.2a) basically implies that the state does not change spontaneously, and the group property in (5.2b) means that the evolution operator of the system does not change in time (i.e. The system is autonomous).

5.1.1 Discrete maps and iterated maps

A *discrete map* or simply a *map*, is an evolution rule defined in discrete time and in a continuous state space. A map $\pi : \mathbb{R}^n \times \mathbb{Z} \to \mathbb{R}^n$ defines a dynamical system where $t \in \mathbb{Z}$.
The time evolution can be defined in an iterative form as:

$$P : \mathbb{R}^n \to \mathbb{R}^n, \text{ where } x \mapsto P(x) \tag{5.3}$$

with $x \in \mathbb{R}^n$. The iterative operator in (5.3) is often written as $x_{n+1} = P(x_n)$ with $n \in \mathbb{Z}$. Notice that given an initial condition $x(0) = x_0$, a generic element at time $t = n$ can be obtained from:

$$x(n) = P^{(n)}(x_0) \tag{5.4}$$

where $P(n) \triangleq P \circ P \circ \cdots \circ P$, n–times.

Example 5.1. The *logistic map* is an instance of how a very simple nonlinear system can present very complicated behavior. It is a discrete model used to describe demographic evolution, and mathematically is written:

$$x_{n+1} = \mu x_n(1 - x_n), \quad \mu \in [0, 1]. \tag{5.5}$$

where μ is the growth constant of the population (For further details see [May, 1976]).

■

5.1.2 Continuous flows and ODEs

A dynamical system can also be defined by an *initial value problem*, through a Ordinary Differential Equation (ODE) of the type:

$$\dot{x} = F(x) \tag{5.6}$$

In (5.1) $X \equiv \mathbb{R}^n$, $\mathcal{T} \equiv \mathbb{R}$ and the flow is defined by $\phi \equiv \varphi$. The state of the system will be given by:

$$x(t) = \phi(x_0, t) \tag{5.7}$$

where $\phi : \mathbb{R}^n \times \mathbb{R} \to \mathbb{R}^n$ and $x(0) = x_0$. The evolution rule ϕ satisfies (5.6) in the sense that:

$$\frac{d}{dt}(\phi(x, t))\bigg|_{t=\gamma} = F(\phi(x, \gamma)) \tag{5.8}$$

Example 5.2. A periodically forced, damped harmonic oscillator satisfies the second order differential equation:

$$\ddot{q} + 2\zeta\dot{q} + \kappa q = a\cos\omega t,$$

where ζ and κ are damping and spring constants respectively, and ω is the angular velocity of the periodic forcing. We can define the state variables $x_1 = q$, $x_2 = \dot{q}$ and $x_3 = \omega t$ such that (5.2) can be written as a set of ordinary differential equations:

$$\begin{aligned} \dot{x}_1 &= x_2, \\ \dot{x}_2 &= \kappa x_1 - 2\zeta x_2 + a\cos x_3, \\ \dot{x}_3 &= \omega. \end{aligned}$$

■

5.2 Qualitative dynamics

Given a generic dynamical system of the form (5.1), consider an invariant set[1] Λ of the dynamical system in X (i.e. $\Lambda \subset X$).

Definition 5.1. A closed and bounded invariant set is called an *attractor* if:

- for any sufficiently small neighborhood $U \subset X$ of Λ, there exists a neighborhood W of Λ such that $\phi(x,t) \in U$ for all $x \in W$ and all $t > 0$, and
- for all $x \in U$, $\phi(x,t) \to \Lambda$ as $t \to \infty$

A dynamical system may have many competing attractors, with their relative importance being indicated by the set of initial conditions that they attract, that is, their domain of attraction.

Definition 5.2. The *domain of attraction* of an invariant set Λ (also known as the *basin of attraction* or simply the *basin*), is the maximal set of initial conditions x for which $\phi(x,t) \to \Lambda$ as $t \to \infty$.

The qualitative description of a dynamical system is given by the description of the invariant sets that compose its phase portrait. The more common types of invariant sets are:

Equilibria. The simplest form of invariant set is an equilibrium solution x^* which satisfies $\phi(x^*,t) = x^*$ for all t.

Periodic orbits. The most complex kind of invariant set is a periodic orbit; it forms closed curves in phase space and satisfies, for an initial condition x_p, that $\varphi(x_p,T) = x_p$ where T indicates the period (The smallest time $T > 0$ for which the condition held). A periodic orbit that is isolated is termed a limit cycle.

Homoclinic and heteroclinic orbits . Another important class of invariant sets are connecting orbits which tend to other invariant sets as time goes asymptotically to $+\infty$ and to $-\infty$. Consider for example orbits which connect equilibria. A *homoclinic* orbit is a trajectory $x(t)$ that connects an equilibrium x^* to itself; $x(t) \to x^*$ as $t \to \pm\infty$. A *heteroclinic* orbit connects two different equilibria x_1^* and x_2^* ; $x(t) \to x_1^*$ as $t \to -\infty$ and $x(t) \to x_2^*$

[1] See definition of invariant set in §4.4.2

as $t \to +\infty$. Homoclinic and heteroclinic orbits play an important role in separating the basins of attraction of other invariant sets.

Other invariant sets. It is quite possible for dynamical systems to contain certain simple geometric subsets of phase space where trajectories must remain for all time once they enter. The dynamics on this invariant sets could contain equilibria, periodic orbits and other attractors. Similarly, flows can contain invariant tori, invariant spheres, cylinders etc. Invariant sets that are everywhere locally smoothly described by an m–dimensional set of coordinates are called *invariant manifolds*.

5.3 Stability and structural stability on smooth systems

The stability of an orbit of a dynamical system characterizes whether nearby (i.e., perturbed) orbits will remain in a neighborhood of that orbit or be repelled away from it. *Asymptotic stability* additionally characterizes attraction of nearby orbits to this orbit in the long–time limit. The distinct concept of *structural stability* concerns qualitative changes in the family of all solutions due to perturbations to the functions defining the dynamical system.

5.3.1 Stability on smooth systems

An important notion of stability in autonomous dynamical systems in that of either *Lyapunov* or *asymptotic stability* of an invariant set (See §4.4). In general, the former means stability in the weak sense that trajectories starting nearby to the invariant set remain close to it for all time, whereas the latter is more restrictive. Both refer to stability of invariant sets with respect to perturbations of initial conditions, at fixed parameter values.

Limit cycles and Poincaré maps. One of the main building blocks of the dynamics in a set of ODEs is the topology analysis of its periodic solutions (or limit cycles). Limit cycles provide a natural way to transform between flows and maps. Consider a limit cycle solution $x(t) = p(t)$ of period $T > 0$, that is $p(t + T) = p(t)$. To study the dynamics near such a cycle, we can choose a Poincaré section, which is an $(n-1)$–dimensional surface Π that contains a point $x_p = p(t_p)$ on the limit cycle and which is transverse to the flow at x_p. We can use the flow ϕ to define a map $\mathcal{P}$ from Π to Π, called the *Poincaré map*, which is

defined for x sufficiently close to x_p as:

$$\mathcal{P}(x) = \phi(x, \gamma(x)) \tag{5.9}$$

where $\gamma(x)$ is defined implicitly as the time closest to T for which $\phi(x, \gamma(x)) \in \Pi$. We can study the stability of the periodic solution by studying the spectrum of the Jacobian matrix of the Poincaré map at x_p (*i.e.* $eig\{\mathcal{P}_x(x_p)\}$).

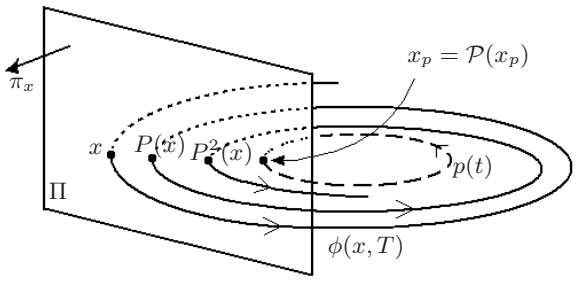

Figure 5.1: Poincaré map definition.

In general, a consequence of using Poincaré maps rather than flows in the stability analysis of invariant sets is that they reduce their dimension of the sets we need to consider. Thus, limit cycles of flows correspond to isolated fixed points of Poincaré maps; invariant tori correspond to closed curves of the map; and a chaotic invariant sets decrease their fractal dimension by one.

5.3.2 Structural stability on smooth systems

Structurally stable systems are ones for which all *nearby* systems have qualitatively *equivalent* dynamics. Thus we need a precise notion of nearby and also of equivalence.
Nearby refers to any possible perturbation of the system itself (the function $F(x)$ for ODE), including for example variation of the system's parameters. We call two systems *equivalent* if their phase spaces have the same dimension, the same number and type of invariant sets, in the same general position with respect to each other. To achieve such a definition, we use mathematical topology.

Definition 5.3. We say that two phase portraits are *topologically equivalent* if there is a smooth transformation that stretches, twists, rotates, but not folds one

phase portrait into the other. Such transformations are called homeomorphisms, which are continuous functions defined over the entire phase space whose inverses are also continuous.

Two dynamical systems defined by operators $\varphi, \psi : X \times \mathcal{T} \to X$ are *topologically equivalent* if there is a homeomorphism h that maps the orbits of the first system onto orbits of the second one, preserving the direction of time.

Definition 5.4 (Hyperbolicity in Flows)**.** Consider an equilibrium x^* of a flow ϕ defined by a system of ODEs $\dot{x} = F(x)$. We refer to the eigenvalues of an equilibrium x^*, to mean the eigenvalues of the associated Jacobian matrix $F_x(x^*)$. An equilibrium is said to be *hyperbolic* if none of its eigenvalues lie on the imaginary axis.

Definition 5.5 (Hyperbolicity in Maps)**.** Consider a fixed point x^* of a map π defined by the iterated equation $x_{n+1} = P(x_n)$. We refer to the multipliers μ_i of a fixed point x^*, to mean the eigenvalues of the associated Jacobian matrix $P_x(x^*)$. A fixed point is said to be hyperbolic if none of the multipliers lie on the unit circle.

One of the key applications of topological equivalence is to show that under *hyperbolicity* condition, linearization of the dynamical systems about the neighborhood of an invariant set are locally topologically equivalent. In addition, it can be proved that the flow local to any two hyperbolic equilibria of n–dimensional systems which have the same number of eigenvalues with negative real part are topologically equivalent to each other.

5.4 Piecewise smooth dynamical systems

A *piecewise smooth (PWS) dynamical system* is a set of smooth dynamical systems (*i.e.* with elements of the form $\mathcal{D}_i = \{X_i, \mathcal{T}_i, \varphi_i(x,t)\}$[2]); plus a set of rules for concatenation in time for some dynamical system $\mathcal{D}_i$ to another $\mathcal{D}_j$, such that identity and group conditions are satisfied. In general the set of rules for concatenation can be expressed through zero level sets of scalar functions, say $\sigma_{ij} : \mathbb{R}^n \to \mathbb{R}$, to commute at time γ from $\mathcal{D}_i$ to $\mathcal{D}_j$; such that the final state $x_\sigma \triangleq x(\gamma) = \varphi_i(x_0, \gamma)$ becomes an initial state as $x(\gamma) \equiv \varphi_j(x_\sigma, 0)$. This is equivalent to say that the state x at commutation time γ can be expressed as function

[2]See definition of smooth dynamical system in §5.1

of both evolution operators.

In [di Bernardo et al., 2007] and [Osorio, 2007] an extensive study of PWS dynamical system can be found. Here, we present some fundamental definitions and properties which will be useful for later analysis in this thesis.

5.4.1 Piecewise smooth maps

A piecewise–smooth map is described by a finite set of smooth maps as:

$$x \mapsto P_i(x, \mu), \text{ for } x \in S_i \tag{5.10}$$

where $\cup_i S_i = D \subset \mathbb{R}^n$ and each S_i has a non–empty interior. The intersection Σ_{ij} between the closure (set plus its boundary) of the sets S_i and S_j (that is, $\Sigma_{ij} \triangleq S_i \cap S_j$) is either an $\mathbb{R}^{(n-1)}$–dimensional manifold included in the boundaries ∂S_j and ∂S_i, or is the empty set. Each function P_i is smooth in both the state x and parameter μ for any open subset U of S_i.

5.4.2 Piecewise smooth flows (ODEs)

A piecewise–smooth flow is given by a finite set of ODEs as:

$$\dot{x} = F_i(x, \mu), \text{ for } x \in S_i \tag{5.11}$$

where $\cup_i S_i = D \subset \mathbb{R}^n$ and each S_i has a non–empty interior. The intersection $\Sigma_{ij} \triangleq S_i \cap S_j$ is either an $\mathbb{R}^{(n-1)}$–dimensional manifold included in the boundaries ∂S_j and ∂S_i, or is the empty set. Each vector field F_i is smooth in both the state x and parameter μ and defines a smooth flow $\phi_i(x, t)$ within any open set $U \in S_i$. In particular, each flow ϕ_i is well–defined on both sides of the boundary S_j.

Example 5.3. The bilinear oscillator, can be written as the first–order system by setting $x_1 = q$, $x_2 = \dot{q}$ and $x_3 = t$ so that

$$\begin{aligned} \dot{x}_1 &= x_2, \\ \dot{x}_2 &= -2\zeta x_2 - \kappa_i x_1 + a\cos(x_3), \\ \dot{x}_3 &= 1, \end{aligned}$$

where the value of κ_i depends on region S_i, with $S_1 = \{x_1 < 0\}, S_2 = \{x_1 > 0\}$.

■

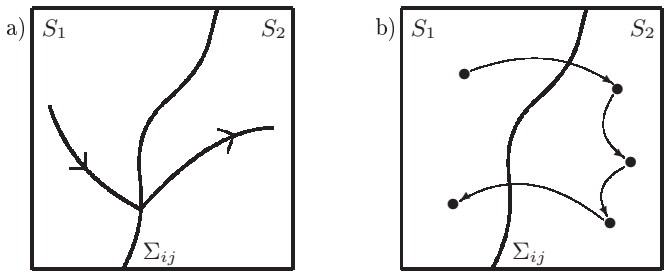

Figure 5.2: Trajectories of (a) a piecewise–smooth flow, and (b) a piecewise–smooth map

5.4.3 Filippov systems

Consider a general piecewise–smooth continuous system with a single boundary Σ, such that:

$$\dot{x} = \begin{cases} F_1(x), & \text{if } H(x) > 0, \\ F_2(x), & \text{if } H(x) < 0, \end{cases} \tag{5.12}$$

where Σ is defined by the zero set of a smooth function H and $F_1(x) \neq F_2(x)$ if $H(x) = 0$. This class of systems must be treated with great care since we have to allow the possibility of *sliding motion*. In order to define sliding, it is useful to think of system (5.12) local to the discontinuity boundary between two regions defined by the zero set of the smooth function $H(x) = 0$.

The *sliding region* of the discontinuity set of a system of the form (5.12) is given by that portion of the boundary of $H(x)$ for which $(H_x F_1) \cdot (H_x F_2) < 0$. That is, $H_x F_1$ (the component of F_1 normal to H) has the opposite sign to $H_x F_2$. Thus the boundary is simultaneously attracting (or repelling) from both sides [Piiroinen and Kuznetsov, 2008].

5.5 Stability of PWS

The extension of well–established concepts for smooth systems to the case of non–smooth systems is still an open research area. Next, we show a pragmatic approach for studying the asymptotic stability of a classical piecewise–smooth linear system presented in [di Bernardo et al., 2007].

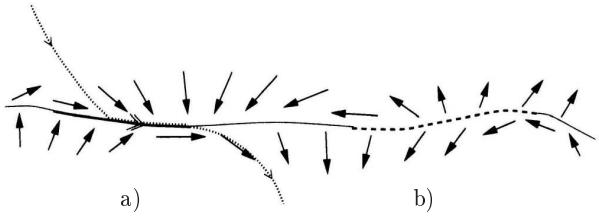

Figure 5.3: Slading region. Bold and dashed regions represent (a) attracting and (b) repelling sliding motion. Dotted lines indicate three individual trajectory segments.

5.5.1 Asymptotic stability

It is a particularly cumbersome task to provide necessary and sufficient conditions that guarantee the asymptotic stability of a desired invariant set of a piecewise–smooth system. Even the problem of assessing the asymptotic stability of an equilibrium that rests on a discontinuity boundary is an open problem in general. Let us focus on the problem for the special case of piecewise–linear systems, which will be of relevance to later discussions in Chapter 6.

Consider the piecewise–linear system:

$$\dot{x} = \begin{cases} A^- x, & \text{if } C^T x \leq 0, \\ A^+ x, & \text{if } C^T x \geq 0 \end{cases} \tag{5.13}$$

where $A^{\pm} \in \mathbb{R}^{n \times n}$ and $c \in \mathbb{R}^n$. We assume that the overall vector field is continuous across the hyperplane $\{x : C^T x = 0\}$, but the degree of smoothness is uniformly one. This means that

$$A^- - A^+ = EC^T \tag{5.14}$$

for some $E \in \mathbb{R}^n$. For the planar case, i.e., $n = 2$, a complete theory is possible and it can be shown that the equilibrium point $x = 0$ of (5.13) is asymptotically stable under certain strict conditions, provided the system obeys the property of observability often used in control theory.

Definition 5.6. Two matrices $A \in \mathbb{R}^{n \times n}$ and $C^T \in \mathbb{R}^{p \times n}$ are said to be *observable*

if the observability matrix $\mathcal{O}$, defined as:

$$\mathcal{O} = \begin{pmatrix} C^T \\ C^T A \\ \vdots \\ C^T A^{n-1} \end{pmatrix} \tag{5.15}$$

has full rank. Equivalently, for single–output systems, observability implies $det(\mathcal{O}) \neq 0$.

Theorem 5.1. *Consider the system* (5.13) *with* $n = 2$. *Assume that the pair* (C^T, A^-) *is observable. Then:*

- *The origin is asymptotically stable if and only if*
  1. *neither* A^- *nor* A^+ *has a real non–negative eigenvalue, and*
  2. *if both* A^- *and* A^+ *have non–real eigenvalues, then* $\sigma^-/\omega^- + \sigma^+/\omega^+ < 0$, *where* $\sigma^\pm \pm \omega^\pm$ *(*$\omega^\pm > 0$*) are the eigenvalues of* $A^\pm$
- *The system* (5.13) *has a non–constant periodic solution if and only if both* A^- *and* A^+ *have non–real eigenvalues and* $\sigma^-/\omega^- + \sigma^+/\omega^+ = 0$, *where* $\sigma^\pm \pm \omega^\pm$ *(*$\omega^\pm > 0$*) are the eigenvalues of* $A^\pm$. *Moreover, if there is one periodic solution, then all other solutions are also periodic. Moreover any such periodic solution has period equal to* $\pi/\omega^- + \pi/\omega^+$.

In higher dimensions, the problem becomes considerably more difficult.

In the control theory literature, a more general tool has been proposed for the stability analysis of piecewise–smooth dynamical systems. Take, for example, the problem of establishing whether an equilibrium point in a discontinuity boundary of a piecewise–smooth dynamical system is asymptotically stable. One technique for proving such stability is to find a common Lyapunov function, that is, a function $V(\mathbf{x})$ that is Lyapunov for each of the vector fields defining the system dynamics in each of the phase space regions. However, finding such functions in practice is at best difficult.

5.6 Numerical methods

In general we referred to numerical analysis tools for differential equations. For smooth flows, there are broadly speaking two classes of numerical methods for

investigating the possible dynamics for a range of parameter values namely; *direct numerical simulation*, and *path–following* [Kuznetsov, 2004]. This classification also applies to piecewise–smooth systems, The rigorous numerical analysis of nonsmooth dynamical systems remains a theory that is far from complete.

5.6.1 Direct numerical simulation

When computing solutions to piecewise–smooth systems it is usually not possible to use general purpose software directly, as they typically use numerical integration routines that assume a high degree of smoothness of the solution. All numerical computations must make special allowance for the nonsmooth events which occur when a discontinuity boundary is reached. Simulation methods for nonsmooth systems fall broadly into two categories; *time–stepping* and *event–driven*. The former is most often used in many–particle rigid body dynamics written in complementarity form for which there can be a big number of constraints. For such problems, to accurately solve for events when one of the every one of the constraint functions becomes zero within each time–step and to subsequently re–initiate the dynamics would be prohibitively computationally expensive. In contrast, the basic idea of *time–stepping* is to only check constraints at fixed times. There are adaptations to standard methods for integrating ODE for complementarity systems, some of which are based on linear complementarity problem solvers that have been developed in optimization theory and that can be directly used on simulation of piecewise smooth dynamical systems. Clearly there are errors introduced by not accurately detecting the transition times, and therefore time–stepping schemes are often of low–order accuracy. In this thesis we are concerned with low–dimensional systems with just a discontinuity boundary. In this context, explicit event driven schemes are feasible, fast and accurate. In these methods, trajectories far from boundaries are solved using standard numerical integration algorithms for smooth dynamical systems (e.g. Runge–Kutta, implicit solvers, etc.), then times at which a discontinuity boundary is hit are accurately solved. Here it is necessary to consider the capability of simulating sliding flow by defining a sliding vector fields.

Chapter 6

Stability analysis of RTS testing on non–linear dampers

Contents

As it was pointed out before in chapter 3, the success of real–time substructuring tests is highly dependent on the control of the signal delays. We intend to analyse the close loop behaviour of a model when testing a supplemental energy dissipation system for structural control. In the seismic protection system considered, the most non–linear and complex-to-model component is a passive non–linear fluid viscous damper added to the structure. In the next chapter, an extensive description of this system is presented. In accord with the fundamentals on RTST, the damper (the critical element) must be extracted from the system and tested physically in the lab, while the remaining part of the structure is modelled mathematically and becomes the numerical substructure. In our tests, the displacements computed form the numerical substructure are applied through an actuator to the damper, and in turn, the resisting force is measured and feed back into the numerical substructure. Although sources of delay are the electronic measuring and actuator assemblage, the delay comes mostly from the actuator dynamics. It is worthy noticing that, the practical effect of this on our system, is

a lag time on the effective damper force applied to the structure.
In this chapter, we present a stability analysis to highlight the harmful effects caused by delays in dynamic systems when timing errors are considered on the damper's response. Our goal is to assess the constraints on delays, in such a way that the stability and reliability of the closed loop simulation can be guaranteed. The present study will be addressed in the context of both classic stability theory for linear/non–linear systems (See Chapter 4) and the qualitative theory of Piecewise Smooth Dynamical Systems (See Chapter 5) according to the particular case which is discussed throughout each section.

6.1 SDOF oscillator with a delayed damper

Let us suppose a simple oscillator compounded of a single–degree of freedom system (SDOF) with an energy dissipation device, as shown in Figure 6.1. Without loss of generality, the damper is considered placed atop of a chevron–type brace and attached to the frame in horizontal position. Thus, by assuming a very stiff brace (much more than the frame), the relative displacement between the ends of the damper can be considered equal to the relative inter–storey drift. Then, we

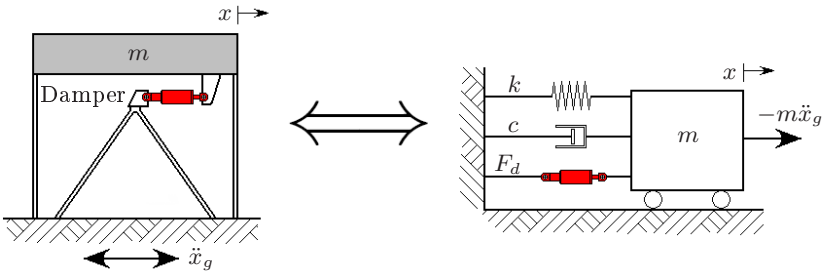

Figure 6.1: SDOF oscillator with an added damper.

can write a mathematical expression to describe the dynamics of this system as in equation (6.1).

$$m\ddot{x}(t) + c\dot{x}(t) + kx(t) + F_d(t, \tau, c_d, \alpha, \dot{x}) = -m\ddot{x}_g(t) \tag{6.1}$$

where:

m : is the mass of the system;
c : is the intrinsical damping coefficient of the system;
k : is the stiffness of the system;
t : is time;
F_d : is the force in the damper;
τ : is the signal delay;
c_d : is the damping coefficient of the damper;
α : is the velocity exponent of the damper; $0<\alpha<1$;
$\ddot{x}_g$: is the base excitation;
$\ddot{x}, \dot{x}, x$: are respectively the system acceleration, velocity and displacements.

Note that the damper force is depending not only on time, damper coefficient and velocity but also on the delay considered on the damper response (assumed as constant). In what follows, we shall examine this system in light of different situations in accord with the behaviour of the damper. We shall cover both linear and non–linear cases.

6.2 Oscillator with added linear damper

Fist of all, let us consider the oscillator with a linear damper. Equation (6.1) can be then rewritten as:

$$m\ddot{x}(t) + c\dot{x}(t) + kx(t) + c_{dl}\dot{x}(t-\tau) = -m\ddot{x}_g(t) \tag{6.2}$$

where c_{dl} is the coefficient of the linear damper.This kind of differential equation, in which the derivative of the unknown function at a certain time is given in terms of the values of the function at previous times, is called a Delay Differential Equation (DDE). We shall describe both the analytical and numerical solutions for x, considering the critical delay value τ_{cr} for which the system may become unstable.

6.2.1 Explicit stability analysis

Let us assume zero external excitation and arbitrary initial conditions. By means of proper substitutions, the system in (6.2) can be rewritten with non–dimensionalised parameters as:

$$x''(\hat{t}) + 2\zeta x'(\hat{t}) + x(\hat{t}) + px'\left(\hat{t} - \hat{\tau}\right) = 0 \tag{6.3}$$

where x' and x'' indicate the first and second–order derivative of x with respect to $\hat{t}$ instead of t; and also:

$$w_n = \sqrt{\frac{k}{m}}\,; \quad \zeta = \frac{c}{2\sqrt{mk}}\,; \quad \hat{t} = w_n t\,; \quad \hat{\tau} = w_n \tau\,; \quad p = \frac{c_{dl}}{m w_n}$$

An accepted and quite common strategy to solve differential equations, is to assume solution of the exponential form, $x = Ae^{\lambda \hat{t}}$. The characteristic equation of the system can be then written as:

$$\lambda^2 + 2\zeta\lambda + 1 + \lambda p e^{-\lambda\hat{\tau}} = 0 \tag{6.4}$$

If we assume that $\hat{\tau}$ is small, instead of $e^{-\lambda\hat{\tau}}$ we can use the first–order approximation $(1 - \lambda\hat{\tau})$ from the series expansion of this exponential function. By substituting this approximation and reordering the parameters, equation (6.4) becomes:

$$(1 - p\hat{\tau})\lambda^2 + (2\zeta + p)\lambda + 1 = 0 \tag{6.5}$$

The real part of the system eigenvalues determines the stability of the linear system (See Lemma 4.1). Solving the last equation for λ we have:

$$\lambda_{1,2} = \frac{1}{2(1 - p\hat{\tau})}\left(-(2\zeta + p) \pm \sqrt{(2\zeta + p)^2 - 4(1 - p\hat{\tau})}\right) \tag{6.6}$$

First, suppose that there is no delay in the damper response. So if $\hat{\tau} = 0$ the system eigenvalues become:

$$\lambda_{1,2} = -\tfrac{1}{2}\left[(2\zeta + p) \pm \sqrt{(2\zeta + p)^2 - 4}\right] \tag{6.7}$$

Since ζ, p are positive quantities (they depend on strictly positive physical characteristics) and $(2\zeta + p) > \sqrt{(2\zeta + p)^2 - 4}$, the real part of the complex roots λ_i will be always negative, so that, the system is globally asymptotically stable as it was expected for a system with an additional linear damper.

Going back to the case when $\hat{\tau}$ is small, we note that by satisfying the relationship $(1 - p\hat{\tau}) > 0$, the quantity $(2\zeta + p)$ is greater than $\sqrt{(2\zeta + p)^2 - 4(1 - p\hat{\tau})}$ being the real part of the complex roots λ_i always negative, what implies global and asymptotic stability. On the other hand, if $(1 - p\hat{\tau}) < 0$ at least one of the roots λ_i will have real part positive and the system will become unstable. Therefore, the system will remain stable if and only if the delay in the damper response satisfies $\hat{\tau} < 1/p$, which converted back to the original parameters can be written as:

$$w_n\tau = \hat{\tau} < \frac{m w_n}{c_{dl}} \quad \Rightarrow \quad \tau < \frac{m}{c_{dl}} \tag{6.8}$$

This expression highlights that structures with strong added dampers will be more susceptible to become unstable due to small delays in the damper response, and

consequently, it will be more difficult to maintain stability when running a real–time substructuring test on it. A system which fulfills the restriction presented in (6.8) has characteristic roots located in the left half complex plane and is always global asymptotically stable. Increasing the value of the bifurcation parameter p results in characteristic roots swarming out from the left to the right half part in the complex plane[1] (i.e. towards the instability).

Although some researchers have demonstrated before, how delay can be understood as negative damping [Horiuchi et al., 1999, Wallace et al., 2005a], equation (6.5) shows how, considering delays in the damping forces, it can manifest itself as negative mass too. In this context delay should be understood like anti-inertial force, a sort of negative mass (in fact, it can be expressed by $m_{neg} = -c_{dl}\tau$) which adds energy into the system. By equaling both sides in the inequality (6.8), it is possible to find the delay τ for which the overall mass in the system is cancelled, as a matter of fact, equation (6.6) is not definite for this value (massless system). Furthermore, do not fulfill inequality (6.8) leads to instability in consequence of the effective negative overall mass operating in the system.

On the other hand, a different approach for determining the stability boundaries of the system, is to search a set of point in the parameters space where the characteristic equation has one pair of pure imaginary roots, that is, just go through a Hopf bifurcation [Kalmár-Nagy et al., 2001]. To find this curve, we substitute into the trial solution previously proposed for equation (6.3), $\lambda = i\hat{w}$, for $w > 0$ and $\hat{w} = w/w_n$.
This analysis is valid for any time delay, even if τ is not small (see [Gilsinn, 2002]). After applying the aforementioned substitution and some algebra, equation (6.4) becomes:

$$-\hat{w}^2 + 2i\zeta\hat{w} + 1 + ip\hat{w}e^{-i\hat{w}\hat{\tau}} = 0 \tag{6.9}$$

Applying the Euler's formula from complex analysis and splitting up into real and imaginary parts, we get two real equations:

$$-\hat{w}^2 + p\hat{w}\sin(\hat{w}\hat{\tau}) + 1 = 0 \tag{6.10a}$$

$$2\zeta + p\cos(\hat{w}\hat{\tau}) = 0 \tag{6.10b}$$

Assuming ζ as known, we can use the last pair of equations to express the parameters $\hat{\tau}$ and p as function of $\hat{w}$.
Dividing equation (6.10a) by (6.10b) and considering periodicity we have:

$$\frac{\hat{w}^2 - 1}{-2\zeta\hat{w}} = \tan(\hat{w}\hat{\tau}) \tag{6.11}$$

[1] Bifurcation and other phenomena are introduced in §4.2.3

$$\hat{\tau} = \frac{1}{\hat{w}} \arctan\left(\frac{1-\hat{w}^2}{2\zeta\hat{w}}\right) + \frac{n\pi}{\hat{w}} \; ; \quad n = 1, 2, 3 \ldots \tag{6.12}$$

where n corresponds to the n-th lobe (parameterized by $\hat{w}$) from the right in the stability diagrams in Figure 6.2 (n must be greater than 0, because $\hat{\tau} > 0$).
The trigonometric terms in Equations (6.10a) and (6.10b) can be eliminated by squaring and adding them to yield:

$$p = \frac{1}{\hat{w}}\sqrt{(\hat{w}^2-1)^2 + (2\zeta\hat{w})^2} \tag{6.13}$$

In Figure 6.2(a), we present the boundaries obtained for $\hat{\tau}$ and p by fixing ζ at 0.03. These curves are parameterized by $\hat{w}$ running from 0 to ∞ and n from 1 to 5. Along these curves the system has a pair of purely imaginary eigenvalues delimiting the parameters space where the system is expected to be stable. Along the line $\hat{\tau} = 0$ the system is stable, consequently, its surrounding area up to the closest boundary is the region of stability (shadow area). The approximate boundary defined by equaling the inequality (6.8) is plotted too (dashed line). The approximation tends to underestimate the critical delay and only holds for very small values of $\hat{\tau}$. The curve with $\hat{\tau}$ for $n = 1$ is the practice stability boundary because encloses the others theoretical boundaries into the unstable region.

In addition, we can rearrange equations (6.10a) and (6.13) assuming p as known, so as to obtain the critical delay $\hat{\tau}$ and ζ as parametric curves in $\hat{w}$ as follows:

$$\zeta = \frac{1}{2\hat{w}}\sqrt{(p\hat{w})^2 - (\hat{w}^2-1)^2} \tag{6.14}$$

$$\hat{\tau}_1 = \frac{1}{\hat{w}} \arcsin\left(\frac{\hat{w}^2-1}{p\hat{w}}\right) + \frac{2\pi n}{\hat{w}} \tag{6.15}$$

where $\hat{w}$ runs from $\frac{1}{2}(-p + \sqrt{p^2+4})$ to $\frac{1}{2}(p + \sqrt{p^2+4})$, and n is any positive integer greater than zero. Seeking for completeness, we have to consider the periodicity of sine function and the range over the arcsin function is defined; thus, the boundary in equation (6.15) should be rounded off with:

$$\hat{\tau}_2 = -\frac{1}{\hat{w}}\left[\arcsin\left(\frac{\hat{w}^2-1}{p\hat{w}}\right) + \pi\right] + \frac{2\pi n}{\hat{w}} \tag{6.16}$$

Figure 6.2(b) shows the stability region for fixed $p = 2$ using the curves defined parametrically by equations (6.14), (6.15) and (6.16). Again, the approximate

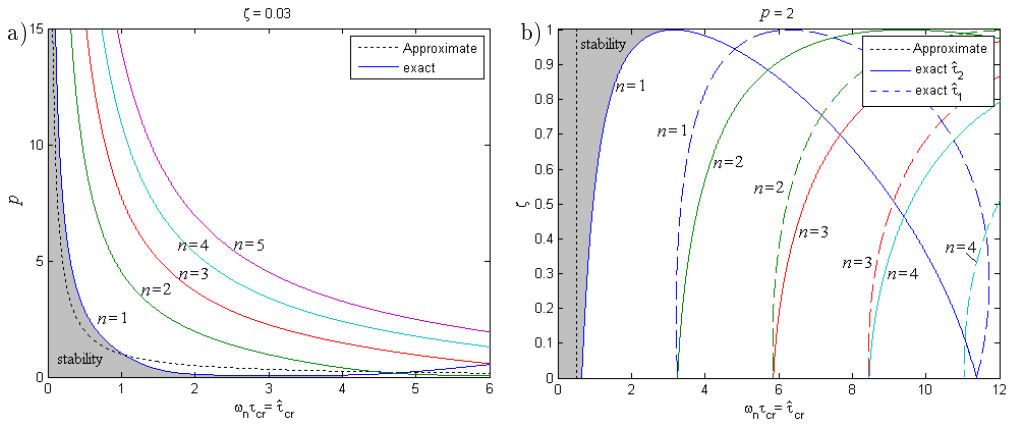

Figure 6.2: Non–dimensionalized complex root solutions: a) Varying added damper capacity, and b) Varying structural damping.

boundary defined by inequality (6.8) is include in dashed line. This approximation is a constant value for any ζ and strongly underestimates the critical delay. Considering the lightly damped systems commonly studied in civil engineering applications ($\zeta < 0.1$), the curve for $\hat{\tau}_2$ with $n = 1$ can be used as the practical stability boundary in the $(\hat{w}, \zeta)$–plane.

6.2.2 Numerical stability analysis

For more complex Delay Differential Equations (DDEs) than equation (6.2) it may become impossible to find stability regions, as before, by analytical calculations. We therefore move to a numerical approach for finding the stability regions. First of all, we shall face the linear case, and afterwards, extend the analysis to more general cases taking into account non–linear substructured systems.

We use a graphical method for studying the qualitative behavior of our second–order linear dynamic system. The phase plane method is concerned with the graphical study of second–order systems described in terms of the equations of state (For further details, see §4.2). Thus, equation (6.3) can be rewritten by means of the simple change of variables $x_1 = x$ and $x_2 = x'$ as:

$$x_1'(\hat{t}) = x_2(\hat{t}) \tag{6.17a}$$

$$x_2'(\hat{t}) = -2\zeta x_2(\hat{t}) - x_1(\hat{t}) - p x_2(\hat{t} - \hat{\tau}) \tag{6.17b}$$

where x_1 and x_2 are the state variables of the system, that is, relative displace-

ment and velocity. In other words, the systems is entirely described by x and x' at any time, that is why the phase plane gives complete information about the system behaviour (See pag. 49).

Firstly, we want to point out how the increasing of the damper coefficient can affect the behaviour of the system and how this circumstances can be distinguished in this kind of plots. To do that, we considered no delay in the equation above ($\hat{\tau} = 0$) and utilized a very easy–to–use program called `pplane`[2]. This program is designed for phase plane analysis of differential equations and allows the user to plot the vector field[3] for the system and also the solution curves. Figure 6.3 shows the vector fields and some solution trajectories for the system in equations (6.17) considering no delay, a structural damping ratio $\zeta = 0.03$ and different capacities for the added damper.
The first two cases with $p = 0.3$ and $p = 1.0$ correspond to a stable focus[4] (Figs. 6.3(a) and (b)). This means that the real part of the eigenvalues in formula (6.7) are negative while the imaginary part are different from zero, which implies that $x(\hat{t})$ and $x'(\hat{t})$ both goes to zero as $\hat{t} \to \infty$. Note that the trajectories encircle the equilibrium point one or more times before converging to it.
The other two cases with $p = 2.0$ and $p = 4.0$ correspond to a stable node. Now, the eigenvalues are real and negatives, which implies that both $x(\hat{t})$ and $x'(\hat{t})$ converge to zero exponentially, as shown in Figures 6.3(c) and (d). It is worth noticing that no oscillation are presented in the trajectories, moreover, the velocity tends to zero faster than the displacement. As the trajectories approach the origin, they become tangent to the line whose slope corresponds to the slow eigenvalue (the smallest). If the damper capacity if large enough to cause an eigenvalue close to zero, this line will be almost horizontal and will become close an equilibrium subspace, being all trajectories almost normal to it. That would imply that the velocity will decrease very rapidly while the displacement will not do it. The physical meaning of this limit behavior is that the system will remain blocked in a position different from zero.

From now on, let us consider $\hat{\tau}$ not null. Due to there is no a software able to draw the phase plane for delay differential equations, we decided to construct the vector field from some solution trajectories of the system in (6.17). A popular approach for solving DDEs is to extend one of the methods used to solve Ordinary Differential Equations (ODEs), most of the codes are based on explicit Runge–Kutta methods (See §3.6.2). In this section, we use a program developed on

[2] `pplane` is copyrighted in the name of John C. Polking, Department of Mathematics, Rice University.
[3] See key definitions in §4.2.1
[4] For a comprehensive description of this behaviour, see §4.2.2

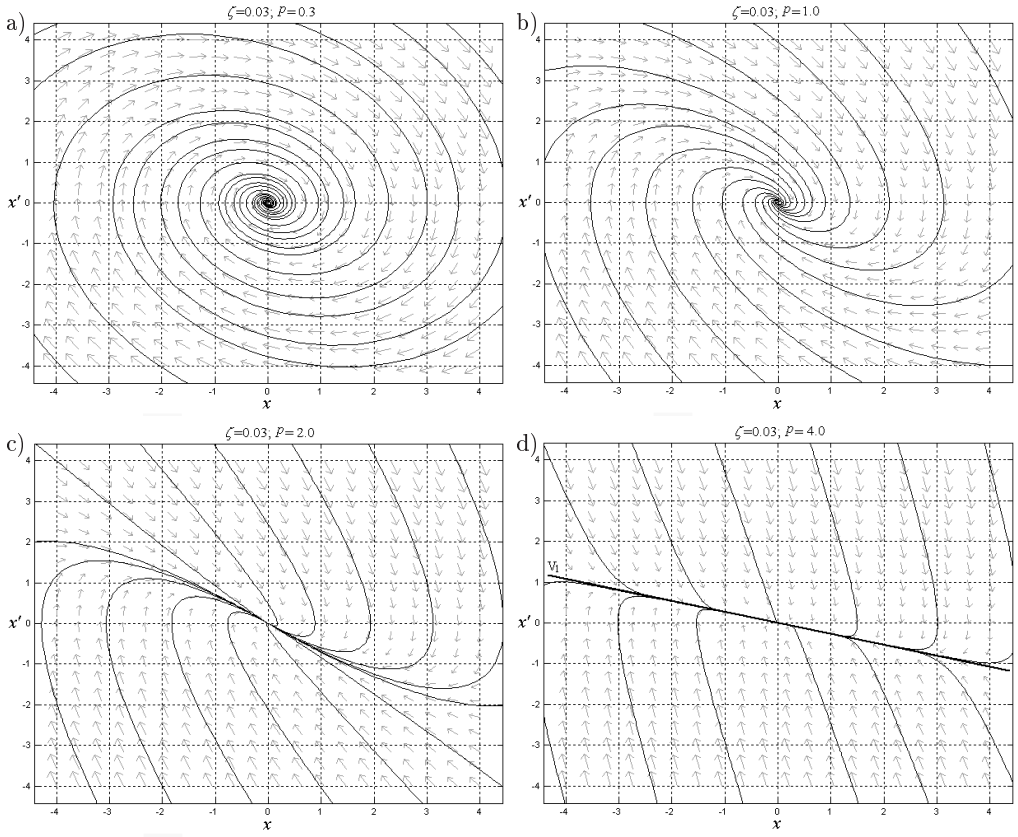

Figure 6.3: Vector fields and trajectories for $\hat{\tau} = 0$ (no delay) varying the added damper capacity for the linear case: a) and b) Stable focus; c) and d) Stable node.

MATLAB[5] called `dde23` which extends the method of the MATLAB ODE solver `ode23` and allows the user to solve DDEs with constant delays including also problems with discontinuities. The program was written by L. Shampine and S. Thompson, a detailed discussion of the numerical methods used by `dde23` can be found in [Shampine and Thompson, 2001].

Figure 6.4 shows the vector fields and some solution trajectories for the system in (6.17) considering $\zeta = 0.03$, $p = 2$ and different delays in the damper's response. For small delays, the system stability does not change, to confirm that, it is sufficient to compare Figure 6.3(c) with Figure 6.4(a), we still have a stable node. Nevertheless, increasing the delay just before the stability limit, the systems behaves as a stable focus, that is, the trajectories encircle the equilibrium point

[5]MATLAB is a registered trademark of The MathWorks, Inc. www.mathworks.com

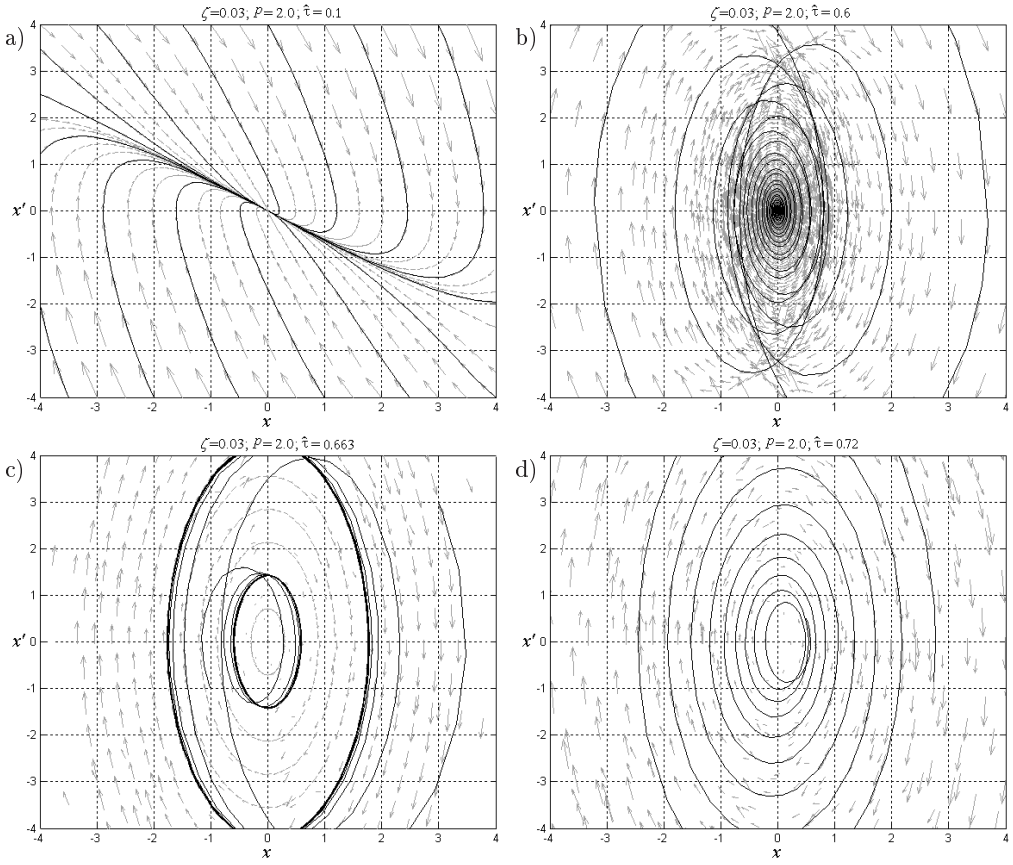

Figure 6.4: Vector fields for $\zeta = 0.03$; $p = 2.0$ and different delays in the feedback loop: a) Stable node; b) Stable focus; c) Center; d) Unstable focus.

several times before converging to it (See Fig. 6.4(b)). On the other side, taking into consideration a delay larger than the stability boundary, the system behaves as an unstable focus, although the trajectories encircle the equilibrium point, both x and x' tend to infinity as $\hat{t} \to \infty$ as shown in Figure 6.4(d). Additionally, just on the stability boundary, the system neither converges to the equilibrium point nor diverges from it, but goes to periodical closed trajectories in phase space which are neighbored by other closed trajectories. This case corresponds to a center point as shown in Figure 6.4(c). The name comes from the fact that all trajectories are ellipses and the equilibrium point is the center of these ellipses.

In order to find the region of stability for the linear substructured system un-

der discussion, we use the conditions explained above to define the critical time lag $\hat{\tau}_{cr}$ as the delay in the damper's response that causes the system to behave as a central point, that is, when it describes sustained closed orbits. We wanted a simple and robust search method for $\hat{\tau}_{cr}$ (in the sense that it always converges to the solution), so we selected and implemented the bisection search method. Although it is relatively slow, it is always reliable.

Roughly speaking, the search process can be illustrated as follows. For a ζ and p known and an arbitrary small value of $\hat{\tau}$ the DDE in formula (6.17) is solved. The initial delay $\hat{\tau}_0$ is chosen small enough such that the systems is stable. Then, the delay is increased of a predetermined quantity $\Delta\hat{\tau}$ and the DDE is solved again. The delay is continuously increased until the system became unstable, without loss of generality, let us call that delay as $\hat{\tau}_n$. In the absence of any other information, the best estimate for the location of the solution ($\hat{\tau}_{cr}$) is the midpoint of the range between the last two values of $\hat{\tau}$ found. Let us call this first estimation as $\hat{\tau}_{cr_0}$. Subsequently, the estimate for the critical delay is used to solve de DDE and either: (i) the system behaves stable, in such a case the interval to be bisected for the next estimate of the critical delay (let us call it $\hat{\tau}_{cr_1}$) is the right–side interval between $\hat{\tau}_{cr_0}$ and $\hat{\tau}_n$; (ii) the system behaves unstable, in such a case the interval to be bisected for the next estimation of the critical delay, is the left–side interval between $\hat{\tau}_{n-1}$ and $\hat{\tau}_{cr_0}$. Now, the new estimation of the critical delay is used to solve de DDE and the process is iteratively applied until the system behaves closely as a central point. The last estimate for the critical delay can be selected as the stability boundary for the system defined by ζ and p.

The above iterative procedure was implemented in a Matlab routine. It allowed us to obtain numerically the regions of stability presented in what follows. Figure 6.5(a) presents the boundaries obtained for $\hat{\tau}$ and p fixing ζ at 0.03. We use red crosses for the numerical solution. We also compare this limit against the theoretical stability boundaries, both exact and approximate, already shown in Figure 6.2(a). As before, the region of stability is emphasized as a shadow area. Additionally, Figure 6.5(b) shows the stability region for $\hat{\tau}$ and ζ fixing $p = 2.0$. Again, the approximate and exact theoretical boundaries are included. Overall, the numerical results in this subsection agree with the explicit stability analysis presented before in §6.2.1. This makes evident the potential of the numerical stability analysis, with the added advantage that it works also for much more complex and non–linear systems.

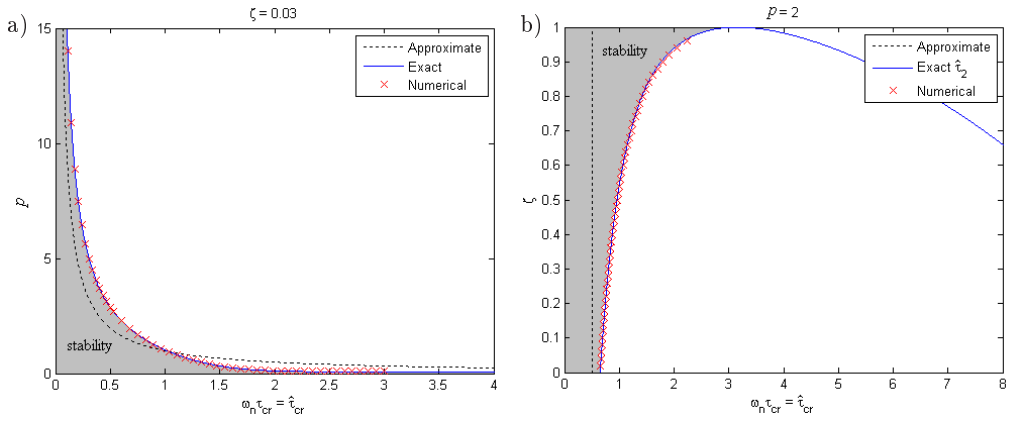

Figure 6.5: Stability region for numerical solution (Linear case): a) Varying added damper capacity, and b) Varying structural damping.

6.3 Oscillator with added non–linear damper

Now, let us consider a non–linear added damper with constant delay in the single degree of freedom system shown in Figure 6.1. The delay differential equation in (6.2) can be now rewritten as:

$$m\ddot{x} + c\dot{x} + kx + c_d|\dot{x}(t-\tau)|^{\alpha} \cdot \text{sign}(\dot{x}(t-\tau)) = -m\ddot{x}_g \tag{6.18}$$

where:

m :	is the mass of the system;
c :	is the intrinsical damping coefficient of the system;
k :	is the stiffness of the system;
t, τ :	are respectively time and the signal delay;
c_d :	is the damping coefficient of the damper;
α :	is the non–linear exponent of the damper; $0<\alpha<1$;
$\lvert\cdot\rvert$:	represent the absolute value of $\cdot$;
$\ddot{x}_g$:	is the base excitation; and
$\ddot{x}, \dot{x}, x$:	are respectively the system acceleration, velocity and displacements.

The same as before, let us consider on equation (6.18) zero external excitation, arbitrary initial conditions and some appropriate substitutions to get a non–dimensionalised formulation in terms of dimensionless parameters. Thus, after some algebra we have:

$$z''(\hat{t}) + 2\zeta z'(\hat{t}) + z(\hat{t}) + p_n|z'(\hat{t}-\hat{\tau})|^{\alpha} \cdot \text{sign}\left(z'(\hat{t}-\hat{\tau})\right) = 0 \tag{6.19}$$

where:

$$\zeta = \frac{c}{2\sqrt{mk}}\,; \quad \hat{t} = w_n t\,; \quad \hat{\tau} = w_n \tau\,; \quad w_n = \sqrt{\frac{k}{m}}$$
$$x = x_0 z; \quad p_n = \frac{c_d}{m} w_n^{\alpha-2} |x_0|^{\alpha-1}$$

The differentiating operator $'$ indicates the derivative with respect to $\hat{t}$, and x_0 stands for an arbitrary initial condition.

Due to the fact that for non–linear delay differential equations there is not a suitable method to perform explicit stability analysis, at first we carried out some numerical investigations in order to understand, identify and characterize qualitatively the behavior of the system.

6.3.1 Numerical stability analysis

Again, we will take advantage of the phase plane analysis to obtain qualitative information about the system behaviour. The qualitative description of a dynamical system is given by the description of the invariant sets that compose its phase portrait. As before, the system is represented in terms of the equations of state, where the system's relative displacement and velocity are the state variables, named respectively $x_1 = z$ and $x_2 = z'$.

$$x_1'(\hat{t}) = x_2(\hat{t}) \tag{6.20a}$$
$$x_2'(\hat{t}) = -2\zeta x_2(\hat{t}) - x_1(\hat{t}) - p_n |x_2(\hat{t}-\hat{\tau})|^{\alpha} \cdot \operatorname{sign}\left(x_2(\hat{t}-\hat{\tau})\right) \tag{6.20b}$$

Seeking for better understanding of the system behaviour, first of all we shall perform a parametric analysis. Our interest is to determine the relationship of the multiple variables in (6.20) and see their effect on overall system performance. By simulations we shall try to identify which parameters could drastically change the system dynamics.

Let us start with the structural damping ration ζ. Note that the vast majority of structures, especially in the civil engineering field, are lightly damped, typically operating between 0.5% and 7%. Figure 6.6 shows vector fields for the system in (6.20) assuming, without loss of generality, constant parameters $p_n = 1.0$; $\alpha = 0.15$ and $\hat{\tau} = 0.8$. Damping ratio is varying from 0.1% to 10%. From those graphics and considering civil engineering structures, it is worth noticing that the system dynamics is not prone to be affected by changes of the damping ration ζ, so that we can disregard its effects.

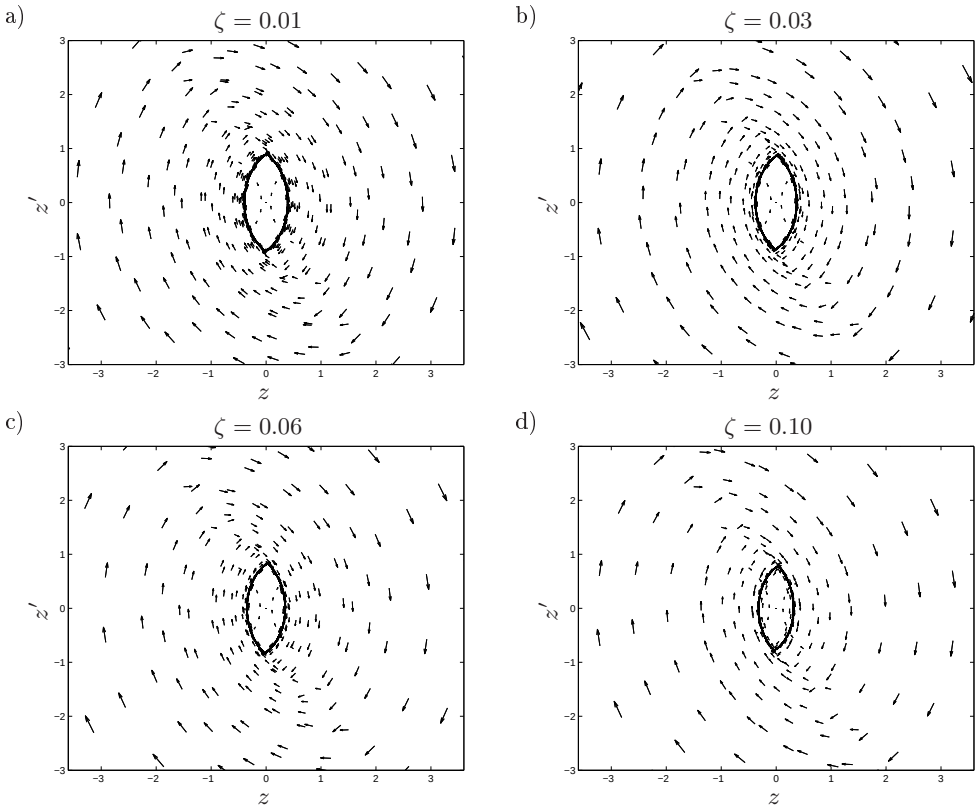

Figure 6.6: Vector fields of system in (6.19) for $p_n = 1.0$; $\alpha = 0.15$; $\hat{\tau} = 0.8$ and different damping ratio: a) $\zeta = 0.01$; b) $\zeta = 0.03$; c) $\zeta = 0.06$; d) $\zeta = 0.10$.

The next parameter to be evaluated is p_n. The vector fields of the system in (6.20) for p_n equals to 0.5, 1.0, 2.0 and 4.0 are presented in Figure 6.7. The other parameters are considered to be constant as: $\zeta = 0.03$, $\alpha = 0.15$ and $\hat{\tau} = 0.8$. Although the graphs may initially seem different, by plotting them at proper scales, the dynamic equivalence among those systems can be evidenced. Note that for a particular structure (represented by m and w_n), the parameter p_n increases by either increasing the damper coefficient c_d or reducing the arbitrary initial condition x_0. Thus, from simulations we can say that even an important increase in the damper's strongness will not change significantly the qualitative description of the dynamics, as it would just imply a change in the scale over which the system should be evaluated. Even more, although the changes in the behaviour are certainly not proportional to p_n, a change of the scale on the state variables which is proportional to the change of p_n, will be enough to catch the

dynamics of the new system.

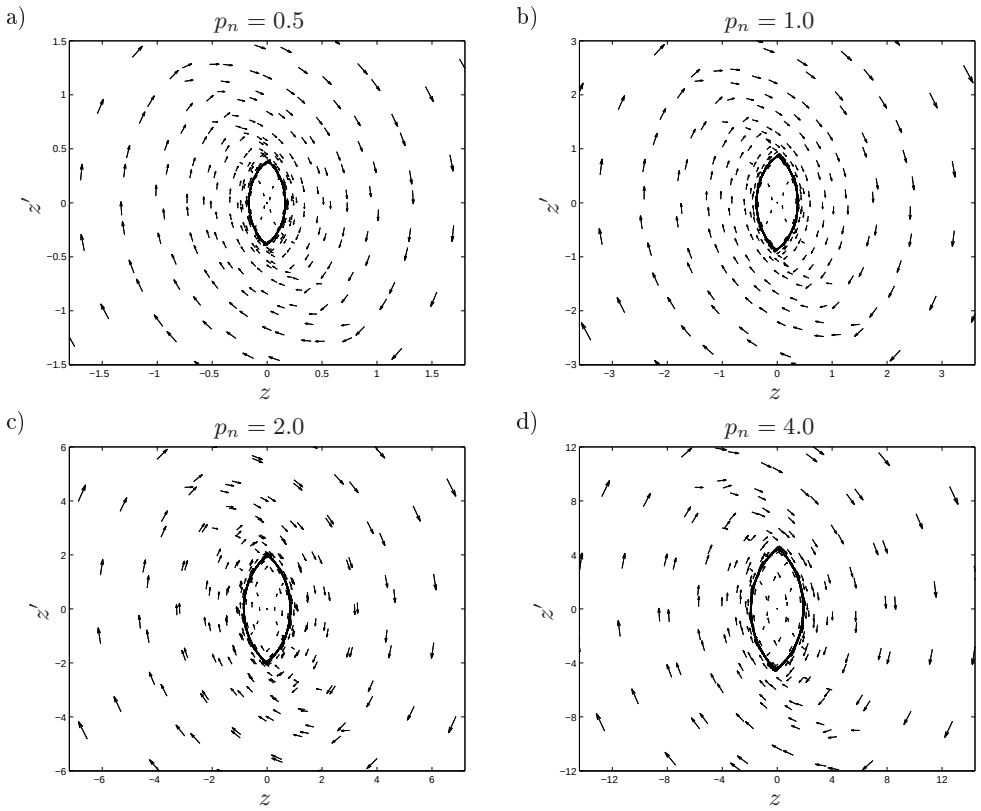

Figure 6.7: Vector fields of system in (6.19) for $\zeta = 0.03$; $\alpha = 0.15$; $\hat{\tau} = 0.8$ and different values of p_n: a) $p_n = 0.5$; b) $p_n = 1.0$; c) $p_n = 2.0$; d) $p_n = 4.0$.

Next, let us skip to the velocity exponent of the damper. A value of α=1 means linear damping (velocity–proportional response). The hysteresis loop for a linear damper is a pure ellipse as shown in Figure 6.8. Nonlinear damping with low exponent ($0<\alpha<1$) shows a hysteresis curve much more rectangular, what implies more energy dissipation capacity. That is why nonlinear fluid devices are very appreciated for real applications in structural engineering, as they provide significantly higher forces at lower velocities compared to linear dampers. Any α above 1.0 produces very poor performance. Figure 6.9 shows the vector fields for the system in (6.20) considering several values of α.
According with our numerical simulation, systems equipped with nonlinear damper at low damper's velocity exponents, let say $\alpha \leq 0.20$, exhibit substantially the

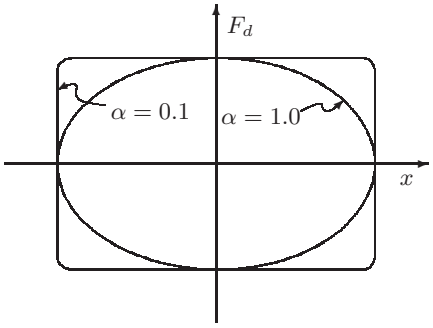

Figure 6.8: Hysteresis loops for a linear ($\alpha = 1.0$) and a nonlinear viscous fluid damper (e.g. $\alpha = 0.1$)

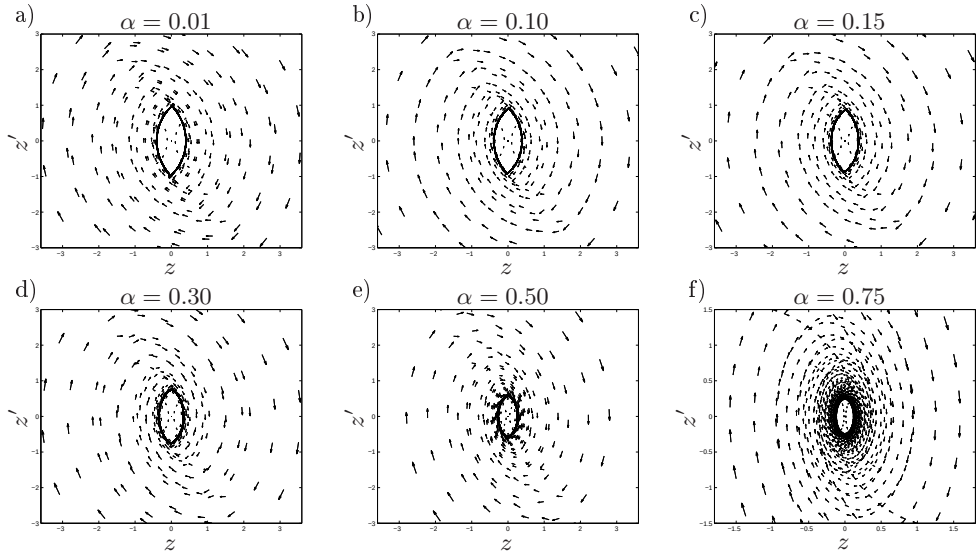

Figure 6.9: Vector fields of system in (6.19) for $\zeta = 0.03$; $p_n = 1.0$; $\hat{\tau} = 0.8$ and different values of α: a) $\alpha = 0.01$; b) $\alpha = 0.1$; c) $\alpha = 0.15$; d) $\alpha = 0.3$; e) $\alpha = 0.5$; and f) $\alpha = 0.75$.

same dynamics. Hence, when analysing stability of systems with added nonlinear dampers with low α, we can consider a *dynamically equivalent model*[6] fixing $\alpha = 0$; that is a model which uses dry friction (Coulomb Friction) instead of viscous nonlinear damping. This will not compromise the general result of the stability analysis. The idea is to use a simpler mathematical model for the damper, having qualitatively equivalent dynamics, in such a way that the explicit stability

[6] A definition of Equivalent Dynamics can be found in §5.3.2

analysis can be achieved in a closed–form.

The former observation is fundamental in this study, as it allowed us to transform a continuous nonlinear dynamical system into a piecewise smooth dynamical system comprised of two linear systems as it shall be explained later.

Finally, let us consider the effects of the delay $\hat{\tau}$. Figure 6.10 shows the vector fields of the system in (6.20) varying $\hat{\tau}$ and considering the constant parameters $\zeta = 0.03$; $p_n = 1.0$ and $\alpha = 0.15$. Even when the delay is very small, this results in self–sustaining oscillations of the system's response. The larger the delay, the longer the limit cycle extension (See Fig. 6.10f). This limit cycle is characterized for a high frequency, much higher than the natural frequency of the system. The smaller the delay, the higher the frequency of the limit cycle.
In addition, for small delays (in the sense that will be defined later), there exists a region in the neighborhood of the limit cycle, where the system behaviour changes drastically. When the system state gets into this area (See dark spots in Figs. 6.10a to 6.10d), it changes suddenly the amplitude and frequency of oscillation. The frequency is increased strongly. These oscillations tend to match the limit cycle; however, if the delay is very small, such convergence to the limit cycle is very slow in terms of the displacement. In other words, whilst in terms of the velocity (z'), the oscillations are very close to those exhibit for the limit cycle, in terms of the displacement, the oscillations converge very slowly to those in the limit cycle. This *high frequency region* only occurs for small delays. When $\hat{\tau}$ becomes larger, the system goes rapidly to the limit cycle without any other phenomenon in between.

An equivalent system

Henceforth, we shall assume systems provided with added nonlinear damper with low velocity exponent. Based on the previous parametric analysis, in place of studying the system in (6.19), we shall considerer a dynamically equivalent system which includes dry friction. Such a system can be expressed as:

$$z''(\hat{t}) + 2\zeta z'(\hat{t}) + z(\hat{t}) + p_s \text{sign}\left(z'(\hat{t} - \hat{\tau})\right) = 0 \tag{6.21}$$

where the damper force F_d is represented by $p_s \text{sign}(z'(\hat{t} - \hat{\tau}))$; $p_s = c_d/(m x_0 w_n^2)$ and the other parameters the same as in pages 90 and 91. Again, the system is represented in terms of the equations of state as in equation (6.22), where $x_1 = z$ and $x_2 = z'$.

$$x_1'(\hat{t}) = x_2(\hat{t}) \tag{6.22a}$$
$$x_2'(\hat{t}) = -2\zeta x_2(\hat{t}) - x_1(\hat{t}) - p_s \text{sign}\left(x_2(\hat{t} - \hat{\tau})\right) \tag{6.22b}$$

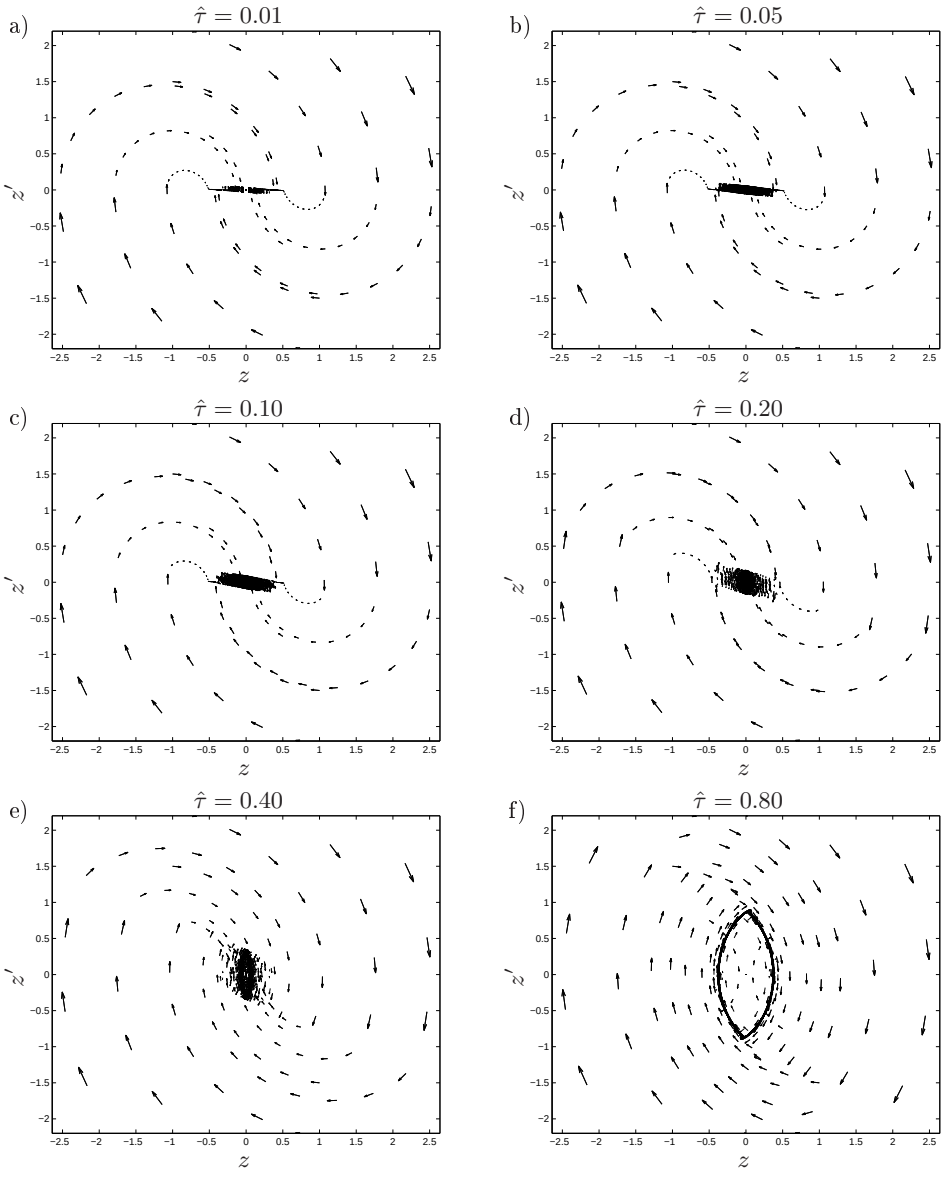

Figure 6.10: Vector fields of system in (6.19) for $\zeta = 0.03$; $p_n = 1.0$; $\alpha = 0.15$ and different delays: a) $\hat{\tau} = 0.01$; b) $\hat{\tau} = 0.05$; c) $\hat{\tau} = 0.1$; d) $\hat{\tau} = 0.2$; e) $\hat{\tau} = 0.4$; and f) $\hat{\tau} = 0.8$.

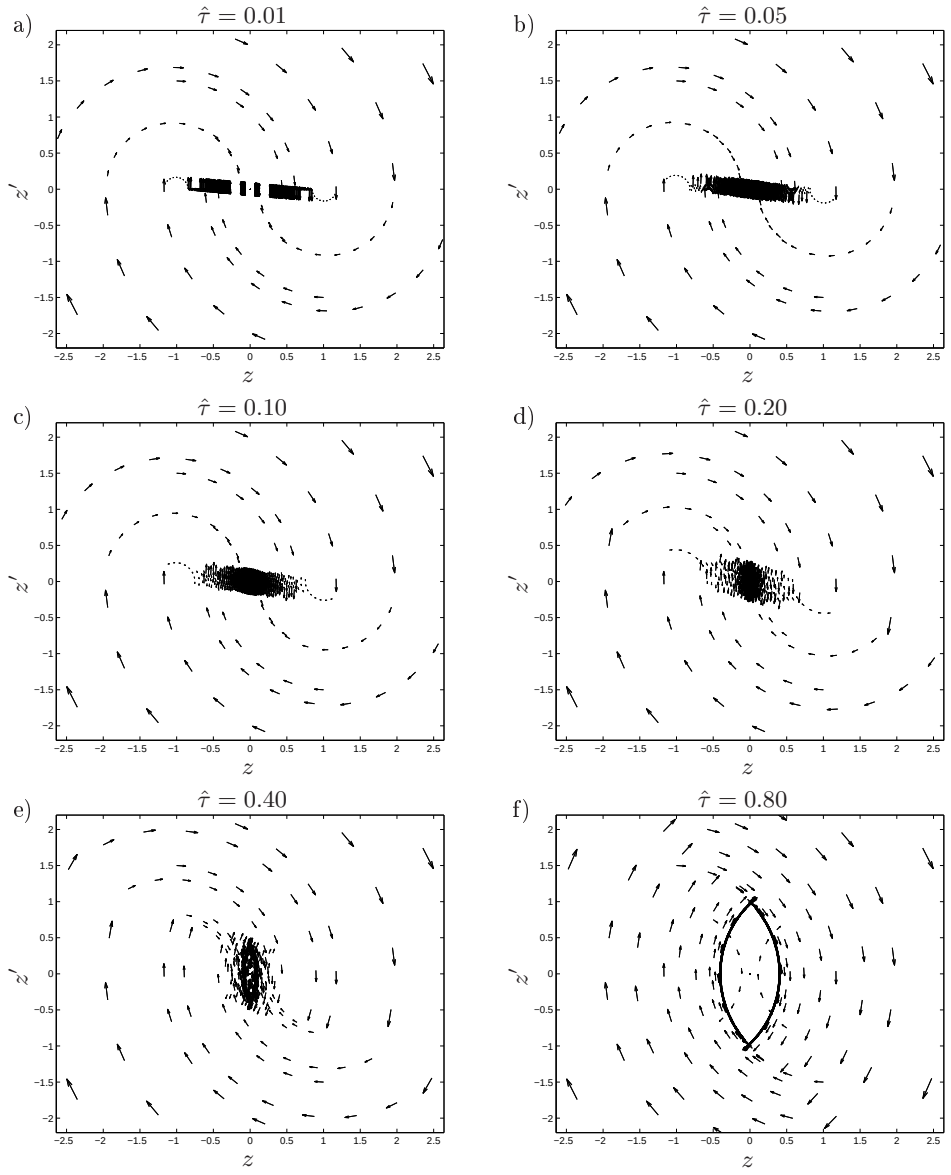

Figure 6.11: Vector fields of system in (6.21) for $\zeta = 0.03$; $p_s = 1.0$; and different delays: a) $\hat{\tau} = 0.01$; b) $\hat{\tau} = 0.05$; c) $\hat{\tau} = 0.1$; d) $\hat{\tau} = 0.2$; e) $\hat{\tau} = 0.4$; and f) $\hat{\tau} = 0.8$.

For completeness, Figure 6.11 shows the vector fields of the equivalent system in (6.21) varying $\hat{\tau}$ and considering the constant parameters $\zeta = 0.03$ and $p_s = 1.0$. The equivalent system behaviour can be described in the same way than the original one, i.e., any delay causes self–sustaining oscillations, and large delays imply

large oscillations and low frequency in the resultant limit cycle. Nevertheless, two main differences could be pointed out. (i) For small $\hat{\tau}$, the self–sustaining oscillations in the equivalent system (6.21) are larger than those exhibited for the original system in (6.19); this is due to the fact that the simplified model (6.21) involves the same damper force F_d even for very small velocities whilst in (6.19) F_d is strongly lessened as velocities tend to zero. And (ii), for small delays the equivalent system (6.21) cannot reproduce the sliding motion[7] in (6.19) just before the self–sustaining oscillations start.

6.3.2 Explicit stability analysis

We intend to investigate analytically the stability of the system in equation (6.19). For starting and just in the seek of the completeness of this thesis, we will demonstrate the system's stability when no delay is considered in the feedback loop. Such stability is expected from a physical point of view, as the nonlinear damper is a passive device which dissipates energy from the system.

Let us considerer the system (6.20) and assume $\hat{\tau} = 0$, the dynamics may be rewritten as:

$$x_1'(\hat{t}) = x_2(\hat{t}) \tag{6.23a}$$
$$x_2'(\hat{t}) = -2\zeta x_2(\hat{t}) - x_1(\hat{t}) - p_n|x_2(\hat{t})|^{\alpha} \cdot \text{sign}\left(x_2(\hat{t})\right) \tag{6.23b}$$

By using the classic stability theory for non–linear systems[8], we can assert that the system in (6.23) is a time–invariant system (autonomous system) with only one singular or equilibrium point at the origin, i.e., at $(x_1, x_2) = (0, 0)$.
Let $V(\mathbf{x}) : \mathbb{R}^2 \to \mathbb{R}$ be the Lyapunov candidate function such as:

$$V(\mathbf{x}) = \frac{1}{2}x_1^2 + \frac{1}{2}x_2^2 \tag{6.24}$$

Note that $V(\mathbf{x})$ is globally positive definite, has continuous partial derivatives and is radially unbounded in domain $\mathbb{R}^2$. Now, we will find the time derivative of $V(\mathbf{x})$ along the state trajectories of system (6.23) as follows:

$$\begin{aligned} V'(\mathbf{x}) &= x_1 x_1' + x_2 x_2' \\ &= x_1 x_2 + x_2\left(-2\zeta x_2 - x_1 - p_n|x_2|^{\alpha} \cdot \text{sign}(x_2)\right) \\ &= x_1 x_2 + -2\zeta x_2^2 - x_1 x_2 - p_n x_2 |x_2|^{\alpha} \cdot \text{sign}(x_2) \\ &= -2\zeta x_2^2 - p_n |x_2|^{\alpha+1} \end{aligned} \tag{6.25}$$

[7] See phenomena on Filippov systems in §5.4.3
[8] See the main concepts of this theory in §4.4

where the property $|x| = x \cdot \text{sign}(x)$ was used.
Due to the fact that ζ, p_n and α are all strictly positive parameters, the final expression for $V'(\mathbf{x})$ is negative for all $x_2 \neq 0$. Nonetheless, in consequence of x_1 does not appear in that expression, the derivative of $V(\mathbf{x})$ is said to be negative semi–definite. Based on Theorem 4.4, we can conclude that the system is stable; even so, the demonstration is still uncompleted because we cannot draw conclusions on asymptotic stability.
So, in what follows we will apply a powerful tool for system analysis known as invariant set theorems[9], particularly, the Theorem 4.8 known as LaSalle's Theorem.

Let $\mathcal{R}$ be the set of all points where $V'(\mathbf{x}) = 0$. Notice that $V'(\mathbf{x})$ is equal to zero only for $x_2 = 0$. Now, by substituting $x_2 = 0$ in (6.23), just a single trajectory[10] can be settled, that is $x_1 = 0$, therefore, no solution can be stay in $\mathcal{R}$ other than the trivial solution $\mathbf{x}(\hat{t}) = 0$. Thus, given that the largest invariant set $\mathcal{R}$ for the system in (6.23) is the origin, and invoking Theorem 4.8, we can conclude that the system with no delay in the damper response is *asymptotically stable*, what implies that $\mathbf{x}(\hat{t}) \to 0$ as $\hat{t} \to \infty$.

In a similar manner, we can also verify the stability conditions for the dynamically equivalent system (using dry friction) with no delay. Let us considerer now, the system (6.22) and assume $\hat{\tau} = 0$, the dynamics may be rewritten as:

$$x_1'(\hat{t}) = x_2(\hat{t}) \tag{6.26a}$$
$$x_2'(\hat{t}) = -2\zeta x_2(\hat{t}) - x_1(\hat{t}) - p_s \text{sign}\left(x_2(\hat{t})\right) \tag{6.26b}$$

As before, it is about a time–invariant system but now the equilibrium is not longer a point but a set of points (continuum). To see that, consider the dynamics of (6.26). When x_2 goes near to zero from the positive domain, i.e, $x_2 \to 0^+$, the vector field component $x_1' \to 0$ while the component $x_2'^+ \to -x_1 - p_s$. On the other side, when $x_2 \to 0^-$ then $x_1' \to 0$ while $x_2'^- \to -x_1 + p_s$.
Note that for all x_1 such that $-p_s \leq x_1 \leq p_s$, the vectors $(x_1', x_2'^-)$ and $(x_1', x_2'^+)$ are normal to x_1–axis and opposite, both pointing towards $x_2 = 0$, what implies that the dynamics from both sides close to the boundary $x_2 = 0$, in the region already indicated, will cancel each other. In other words, that set of point is an attractor of the system. We can formalise the former observation as:

$$\mathbf{x}' = 0, \quad \forall \mathbf{x} \in \mathcal{H} \quad \text{where} \quad \mathcal{H} := \{\mathbf{x} \in \mathbb{R}^2 : x_2 = 0, -p_s \leq x_1 \leq p_s\} \tag{6.27}$$

Again, let us assume the Lyapunov candidate function in (6.24) and find the time

[9] A brief description is presented in §4.4.2
[10] Solution for null dynamics ($\mathbf{x}' = 0$)

derivative of $V(\mathbf{x})$ along the state trajectories of system (6.26), as follows:

$$\begin{aligned} V'(\mathbf{x}) &= x_1x_1' + x_2x_2' \\ &= x_1x_2 + x_2\left(-2\zeta x_2 - x_1 - p_s\text{sign}(x_2)\right) \\ &= x_1x_2 + -2\zeta x_2^2 - x_1x_2 - p_sx_2\text{sign}(x_2) \\ &= -2\zeta x_2^2 - p_s|x_2| \end{aligned} \tag{6.28}$$

Since all parameters in (6.28) are strictly positives, $V'(\mathbf{x})$ is negative for all $x_2 \neq 0$. As it was previously, in consequence of x_1 does not appear in the derivative of $V(\mathbf{x})$, it is a negative semi–definite function and we cannot concluded asymptotic stability yet.
Newly, Let $\mathcal{R}$ be the set of all points where $V'(\mathbf{x}) = 0$, that is, $x_2 = 0$. Nonetheless, in the light of condition (6.27), the largest invariant set $\mathcal{R}$ for the system in (6.26) is $\mathcal{H}$. Thus, by means of the Theorem 4.8 (LaSalle's Theorem), we can assert that the system is *asymptotically stable* respect to the invariant set $\mathcal{H}$, what implies that $\mathbf{x}(\hat{t}) \to \mathcal{H}$ as $\hat{t} \to \infty$. In addition, due to $V(\mathbf{x})$ is globally positive definite and radially unbounded in $\mathbb{R}^2$, this stability is global.

Piecewise linear dynamical system

As it was pointed out earlier from the numerical analysis, we shall considerer the simplified system in (6.22) which preserves dynamic equivalence with our original system in equation (6.20). The advantage of this exchange lies in the fact that such a system can be modelled by a piecewise linear set of ODEs of the form:

$$\Psi_{\hat{\tau}} : \mathbf{x}' = A\mathbf{x} + Bu \tag{6.29}$$

where $\mathbf{x} \in \mathbb{R}^2$ is the two–dimensional state vector; A and B are the system matrices in controllable canonical form as presented in (6.30), and the switching parameter u obeys the switching rule in equation (6.31).

$$A = \begin{bmatrix} 0 & 1 \\ -1 & -2\zeta \end{bmatrix}; \qquad B = \begin{bmatrix} 0 \\ -p_s \end{bmatrix} \tag{6.30}$$

$$u = \begin{cases} 1.0, & \text{if } \; x_2(\hat{t} - \hat{\tau}) > 0, \\ -1.0, & \text{if } \; x_2(\hat{t} - \hat{\tau}) < 0, \end{cases} \tag{6.31}$$

In what follows, we will term $F_1(\mathbf{x})$ the system vector field of $\Psi_{\hat{\tau}}$ when $u = 1.0$, $F_2(\mathbf{x})$ the vector field of $\Psi_{\hat{\tau}}$ when $u = -1.0$. In addition, we will label as $\phi_i(\mathbf{x_0}, t)$ the flow generated by F_i $(i = 1, 2)$ as explained in §5.1.2, such that:

$$\frac{d}{dt}(\phi_i(\mathbf{x}, \hat{t})) = F_i(\phi_i(\mathbf{x}, \hat{t})); \quad \phi_i(\mathbf{x_0}, 0) = \mathbf{x_0} \tag{6.32}$$

Finally, note that the system's evolution in time is uniquely determined once we have defined the values of x_1, x_2, and u. Thus, in the three–dimensional space (x_1, x_2, u), we can visualise the state space as two parallel half–planes, partially overlapping wherever u can have two different values for the same pair (x_1, x_2).

To get a better understanding about how a piecewise system can be interpreted, let us considerer firstly the system with no delay, as written in equation (6.33), together with the corresponding switching rule in (6.34).

$$\Psi_0 : \mathbf{x}' = A\mathbf{x} + Bu \tag{6.33}$$

$$u = \begin{cases} 1.0, & \text{if } \; x_2(\hat{t}) > 0, \\ -1.0, & \text{if } \; x_2(\hat{t}) < 0, \end{cases} \tag{6.34}$$

The system vector fields F_1 and F_2 of the system in (6.33) for $\zeta = 0.03$ and $p_s = 1.0$ are shown in Figure 6.12, notice that both equilibrium points are stable foci (located at (0,-$p_s u$)).

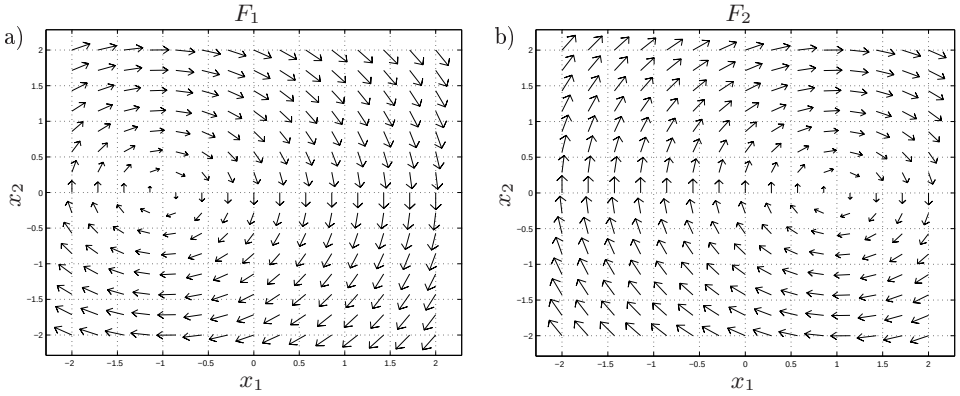

Figure 6.12: Vector fields F_1 and F_2 of the system in (6.33) for $\zeta = 0.03$, $p_s = 1.0$: a) For $u = 1.0$ and b) for $u = -1.0$.

Note however that for the system Ψ_0, the vector field F_1 is valid only when the switching rule (6.34) is satisfied, that is, for all $x_2 > 0$; in the same way that F_2 is valid only when $x_2 < 0$. Thus, the complete vector field of the piecewise linear system Ψ_0 is made of the combination of F_1 and F_2, in their respective valid domains.
The system phase plane can be partitioned into the following two regions, being

S_i the valid domain for F_i $(i = 1, 2)$:

$$\begin{aligned} S_1 &:= \{\mathbf{x} \in \mathbb{R}^2 : x_2 > 0\} \\ S_2 &:= \{\mathbf{x} \in \mathbb{R}^2 : x_2 < 0\} \end{aligned} \tag{6.35}$$

Also, we label the boundaries between the regions above as:

$$\begin{aligned} \Sigma_{12}^{+} &:= \{\mathbf{x} \in \mathbb{R}^2 : x_1 > -p_s,\ x_2 = 0\} \\ \Sigma_{12}^{-} &:= \{\mathbf{x} \in \mathbb{R}^2 : x_1 < p_s,\ x_2 = 0\} \end{aligned} \tag{6.36}$$

Note that Σ_{12}^{+} is the subset where the switching condition (6.34) is satisfied for changing from F_1 to F_2, whilst Σ_{12}^{-} is the subset where (6.34) is satisfied for going back from F_2 to F_1. Henceforth, they will be referred as *switching sets*.

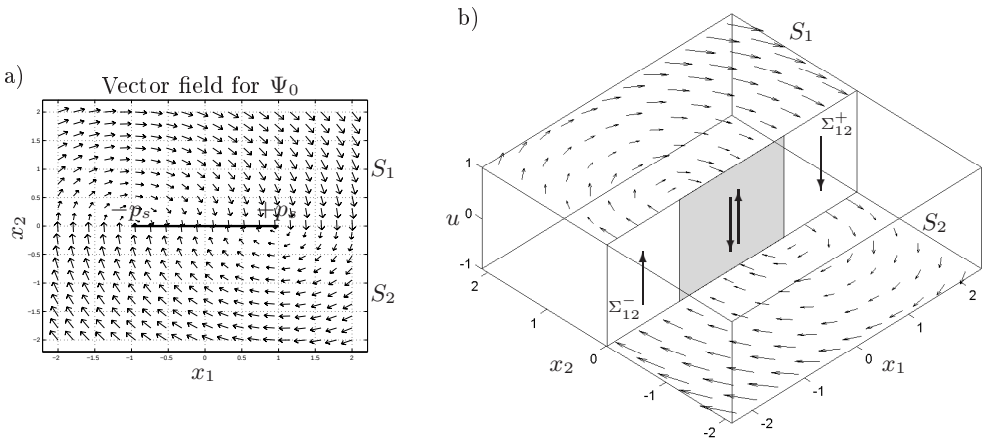

Figure 6.13: Vector fields of the piecewise linear system Ψ_0 for $\zeta = 0.03$, $p_s = 1.0$: a) (x_1, x_2)–plane; b) three–dimensional space (x_1, x_2, u).

Figure 6.13 presents the vector field of system Ψ_0. On the left, the (x_1, x_2)–plane shows that the invariant set (the equilibrium) of the system. The attractor is no longer a focus point (as it was for F_1 and F_2), but the invariant set $\mathcal{H}$ as defined before in formula (6.27). This set also corresponds to the region where the switching sets overlap each other, i.e., the set $\Sigma_{12}^{+} \cap \Sigma_{12}^{-}$. This implies that any trajectory of (6.33) lying on this intersection will stay there for all future time. From a physical point of view this indicates that, when an oscillation reaches its maximum displacement, and therefore zero velocity, but this displacement is such that the distance from the origin is less than the parameter p_s, the system will remain blocked at that position (different from zero). It is due to the system

internal forces cannot overcome the static friction inside the damper, and so, the system cannot be recentered by itself.
It is worthy of note that p_s grows as c_d does, so larger nonlinear dampers will have a longer "dead zone" where the system may remain blocked.

Similarly, Figure 6.13b shows the three–dimensional space (x_1, x_2, u). From a mathematical point of view, when the system's state hits the switching sets intersection $\Sigma_{12}^{+} \cap \Sigma_{12}^{-}$ (shadowed plane in the figure), the system keep trapped into this plane and remains continuously switching between F_1 and F_2.

Flows of the piecewise linear system

The flows ϕ_1 and ϕ_2 are well–defined on each corresponding region S_1 and S_2. To find the mathematical expression of these flows generated by the system vector fields F_1 and F_2, we have to solve each ODE in the set of equations (6.29). Let us consider a general expression for the linear model $\Psi_{\hat{\tau}}$ as:

$$\begin{aligned} x_1' &= x_2 && \text{(6.37a)} \\ x_2' &= -2\zeta x_2 - x_1 - p_s u && \text{(6.37b)} \end{aligned}$$

where u is equals to 1.0 for F_1 and equals to -1.0 for F_2. To make things easier, let us rewrite the system in (6.37) through a new set of state variables by substituting $y_1 = x_1 + p_s u$ and $y_2 = x_2$. Thus, we have:

$$\begin{aligned} y_1' &= y_2 && \text{(6.38a)} \\ y_2' &= -2\zeta y_2 - y_1 && \text{(6.38b)} \end{aligned}$$

This system can be expressed in matrix notation as $\mathbf{y}' = A\mathbf{y}$, where A is the same matrix presented in formula (6.30). For this ODE, the solution is of the form in (6.39) being $\lambda_{1,2}$ the eigenvalues of matrix A, and $C_{1,2}$ two arbitrary constants depending on the initial conditions $y_1(0) = y_{10}$ and $y_1'(0) = y_2(0) = y_{20}$.

$$y_1(\hat{t}) = C_1 e^{\lambda_1 \hat{t}} + C_2 e^{\lambda_2 \hat{t}} \tag{6.39}$$

where

$$\begin{aligned} \lambda_1 &= -\zeta + \sqrt{\zeta^2 - 1} \\ \lambda_2 &= -\zeta - \sqrt{\zeta^2 - 1} \end{aligned} \tag{6.40}$$

taking the first derivative of y_1 respect to $\hat{t}$, we get:

$$y_1'(\hat{t}) = C_1 \lambda_1 e^{\lambda_1 \hat{t}} + C_2 \lambda_2 e^{\lambda_2 \hat{t}} \tag{6.41}$$

By equaling equations (6.39) and (6.41) at $\hat{t}$=0 with the respective initial conditions, the set of equations for C_i can be found as:

$$\begin{aligned} C_1 + C_2 &= y_{10} \\ C_1\lambda_1 + C_2\lambda_2 &= y_{20} \end{aligned} \tag{6.42}$$

solving for C_1 and C_2 we get:

$$\begin{aligned} C_1 &= C_\lambda(y_{20} - y_{10}\lambda_2) \\ C_2 &= C_\lambda(-y_{20} + y_{10}\lambda_1) \\ C_\lambda &= \tfrac{1}{\lambda_1 - \lambda_2} \end{aligned} \tag{6.43}$$

replacing these constants in (6.39) and (6.41), converting back to the original parameters and taking into account that $x_1(0) = x_{10} = y_{10} - p_s u$ and $x_2(0) = x_{20} = y_{20}$, we can write the solution for x_1 and x_2 as:

$$\begin{aligned} x_1(\hat{t}) &= C_\lambda\left((x_{20} - (x_{10} + p_s u)\lambda_2)e^{\lambda_1\hat{t}} + (-x_{20} + (x_{10} + p_s u)\lambda_1)e^{\lambda_2\hat{t}}\right) - p_s u \\ x_2(\hat{t}) &= C_\lambda\left((x_{20} - (x_{10} + p_s u)\lambda_2)\lambda_1 e^{\lambda_1\hat{t}} + (-x_{20} + (x_{10} + p_s u)\lambda_1)\lambda_2 e^{\lambda_2\hat{t}}\right) \end{aligned} \tag{6.44}$$

Thus, the flows ϕ_1 and ϕ_2 can be obtained from (6.44) by substituting u according to the respective vectorial field F_1 and F_2 as follows:

$$\phi_1(\mathbf{x_0}, \hat{t}) = \begin{bmatrix} a_{11}e^{\lambda_1\hat{t}} + a_{12}e^{\lambda_2\hat{t}} - p_s \\ a_{11}\lambda_1 e^{\lambda_1\hat{t}} + a_{12}\lambda_2 e^{\lambda_2\hat{t}} \end{bmatrix} \tag{6.45a}$$

$$\phi_2(\mathbf{x_0}, \hat{t}) = \begin{bmatrix} a_{21}e^{\lambda_1\hat{t}} + a_{22}e^{\lambda_2\hat{t}} + p_s \\ a_{21}\lambda_1 e^{\lambda_1\hat{t}} + a_{22}\lambda_2 e^{\lambda_2\hat{t}} \end{bmatrix} \tag{6.45b}$$

where $\mathbf{x_0} = (x_{10}, x_{20})$ and

$$\begin{aligned} a_{11} &= C_\lambda\left(x_{20} - (x_{10} + p_s)\lambda_2\right) & a_{12} &= C_\lambda\left(-x_{20} + (x_{10} + p_s)\lambda_1\right) \\ a_{21} &= C_\lambda\left(x_{20} - (x_{10} - p_s)\lambda_2\right) & a_{22} &= C_\lambda\left(-x_{20} + (x_{10} - p_s)\lambda_1\right) \end{aligned} \tag{6.46}$$

The above explicit expressions for the flows allows us to get any trajectory in the (x_1, x_2)–plane from any initial condition.

Delay by changing the switching rule

The main idea behind the use of piecewise smooth dynamical systems for the present stability analysis, is to reap the benefits of including, in a very easy way,

the effects of the delay in the system dynamics. Thus, after some proper transformations, we can study the stability of an equivalent non–delayed system, rather than focusing on a complex delayed system. All this without compromising the integrity of the stability analysis results.

Consider the dynamics of system (6.29), note that the delay $\hat{\tau}$ is only explicit in the switching rule. The system phase plane can be partitioned into the two regions as follows:

$$\begin{aligned} S_1 &:= \{\mathbf{x} \in \mathbb{R}^2 : x_2(\hat{t} - \hat{\tau}) > 0\} \\ S_2 &:= \{\mathbf{x} \in \mathbb{R}^2 : x_2(\hat{t} - \hat{\tau}) < 0\} \end{aligned} \tag{6.47}$$

To introduce the effects of the delay in the system dynamics, observe that if a trajectory crosses one of the switching sets Σ_{12}^{+} or Σ_{12}^{-}, because of the delay, the actual switching from one system configuration to the other will occur after some time defined by $\hat{\tau}$. Indeed, switchings occur on the *delayed switching sets* $\Sigma_{12}^{\hat{\tau}+}$ and $\Sigma_{12}^{\hat{\tau}-}$ which are images of Σ_{12}^{+} and Σ_{12}^{-} under the system flow ϕ_i for some time delay. Specifically we have,

$$\begin{aligned} \Sigma_{12}^{\hat{\tau}+} &:= \{\phi_1(\mathbf{x}, \hat{\tau}),\ \mathbf{x} \in \Sigma_{12}^{+}\} \\ \Sigma_{12}^{\hat{\tau}-} &:= \{\phi_2(\mathbf{x}, \hat{\tau}),\ \mathbf{x} \in \Sigma_{12}^{-}\} \end{aligned} \tag{6.48}$$

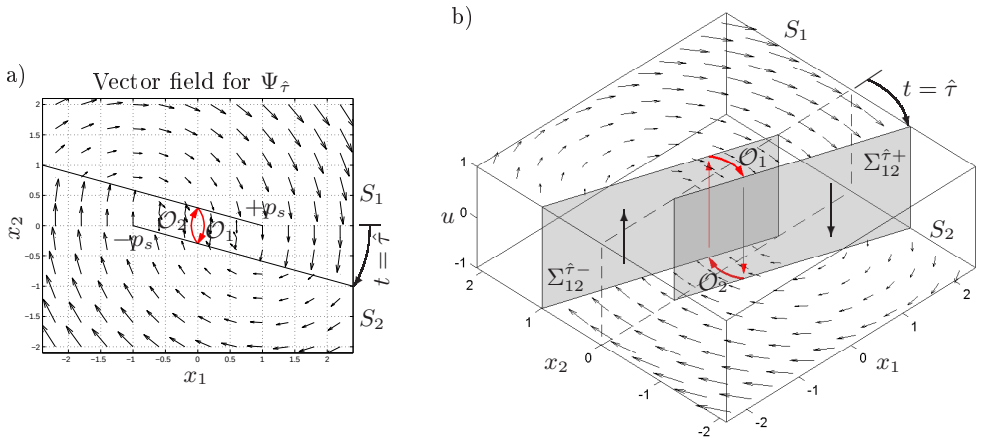

Figure 6.14: Vector fields of the piecewise linear system $\Psi_{\hat{\tau}}$ in (6.29) for $\hat{\tau} = 0.4$, $\zeta = 0.03$, $p_s = 1.0$: a) (x_1, x_2)–plane; b) three–dimensional space (x_1, x_2, u).

Thus, the original switching sets rotate clockwise around the corresponding point (0,-$p_s u$) as shown in Figure 6.14. The position of $\Sigma_{12}^{\hat{\tau}+}$ in the (x_1, x_2)–plane

can be easily determined by computing ϕ_1 for any initial condition falling on Σ_{12}^{+} and $t = \hat{\tau}$. Similar procedure can be done for $\Sigma_{12}^{\hat{\tau}-}$ by considering ϕ_2 and Σ_{12}^{-}.

Therefore, instead of analysing a delayed model, we can replace the system in (6.29) by a non–delayed system which includes the dynamic effects of the delay by moving the original switching sets towards the corresponding position as it was explained before. Thus, we can rewrite the delayed system (6.29) as follows:

$$\Psi_0 : \mathbf{x}' = A\mathbf{x} + Bu \tag{6.49}$$

$$u \mapsto \begin{cases} 1.0, & \text{if } \mathbf{x} \in \Sigma_{12}^{\hat{\tau}-}, \\ -1.0, & \text{if } \mathbf{x} \in \Sigma_{12}^{\hat{\tau}+}, \end{cases} \tag{6.50}$$

where the above switching rule establishes that, parameter u switch to 1.0 (or -1.0) only when the respective condition in (6.50) is satisfied, that is to say, when the trajectory hits $\Sigma_{12}^{\hat{\tau}-}$ (or $\Sigma_{12}^{\hat{\tau}-}$), and will remain fixed at this value until a new condition in (6.50) is satisfied. In other words, the switching parameter u changes if and only if a delayed switching set (6.48) is reached for the non–delayed system states.

This effect of the delay on the switching rule, was firstly envisaged when studying the dynamics of a delayed hysteretic relay feedback system [Colombo et al., 2007]. In that work, the authors demonstrated that the dynamics of the delayed system remain qualitatively the same as those of a system with properly constructed switching sets. In other words, all the dynamics observed in a non–delayed system with switching sets selected as (6.50) can be found in an equivalent delayed system with properly switching set as (6.31).
The prior statement is true for all $\hat{\tau} \leq \pi$. For larger delays, those researchers identified a new bifurcation phenomenon, so–called *event collision*, where the delayed switching manifold $\Sigma_{12}^{\hat{\tau}+}$ intersects the switching set Σ_{12}^{-} (or equivalently, $\Sigma_{12}^{\hat{\tau}-}$ intersects Σ_{12}^{+}). In such a case, the dynamics become much more complicated, whereby it will not be considered here, since according to us, the case is outside the core to research of this thesis. Further details can be found in the reference cited above and some references within.

Existence of limit cycle

We now investigate the existence of limit cycles induced by the delay in the damper's response. Let us note $\mathcal{O}$ the limit cycle generated by (6.49). We can then partition the limit set $\mathcal{O}$ in two different segments $\{\mathcal{O}_1, \mathcal{O}_2\}$ that corresponds

to the discrete values of u as shown in Figure 6.14. Let us define $\mathbf{x}^*$ the point on the (x_1, x_2)–plane where the limit cycle hits the switching set $\Sigma_{12}^{\hat{\tau}-}$ and $\mathbf{x}^{**}$ the analogous point where $\mathcal{O}$ hits $\Sigma_{12}^{\hat{\tau}+}$.
The part $\mathcal{O}_1$ belongs to the vector field F_1 and corresponds to the trajectory under the system flow ϕ_1 which starts on $\mathbf{x}^*$ and ends on $\mathbf{x}^{**}$ after some time named $\hat{t}^*$. Similarly, the part $\mathcal{O}_2$ belongs to the vector field F_2 and corresponds to the trajectory under the system flow ϕ_2 which starts on $\mathbf{x}^{**}$ and ends on $\mathbf{x}^*$ after some time named $\hat{t}^{**}$. We can formally define them as:

$$\mathcal{O}_1 = \left\{\mathbf{x} : \mathbf{x}(\hat{t}) = \phi_1(\mathbf{x}^*, \hat{t}),\ \forall \hat{t} \in [0, \hat{t}^*]\right\}, \tag{6.51}$$

$$\mathcal{O}_2 = \left\{\mathbf{x} : \mathbf{x}(\hat{t}) = \phi_2(\mathbf{x}^{**}, \hat{t}),\ \forall \hat{t} \in [0, \hat{t}^{**}]\right\}, \tag{6.52}$$

Geometric arguments can be used to establish the topology of the cycles that we can expect from the system. We will show that, if the limit cycle exists, it is symmetric and unimodal, i.e., characterised by only two switching events.

First, note that the equilibria of both linear systems in equation (6.49) are foci (See Fig 6.12), even more, since both systems share the same matrix A, they have the same eigenvectors, and then, the vector fields F_1 and F_2 are exactly the same but converging to different points; in other words, if the vector field F_1 is displaced through the (x_1, x_2)–plane from ($-p_s$,0) to (p_s,0), it will perfectly match the vector field F_2.
In addition, both delayed switching sets are images of a portion of the x_1–axis under the respective flow ϕ_i. Due to F_1 and F_2 have the same dynamics characteristics (the same eigenvalues), the flows ϕ_1 and ϕ_2 are equivalents, and so, the angles covered for both flows on (x_1, x_2)–plane throughout a time equals to $\hat{\tau}$ will be the same. This implies that both delayed switching sets $\Sigma_{12}^{\hat{\tau}+}$ and $\Sigma_{12}^{\hat{\tau}-}$ have the same slope. Putting together the above particularities, we can say that the system's dynamics in the phase plane are symmetrical with respect to the origin. That means, every point on the right–hand side in the plane (x_1, x_2)–plane is reflected through the origin.
Because of this symmetry, the part of the limit cycle $\mathcal{O}_1$ which corresponds to the trajectory under the flow ϕ_1 starting in a point $\mathbf{x}^*$ on $\Sigma_{12}^{\hat{\tau}-}$ should hit the other delayed switching set $\Sigma_{12}^{\hat{\tau}-}$ just in the symmetrical point with respect to the origin, what suggests that, the aforementioned point $\mathbf{x}^{**}$ cannot be other than $-\mathbf{x}^*$. Furthermore, in consequence of the symmetry and the correlation between the flows ϕ_1 and ϕ_2 pointed out before, the evolution time for completing the trajectory of the limit cycle $\mathcal{O}_1$, is exactly the same as the evolution time corresponding to $\mathcal{O}_2$. This implies that $\hat{t}^{**} = \hat{t}^*$, and that the period for a complete limit cycle $\mathcal{O}$ is $\hat{T}^* = 2\hat{t}^*$.

Thus, if the limit cycle exits and is symmetric, the following conditions must be satisfied.

- No intersection must exist between the delayed switching sets, i.e.,

$$\Sigma_{12}^{\hat{\tau}+} \cap \Sigma_{12}^{\hat{\tau}-} = \emptyset \tag{6.53}$$

- The limit cycle must hit the delayed switching sets in symmetrical points with respect to the origin, i.e.,

$$\phi_1(\mathbf{x}^*, \hat{t}) = -\mathbf{x}^* \quad \text{for some} \quad \mathbf{x}^* \in \Sigma_{12}^{\hat{\tau}-} \ \wedge \ \hat{t} = \hat{t}^* \tag{6.54}$$

$$\phi_2(-\mathbf{x}^*, \hat{t}) = \mathbf{x}^* \quad \text{for some} \quad -\mathbf{x}^* \in \Sigma_{12}^{\hat{\tau}+} \ \wedge \ \hat{t} = \hat{t}^* \tag{6.55}$$

Due to the fact that even a small delay causes no intersection between the switching sets $\Sigma_{12}^{\hat{\tau}+}$ and $\Sigma_{12}^{\hat{\tau}-}$, we can assert that the presence of delay implies the existence of the limit cycle.

In what follows, we will find some closed–form expressions for describing the main characteristics of such a limit cycle, namely, amplitude and period of oscillation.

Firstly, we will write two new equations for the switching sets in order to make easier this mathematical development.

$$\begin{aligned} \Sigma_{12}^{\hat{\tau}+} &:= \{\mathbf{x} \in \mathbb{R}^2 : x_2 = m_\Sigma x_1 - b_\Sigma, \ x_2 > 0\} \\ \Sigma_{12}^{\hat{\tau}-} &:= \{\mathbf{x} \in \mathbb{R}^2 : x_2 = m_\Sigma x_1 + b_\Sigma, \ x_2 < 0\} \end{aligned} \tag{6.56}$$

Without loss of generality, we will focus our attention on trajectories generated by the vector field F_1 along its valid domain S_1. We can define the slope and the x_2–intercept of the switching sets on the (x_1, x_2)–plane, by calculating the final states under the flow ϕ_1, for an initial condition $\mathbf{x}_{p_s} = (p_s, 0) \in \Sigma_{12}^{+}$ and an evolution time equals to the delay $\hat{\tau}$, as:

$$m_\Sigma = \frac{\phi_{1_2}(\mathbf{x}_{p_s}, \hat{\tau})}{\phi_{1_1}(\mathbf{x}_{p_s}, \hat{\tau}) + p_s}; \quad b_\Sigma = -p_s m_\Sigma \tag{6.57}$$

where the second–order subscript indicates the element position in the vector ϕ_1.

Now, we are interested in finding the conditions for which the expression (6.54) is satisfied. Let $\mathbf{x}^* = (x_1^*, x_2^*)$ be the initial condition on the plane $\Sigma_{12}^{\hat{\tau}-}$ for a trajectory under the flow ϕ_1. Because of this point falls just on the switching set,

by using equation (6.56) we can express x_2^* as function of x_1^* as $x_2^* = m_\Sigma x_1^* + b_\Sigma$. Then, the trajectory under ϕ_1 can be written as:

$$\mathbf{x}(\hat{t}) = \phi_1(\mathbf{x}^*, \hat{t}) = \phi_1((x_1^*, x_2^*), \hat{t}) = \phi_1((x_1^*, m_\Sigma x_1^* + b_\Sigma), \hat{t}) \tag{6.58}$$

If it is about a limit cycle, in accord with (6.54), there must exist an evolution time $\hat{t} = \hat{t}^*$ such that,

$$\phi_1((x_1^*, m_\Sigma x_1^* + b_\Sigma), \hat{t}^*) = -\mathbf{x}^* = (-x_1^*, -m_\Sigma x_1^* - b_\Sigma) \tag{6.59}$$

By using definition in (6.45a), we can write explicit expressions for the flow in equation (6.59) as:

$$\begin{aligned} &\phi_{1_1}((x_1^*, x_2^*), \hat{t}^*) = \\ &C_\lambda \left((x_2^* - (x_1^* + p_s)\lambda_2) e^{\lambda_1 \hat{t}^*} + (-x_2^* + (x_1^* + p_s)\lambda_1) e^{\lambda_2 \hat{t}^*} \right) - p_s = -x_1^* \end{aligned} \tag{6.60}$$

and

$$\begin{aligned} &\phi_{1_2}((x_1^*, x_2^*), \hat{t}^*) = \\ &C_\lambda \left((x_2^* - (x_1^* + p_s)\lambda_2)\lambda_1 e^{\lambda_1 \hat{t}^*} + (-x_2^* + (x_1^* + p_s)\lambda_1)\lambda_2 e^{\lambda_2 \hat{t}^*} \right) = -x_2^* \end{aligned} \tag{6.61}$$

We have to derive two new expression in order to solve the above flow for $\hat{t}^*$ and $\mathbf{x}^*$. Multiplying formula (6.60) by λ_1, subtracting (6.61) from this product, and after some known substitutions and rearrangement, we get:

$$e^{\lambda_2 \hat{t}^*} \left(-x_1^*(m_\Sigma - \lambda_1) - b_\Sigma + p_s\lambda_1 \right) = x_1^*(m_\Sigma - \lambda_1) + b_\Sigma + p_s\lambda_1 \tag{6.62}$$

In a similar manner, we can multiply formula (6.60) by λ_2 and subtract (6.61) from this product for getting:

$$e^{\lambda_1 \hat{t}^*} \left(-x_1^*(m_\Sigma - \lambda_2) - b_\Sigma + p_s\lambda_2 \right) = x_1^*(m_\Sigma - \lambda_2) + b_\Sigma + p_s\lambda_2 \tag{6.63}$$

Now, we can solve for $\hat{t}^*$ from either (6.62) or (6.63). By considering equation (6.63), we can write an explicit expression for calculating the evolution time for the half–part of the limite cycle $\mathcal{O}_1$ as:

$$\hat{t}^* = \frac{1}{\lambda_1} \ln \left(\frac{x_1^*(m_\Sigma - \lambda_2) + b_\Sigma + p_s\lambda_2}{-x_1^*(m_\Sigma - \lambda_2) - b_\Sigma + p_s\lambda_2} \right) \tag{6.64}$$

In consequence of the symmetry, the period for the whole limit cycle $\mathcal{O}$, is

$$\hat{T}^* = 2\hat{t}^* \tag{6.65}$$

Furthermore , the evolution time in (6.64) may be substituted into formula (6.62), and then, some logarithmic identities may be applied to yield:

$$\frac{x_1^*(m_\Sigma - \lambda_1) + b_\Sigma + p_s\lambda_1}{-x_1^*(m_\Sigma - \lambda_1) - b_\Sigma + p_s\lambda_1} = \left(\frac{x_1^*(m_\Sigma - \lambda_2) + b_\Sigma + p_s\lambda_2}{-x_1^*(m_\Sigma - \lambda_2) - b_\Sigma + p_s\lambda_2}\right)^{\frac{\lambda_2}{\lambda_1}} \tag{6.66}$$

The former equation is an implicit function of x_1^* and can be solved numerically. It is worthy noticing that all the other variables in formula (6.66) are known and easily derivable from the problem parameters through the closed–form expression presented before.
In this manner, also the maximum velocity developed under the limit cycle can be easily calculated from $x_2^* = m_\Sigma x_1^* + b_\Sigma$.

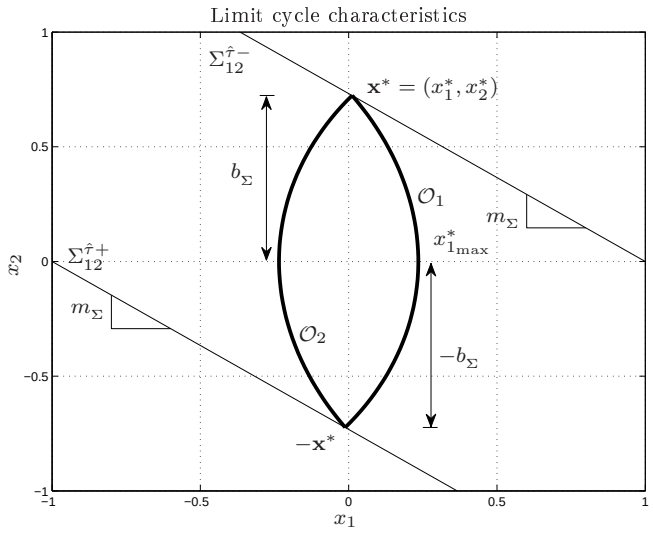

Figure 6.15: Names of the characteristics in the limit cycle.

The other important characteristic of the limit cycle is the maximum displacement reached for the oscillations. To find it, it is enough to determine the point where the velocity under the flow $\phi_1(\mathbf{x}^*, \hat{t})$ vanishes, i.e, the second component of $\phi_1(\mathbf{x}^*, \hat{t})$ must be forced to be equal to zero. Thus, from formula (6.61) we can write:

$$\begin{aligned} &\phi_{1_2}((x_1^*, x_2^*), \hat{t}) = 0 \\ &(x_2^* - (x_1^* + p_s)\lambda_2)\lambda_1 e^{\lambda_1 \hat{t}} + (-x_2^* + (x_1^* + p_s)\lambda_1)\lambda_2 e^{\lambda_2 \hat{t}} = 0 \end{aligned} \tag{6.67}$$

We can solve equation (6.67) for $\hat{t}$. Let us name this time as $\hat{t}_0^*$, which represents the needed evolution time for a trajectory starting from $\mathbf{x}^*$ under the flow ϕ_1 to

get the maximum displacement, and therefore, null velocity. Applying logarithmic properties we can rearrange (6.67) to yield:

$$\hat{t}_0^* = \frac{1}{\lambda_1 - \lambda_2} \ln \left(\frac{(x_2^* - (x_1^* + p_s)\lambda_1)\lambda_2}{(x_2^* - (x_1^* + p_s)\lambda_2)\lambda_1} \right) \tag{6.68}$$

Hence, we can calculate the maximum displacement caused in the limit cycle by evaluating the first component of the flow $\phi_1(\mathbf{x}^*, \hat{t}_0^*)$ for the evolution time previously found.

$$x_{1_{\max}}^* = C_\lambda \left((x_2^* - (x_1^* + p_s)\lambda_2) e^{\lambda_1 \hat{t}_0^*} + (-x_2^* + (x_1^* + p_s)\lambda_1) e^{\lambda_2 \hat{t}_0^*} \right) - p_s \tag{6.69}$$

The above formulas comprise the closed–form solution for defining the limit cycle of SDOF systems which include a delayed dry friction element. In consequence of the dynamic equivalence pointed out in the numerical parametric analysis in §6.3.1, we can assert that these expression are also valid for SDOF systems with delayed nonlinear viscous dampers which exhibit a damping exponent α lower than 0.2.

In what follows, we show a numeric example to clarify how these set of formulas can be applied.

Example 6.1 (*Finding the limit cycle*)**.**
Let us assume a SDOF system with the next properties: mass $m = 1000\text{Kg}$, stiffness $k = 1 \times 10^5 \text{N/m}$ and damping ratio $\zeta = 5\%$. Also, let us suppose a nonlinear viscous damper added to the system with exponent $\alpha = 0.1$ and a nonlinear coefficient $c_d = 50\text{kN}(\text{sec/m})^{0.1}$. We are interested in characterizing the limit cycle of the system, if a constant delay of 0.03sec is considered in the damper response.

To solve this problem, the fist step is to find a dimensionless expression of the form (6.21) by using the proper parameters defined in page 91. Without loss of generality, let us assume an arbitrary initial condition $x_0 = 5\text{cm}$.

$$w_n = \sqrt{\frac{k}{m}} = 10\text{rad/sec}; \qquad p_s = \frac{c_d}{m w_n^2 x_0} = 10; \qquad \hat{\tau} = w_n \tau = 0.3$$

and $z = y/x_0$, where we have named y the displacement of the SDOF system in meters.
The eigenvalues of the system can be obtained from the matrix A in (6.30) as:

$$\text{eig}(A) = \lambda_{1,2} = -\zeta \pm \sqrt{\zeta^2 - 1} = -0.05 \pm 0.9987i;$$

Then, we have to calculate the slope and the x_2–intercept of the switching sets on the (x_1, x_2)–plane in accord with formula (6.57) by using the definition in (6.45a).

$$\begin{aligned}
\phi_{1_1}((p_s,0),\hat{\tau}) &= \phi_{1_1}((10,0),0.3)\\
&= C_\lambda\left((x_{20}-(x_{10}+p_s)\lambda_2)e^{\lambda_1\hat{\tau}}+(-x_{20}+(x_{10}+p_s)\lambda_1)e^{\lambda_2\hat{\tau}}\right)-p_s\\
&= (-0.5006i)\left((0-20\cdot(-0.05-0.9987i))e^{0.3(-0.05+0.9987i)}\ \dots\right.\\
&\quad \left.+(0+(20)(-0.05+0.9987i))e^{0.3(-0.05-0.9987i)}\right)-10\\
&= 9.1156\\
\phi_{1_2}((p_s,0),\hat{\tau}) &= \phi_{1_2}((10,0),0.3)\\
&= C_\lambda\left((x_{20}-(x_{10}+p_s)\lambda_2)\lambda_1 e^{\lambda_1\hat{\tau}}+(-x_{20}+(x_{10}+p_s)\lambda_1)\lambda_2 e^{\lambda_2\hat{\tau}}\right)\\
&= -5.8226
\end{aligned}$$

therefore,

$$\begin{aligned}
m_\Sigma &= \tfrac{\phi_{1_2}(\mathbf{x}_{p_s},\hat{\tau})}{\phi_{1_1}(\mathbf{x}_{p_s},\hat{\tau})+p_s} = \tfrac{-5.8226}{9.1156+10} = -0.3046\\
b_\Sigma &= -p_s m_\Sigma = -10(-0.3046) = 3.046
\end{aligned}$$

So that, we are now able to calculate the point where the limit cycle impacts the switching sets by solving formula (6.66), as follows:

$$\tfrac{x_1^*(-0.3046-(-0.05+0.9987i))+3.046+10(-0.05+0.9987i)}{-x_1^*(-0.3046-(-0.05+0.9987i))-3.046+10(-0.05+0.9987i)} = \cdots$$
$$\left(\tfrac{x_1^*(-0.3046-(-0.05-0.9987i))+3.046+10(-0.05-0.9987i)}{-x_1^*(-0.3046-(-0.05-0.9987i))-3.046+10(-0.05-0.9987i)}\right)^{\frac{-0.05-0.9987i}{-0.05+0.9987i}} \quad \Rightarrow$$

$$\tfrac{x_1^*(-0.2546-0.9987i)+2.546+9.9875i}{x_1^*(0.2546+0.9987i)-3.546+9.9875i} = \left(\tfrac{x_1^*(-0.2546+0.9987i)+2.546-9.9875i}{x_1^*(0.2546-0.9987i)-3.546-9.9875i}\right)^{-0.995+0.099i}$$

Solving the previous formula, we get $x_1^* = 0.0092$. (hint: you can separate real and imaginary part and solve numerically for one of them.). So, we can already know the peak velocity of the limit cycle by calculating $x_2^* = m_\Sigma x_1^* + b_\Sigma = 3.0432$.

Once the point where the limit cycle hits the switching sets is found, we just need to substitute the known parameters into equation (6.64) to obtain the evolution time for the trajectory $\mathcal{O}_1$ between the delayed switching sets.

$$\begin{aligned}
\hat{t}^* &= \tfrac{1}{-0.05+0.9987i}\ln\left(\tfrac{0.0092(-0.3046-(-0.05-0.9987i))+3.046+10(-0.05-0.9987i)}{-0.0092(-0.3046-(-0.05-0.9987i))-3.046+10(-0.05-0.9987i)}\right)\\
&= 0.591
\end{aligned}$$

Thus, the period for the limit cycle can be obtained as $\hat{T}^* = 2\hat{t}^* = 1.182$.

Finally, the evolution time for the maximum displacement under the limit cycle can be calculated from (6.68) as:

$$\hat{t}_0^* = \frac{1}{1.9975i} \ln\left(\frac{(3.0432-(10.0092)(-0.05+0.9987i))(-0.05-0.9987i)}{(3.0432-(10.0092)(-0.05-0.9987i))(-0.05+0.9987i)}\right) = 0.291$$

and the corresponding maximum amplitude from (6.69):

$$\begin{aligned} x_{1_{\max}}^* = \quad & \frac{1}{1.9975i}\left((3.0432-(10.0092)\lambda_2)e^{0.291\lambda_1}\ \ldots\right. \\ & \left.+(-3.0432+(10.0092)\lambda_1)e^{0.291\lambda_2}\right) - 10 = 0.453 \end{aligned}$$

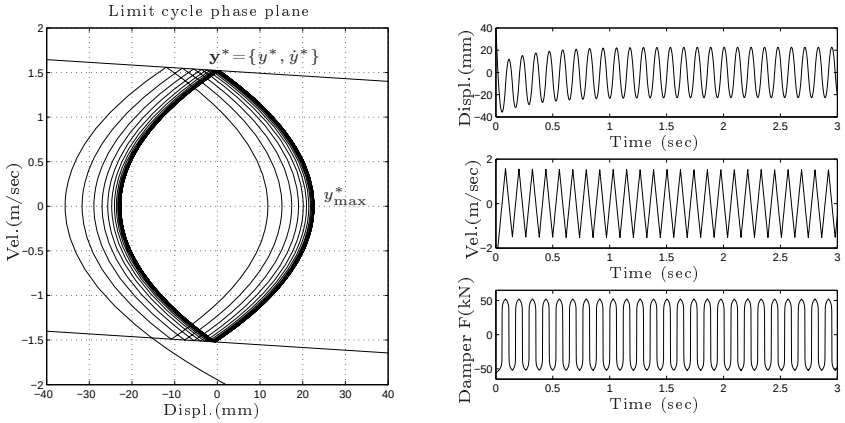

Figure 6.16: Trajectory going to the limit cycle of the system in example 6.1.

The task is almost finished, after converting back the solutions to the original parameters we will get the complete dynamic characterization of the limit cycle. Figure 6.16 shows a numerical solution which confirms the features listed below.
Peak limit cycle displacement, $y^*_{\max} = x^*_{1_{\max}} x_0 = 0.453(0.05)\text{m} = 22.65\text{mm}$.
Peak limit cycle velocity, $\dot{y}^* = x_2^* x_0 w_n = 3.0432(0.05)\text{m}(10)1/\text{sec} = 1.52\text{m/sec}$.
Period of oscillation, $T^* = \hat{T}^*/w_n = 0.118\text{sec} \quad \therefore \quad f^* = 8.46\text{Hz}$.

■

Existence of high frequency region.

At the end of section 6.3.1, we showed through numerical simulation how, for a range of small delay $\hat{\tau}$, the system exhibits a harmful phenomenon which is characterized by oscillations at high frequency. In this section we intend to define the

conditions under which that *high frequency region* takes place.

We identified a system state, named $\mathbf{x}^\star = (x_1^\star, x_2^\star)$, which corresponds to the point where the vectorial field F_1 is tangent to the switching set $\Sigma_{12}^{\hat{\tau}-}$. Similarly and by symmetry, we can also named $-\mathbf{x}^\star$ the point where the vectorial field F_2 is tangent to the switching set $\Sigma_{12}^{\hat{\tau}+}$ (See Fig. 6.17).

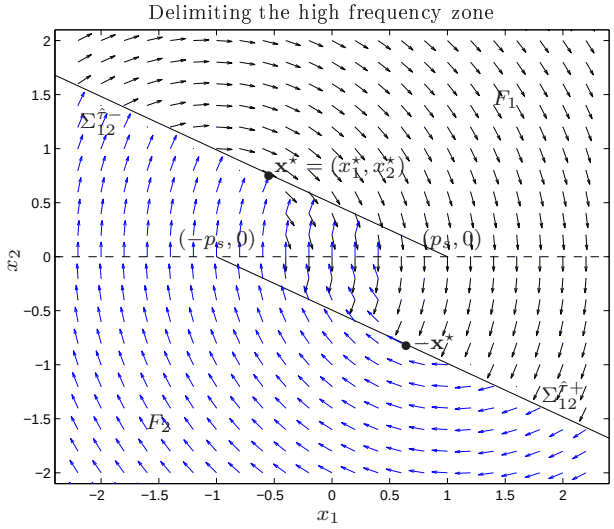

Figure 6.17: Parameter names when delimiting the high frequency zone

We found that, any trajectory under F_2 which hits the switching set $\Sigma_{12}^{\hat{\tau}-}$ in between the segment from $(x_1^\star, x_2^\star)$ to $(p_s, 0)$ (or equivalently, under F_1 the switching set $\Sigma_{12}^{\hat{\tau}-}$ in between the segment from $(-p_s, 0)$ to $(-x_1^\star, -x_2^\star)$), will remain trapped in middle of both switching sets, commuting constantly. This causes the system to increase the frequency of oscillation suddenly. In what follows, we will derive an analytical expression for finding the point $\mathbf{x}^\star$ which allows us to set boundaries of these harmful zone of self–sustained high–frequency oscillations.

As before, without loss of generality, let us concentrate on the flow generated by the system vector field F_1. We will use the concept of *isoclines*. An isocline is a line that connects all the points in a vector field which have the same gradient (slope). We are interested in finding where the vector field is tangent to the switching sets, so that, the target is to find an isocline whose gradient is equals to the switching set slope.
Let us consider the set of equations (6.37) and substitute $u = 1$ for the vector

field F_1. The target isocline can be written as:

$$f(\mathbf{x},t) = \frac{x_2'}{x_1'} = \frac{-2\zeta x_2 - x_1 - p_s}{x_2} = m_{_\Sigma} \tag{6.70}$$

Solving formula (6.70) for x_2 and equaling the resultant expression with the equation in the (x_1, x_2)–plane for $\Sigma_{12}^{\hat{\tau}-}$, we can get the intersection point between both curves (isocline and switching set).

$$x_2 = \frac{-x_1 - p_s}{m_{_\Sigma} + 2\zeta} = m_{_\Sigma} x_1 + b_{_\Sigma} \tag{6.71}$$

Thus, the point where F_1 is tangent to $\Sigma_{12}^{\hat{\tau}-}$, is easily obtained by solving the right–hand–side equation in (6.71) for x_1:

$$x_1^\star = \frac{-b_{_\Sigma}(m_{_\Sigma} + 2\zeta) - p_s}{m_{_\Sigma}(m_{_\Sigma} + 2\zeta) + 1} \tag{6.72}$$

Substituting the former value into the most right–hand part of (6.71), we get the other component as:

$$x_2^\star = m_{_\Sigma} x_1^\star + b_{_\Sigma} \tag{6.73}$$

Besides, if the so-called high frequency zone exits, the following condition must be satisfied. Otherwise, the system just goes rapidly to the limit cycle defined above without any other phenomenon arising.

- Let $\Gamma_{12}^{\hat{\tau}-}$ be the segment of the switching set $\Sigma_{12}^{\hat{\tau}-}$ between $\mathbf{x}^*$ and $(p_s, 0)$. The point $\mathbf{x}^\star$ must not fall on $\Gamma_{12}^{\hat{\tau}-}$, i.e.,

$$\begin{aligned} &\mathbf{x}^\star \notin \Gamma_{12}^{\hat{\tau}-} \\ \text{where} \quad &\Gamma_{12}^{\hat{\tau}-} := \{\mathbf{x} \in \Sigma_{12}^{\hat{\tau}-} : 0 \geq x_2 \geq x_2^*\} \end{aligned} \tag{6.74}$$

Example 6.2 (*Delimiting the high frequency zone*)**.**
Let us assume the SDOF system studied before in example 6.1, and suppose that we are now interested in finding the region where the system would develop high frequency oscillation.
It is really simple. Again the first step is to rewrite the problem in dimensionless terms and find the slope and x_2–intersect of the switching sets. We will use some parameter already calculated in the past in the reference example.
So that, substituting the known parameters into equations (6.72) and (6.73) is

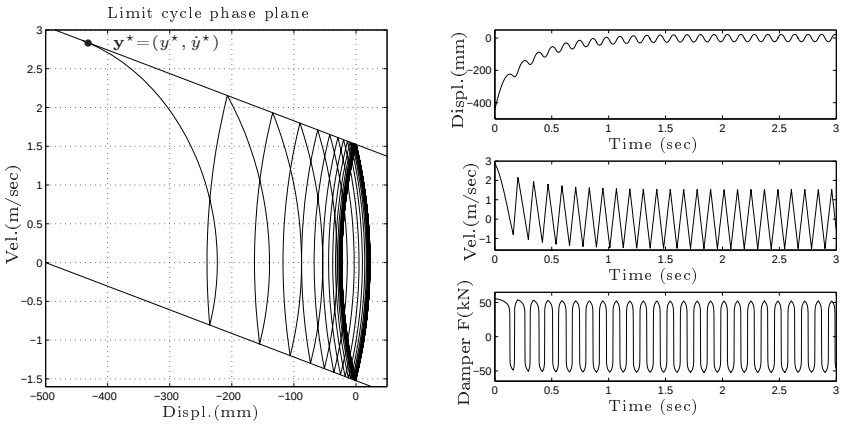

Figure 6.18: Trajectory starting just in the limit of the high frequency zone $\mathbf{x}^\star$ for the system in example 6.1.

enough to define the target region.
From equation (6.72), we have:

$$x_1^\star = \frac{-3.046(-0.3046 + 2 \cdot 0.05) - 10}{-0.3046(-0.3046 + 2 \cdot 0.05) + 1} = -8.827$$

Substituting this and the others known values into (6.73) yields to:

$$x_2^\star = -0.3046(-8.827) + 3.046 = 5.735$$

Since both $\mathbf{x}^\star$ and $\mathbf{x}^*$ fall on $\Sigma_{12}^{\hat{\tau}-}$ and $x_2^\star$ is greater than x_2^*, we can assert that this high frequency region exists and is delimited by the switching sets between $\mathbf{x}^\star$ and $-\mathbf{x}^\star$.

For concluding, Figure 6.18 shows a trajectory of the system in example 6.1 which starts just in the limit of the high frequency zone. We may convert back to the original parameters to get:
Limit in terms of displacement, $y^\star = x_1^\star x_0 = -8.827(0.05)\text{m} = -441.3\text{mm}$.
Limit in terms of velocity, $\dot{y}^\star = x_2^\star x_0 w_n = 5.735(0.05)(10)\text{m} = 2.87\text{m/sec}$.

■

In the next chapter, we shall present experimental result from a campaign on Real Time dynamic substructuring testing considering a full–scale passive–controlled structure which includes a large–scale non–linear viscous fluid damper. Those results exhibit the dynamic phenomena comprehensively described throughout this chapter.

Chapter 7

Case Study

Contents

In this chapter we present the description, analysis and experimental set–up of a Real–Time Dynamic Substructuring Test of a civil structure provided with a passive seismic protection system. Particulary, we considered a building with two nonlinear viscous dampers attached at the first floor to control the vibrations induced by seismic excitations. Our interest is to show how this kind of test can be exploited for the assessment and design of current and new protection systems in earthquake engineering. We believe that this method is very suitable when an accurate mathematical model of the protection device is not yet available.
To evaluate the advantages of real–time dynamic substructuring simulation on testing large–scale energy dissipation devices, an experimental campaign was accomplished in the Earthquake and Large Structures Laboratory at University of Bristol (UK). This experimental activities were carried out in closed collaboration with professors David Wagg and Simon Neild from the Department of Mechanical Engineering of that University.

7.1 Description of the controlled structure

Fluid viscous dampers (FVDs) are a type of supplemental damping devices able to reduce vibrations in structures. Linear fluid viscous dampers have been widely investigated, either experimentally or numerically, because they can be simply modelled through a linear force–velocity constitutive law. However, they can develop excessive damper forces when large structural velocities occur. More recently, both researchers and professional engineers have focused their attention on non–linear FVDs not only to limit the damper forces at large structural velocities but also because of their ability to dissipate more energy at lower velocities [Lee and Taylor, 2001].
This thesis deals with a passive control system installed on a symmetric 3–storey one–bay steel framed building with reinforced concrete slabs. The system is composed by chevron–type braces and non–linear passive viscous fluid dampers (in horizontal position) linking the brace to the hosting structure. As shown in Figure 7.1, two of this braces are placed at the first floor on opposite building's sides. We only considered one–directional base excitation along the axis where the dampers are placed.

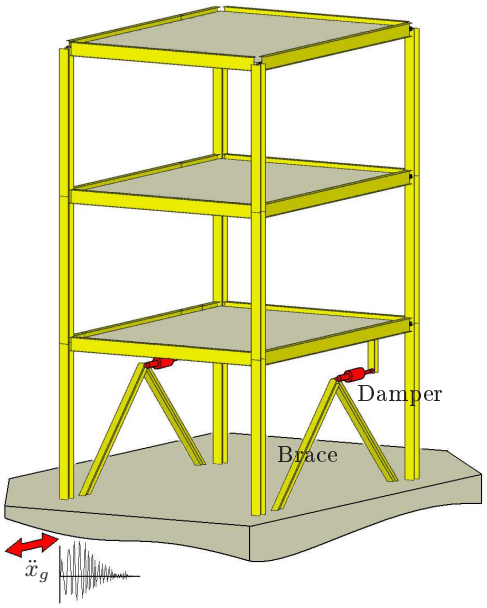

Figure 7.1: Sketch of the passive controlled system analysed.

A supplemental energy dissipation system is optimally designed to absorb vibration energy from the hosting system, thereby reducing energy dissipation

demand on the structure. And so, a typically and widely accepted approach when designing passive control systems is to consider that the structure remains in the linear range. In addition, if the non–linearity and complex behaviour of the viscous dampers are considered, those devices may be easily identified as the critical component of the whole structural system.
Thus, in order to set up the RTDST test, the system is split up into two subsystems, keeping the dampers as the physical substructure while the remains of the structure is modelled numerically. Also, in consequence of the symmetry from both the structural configuration and load, the structural response was expected to be symmetrical. So that, despite the original passive controlled structure has actually two dampers, a RTDST which takes into account just one damper is enough to emulate properly the system, as long as due cares were taken in the subsystems' interaction interface. Namely, the force fed back to the numerical substructure was twice the measured force from the physical substructure.

This symmetry–based simplification is supported not only on several exhaustive numerical simulations but also through a large number of experimental data obtained form an experimental campaign carried out in Italy under the RELUIS project[1], where researchers tested a symmetric and passive controlled structure under earthquake base excitations by using an one–directional shaking table (See e.g. [Ponzo et al., 2008, Sorace and Terenzi, 2008] and some references therein). Most of those results exhibit the symmetrical structural behaviour assumed throughout this thesis.

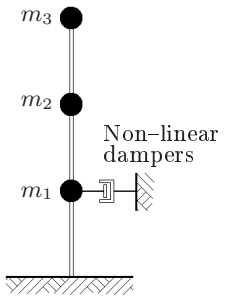

Figure 7.2: Simplified numerical model of the structural system.

According to this, a simplified lumped–mass model of the whole structure has been employed as the numerical substructure. At the beginning we consider such

[1]See more information of this project in www.reluis.it

a simple model because it is the fastest numerical substructure we can get. Once the delay issues are overcome, we can try more complete, complex and of course slower to be calculated numerical models. The dampers are included as a single external force (see Figure 7.2), which will be updated in accord with the measurements taken from the damper during the simulation.
The classical expression for describing this model is given by the ordinary differential equation (ODE) in formula (7.1) where: **M, K, C** represent the structural mass, stiffness and damping matrices; $\ddot{x}_g(t)$ indicates the base excitation; $U(t)$ is twice the force in the damper and X, $\dot{X}$ and $\ddot{X}$ are the structural responses namely: displacement, velocity and acceleration, respectively. The coefficients of the damping matrix **C** have been derived from those of **M** and **K** imposing a mass and stiffness proportional damping (Rayleigh damping) with modal damping ration equal to 3%.

$$\mathbf{M}\ddot{X}(t) + \mathbf{C}\dot{X}(t) + \mathbf{K}X(t) = -\mathbf{M}\ddot{x}_g(t) + \mathbf{L}U(t) \tag{7.1}$$

being:

$$\mathbf{L} = \begin{bmatrix} 0 & 0 \\ -1 & 0 \\ 0 & -1 \end{bmatrix}, \quad \mathbf{M} = \begin{bmatrix} 5430.2 & 0 & 0 \\ 0 & 5430.2 & 0 \\ 0 & 0 & 5430.2 \end{bmatrix} \text{ (Kg)}$$

$$\mathbf{C} = \begin{bmatrix} 9.817 & -2.878 & -0.625 \\ -2.878 & 9.192 & -3.508 \\ -0.625 & -3.504 & 6.313 \end{bmatrix} \times 10^3 \ (\mathrm{N}\tfrac{\mathrm{sec}}{\mathrm{m}})$$

$$\mathbf{K} = \begin{bmatrix} 12.091 & -6.046 & 0 \\ -6.046 & 12.091 & -6.046 \\ 0 & -6.046 & 6.046 \end{bmatrix} \times 10^6 \ (\tfrac{\mathrm{N}}{\mathrm{m}})$$

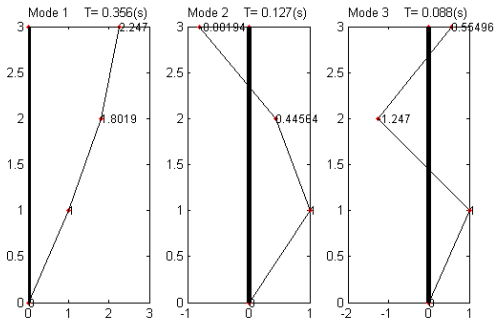

Figure 7.3: Structural mode shapes.

7.1.1 Damper description

The dampers used in these tests were provided by FIP–Industriale[2]. They are characterized by a suitably designed hydraulic circuit which controls the passage of the viscous fluid from one chamber to the other, therefore the energy dissipation is caused by the relative movement between the two damper ends when the fluid is forced to move through the hydraulic circuit. Both ends of the dampers are usually provided with two spherical hinges assuring perfect alignment between piston and cylinder, in spite of possible mounting inaccuracies during installation. In consequence of the non–linear constitutive law in these dampers, an almost constant force is developed over an important range of velocities.

Figure 7.4: Non–linear viscous damper used in the tests.

Figure 7.4 shows a picture of one of the four viscous dampers available for the tests. They are characterized by a peak force up to 50KN, stroke ±25mm and peak velocity about 0,3m/sec. Additionally, their non–linear constitutive force–velocity law may be described by means of equation (7.2) where $\dot{x}_d$ represents the relative velocity between the ends of the damper in meters per second; c_α is the nonlinear damping coefficient equal to $60\text{kN}(\frac{\text{sec}}{\text{m}})^{0.15}$ and α is the velocity exponent equals to[3] 0.15.

$$F_D = c_\alpha \left|\dot{x_d}\right|^\alpha \text{sign}(\dot{x_d}) \qquad \text{(kN)} \tag{7.2}$$

As it will be shown later, the last relationship was verified through several experimental characterization tests performed at the Structural Engineering Laboratory of the University of Naples Federico II (See §7.3.1).

7.2 Numerical simulations

First of all, we completed several numerical simulations of the substructured system described above. We build a full numerical substructured systems in ©simulink[4]. In this model the physical substructure is replaced by a numerical approximation of the damper response as shown in Figure 7.5. As well, a constant

[2]Italian company specialized in design and manufacture of technical products and seismic protection devices for the large-scale construction (See: www.fip-group.it)

[3]Model provided by manufacturer.

[4]Simulink is a registered trademark of The MathWorks, Inc. www.mathworks.com

delay transport is added to the damper force which is fed back to the numerical substructure. This to take into account the actuator dynamics, as explained in the former chapters.

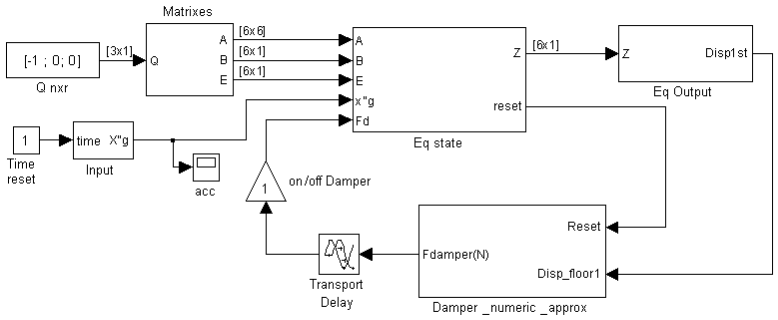

Figure 7.5: Simulink model of the full numerical substructured system.

We consider small delays (between 1 and 4 milliseconds) and run this full–numerical substructured model under both periodic and seismic loads. All the simulations exhibited delay–induced self–sustained oscillations, as described in Chapter 6 for the case of non–linear systems.
In what follows, we present some pictures of the system response under earthquake loads considering a delay equals to 3msec. Figure 7.6 shows the displacement and velocity time histories of the first floor of the structure in (7.1), along with the numerical approximation of the damper force and the phase plane plot.

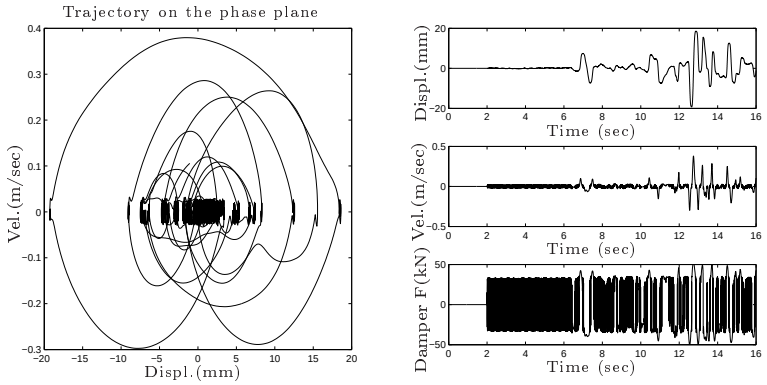

Figure 7.6: Substructured system outcomes for the full numerical substructuring test considering the earthquake 0187.

As explained in previous Chapters, by considering a delay in the feedback loop,

the equilibrium of the system (0,0) becomes unstable and even a small perturbation causes the system to go away from it. The plots evidence how the system goes to the limit cycle (self–sustained oscillations) just before a the earthquake starts (at 2sec in the simulation). Note that even a very tiny displacement at early stages of the system response cause suddenly the limit cycle, and then, very high forces in the damper switching between ± the maximum force. Figure 7.7 shows a zoom–window for the first second just before the external excitation starts. In the other hand, Figure 7.8 presents the steady–state system response from the analytical expressions given along Section 6.3, where the dimensionless parameter were obtained as explain in Example 6.1.

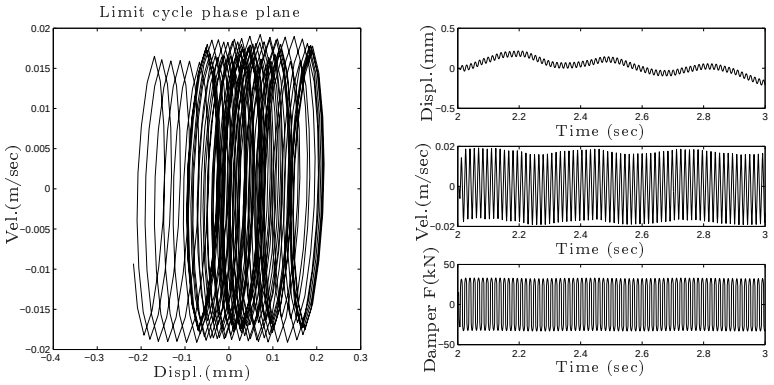

Figure 7.7: One–second zoom window of the substructured system outcomes for the full numerical substructuring test considering the earthquake 0187.

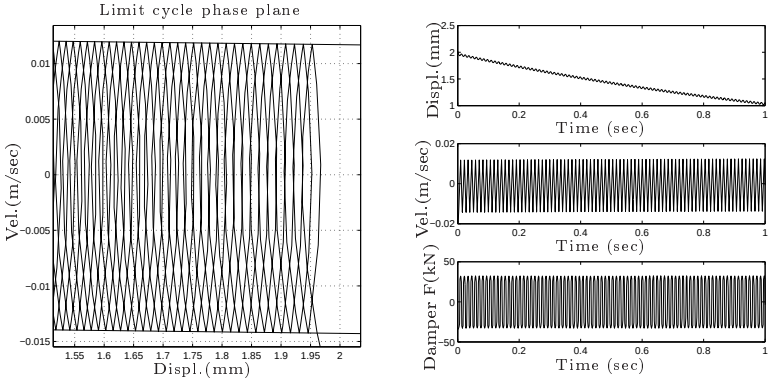

Figure 7.8: Analytical steady–state substructured system responses for the full numerical substructuring test considering the earthquake 0187.

The last figures clearly shows an good agreement between the numerical simulations and the analytical results. In spite of some differences can be found between the displacement time histories, they can be neglected as Figure 7.8 does not consider any external excitation, but just a not null initial condition. That is why these differences arise. From the analytical expressions comes a limit cycle (oscillations as time tends to infinite) with the next characteristics: Frequency=83.44Hz; Peak velocity=$\pm$0.013m/sec; Peak damper force=$\pm$33kN.

7.3 Experimental activities

7.3.1 Damper characterization test

The non–linear viscous fluid dampers were first characterized through a detailed experimental campaign performed at the Structural Engineering Laboratory of the University of Naples Federico II, these experimental tasks were carried out in collaboration with Dr. Mariacristina Spizzuoco from the Department of Structural Engineering in this university. A self–equilibrated testing apparatus was designed and assembled ad–hoc for these tests, it is equipped with a dynamic actuator having a stroke of 250mm and a dynamic horizontal load of up to 1200kN in tension and 440kN in compression within a frequency range from 0 to 5Hz. The external cylinder of the actuator is firmly connected to a main rigid steel plate through four steel bars with a diameter of 24mm each; one damper's end is connected to the actuator through the interposition of a 100kN load cell while the other end is firmly connected to an secondary smaller rigid steel plate which is jointed to the main plate by four rigid steel tubes having an external diameter of 114.3mm and a thickness of 8mm (see Figure 7.9).

The hydraulic actuator applies the load to the device along its longitudinal axis. Table 7.1 lists the channels acquired during the experimental tests whereas Figure 7.10 shows the position of the transducers: a 100kN load cell (F1) measures the force acting on the damper; a horizontal displacement transducer (D2) measures the displacement of the actuator's piston and is used for its displacement–based controller; an additional horizontal displacement transducer (D3) with 50mm stroke was mounted to measure the relative displacement of the damper; and finally, two temperature transducers were installed on the outer surface of damper's body by locking two sensible stainless steel small plates (25mm$\times$25mm) able to house the thin rods of the transducers.

The experiments aiming at characterizing the non-linear viscous dampers has been planned according to both the European Standard prEN 15129 [Eur, 2007] and to the section 11.9.6 (Fluid viscous devices) of the new Italian Technical Regulations for Constructions [Ita, 2008]. According to the normative, two different

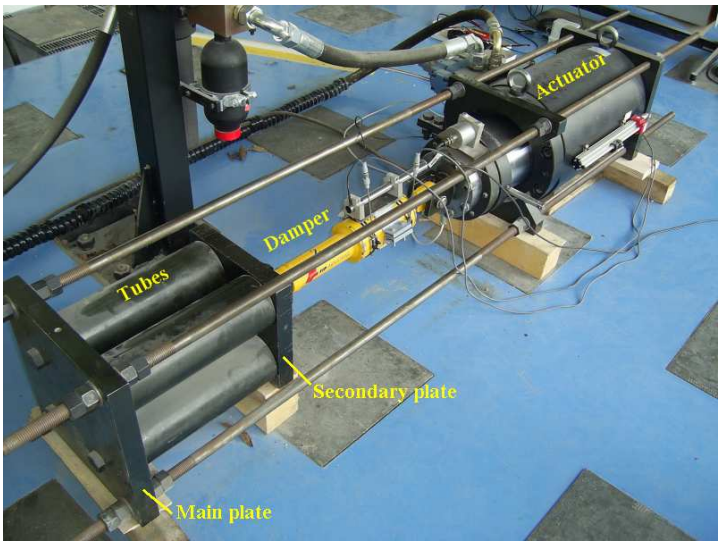

Figure 7.9: Viscous fluid damper mounted in the testing equipment.

Channel	Transducer
F1	Load cell
D2	LVDT
D3	LVDT
T4	Temperature
T5	Temperature

Table 7.1: Acquisition channels and transducers in detailed.

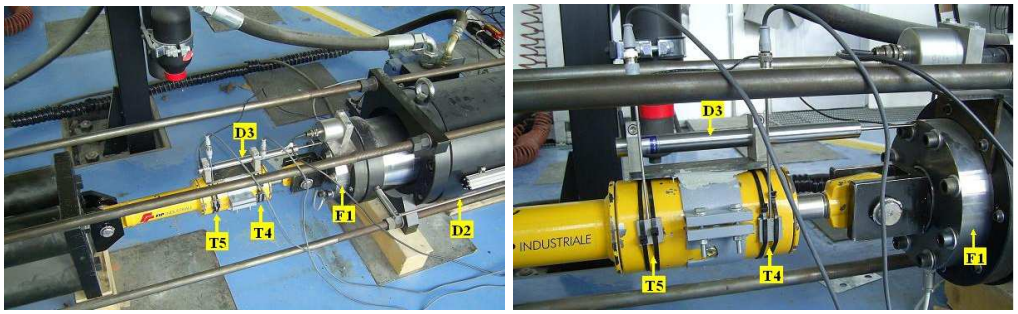

Figure 7.10: Transducers and recording channels.

types of dynamic tests were planned to be imposed on the dampers: dynamic constitutive law tests and dynamic damping efficiency tests. Damper temperature also had to be monitored, we recorded it for three tests at two locations on the main body of the device, considering a period from 5min before until 15min after each test.
In constitutive law tests, cycles with a constant velocity displacement are to be imposed (see table 7.2). Thus, four constant–amplitude triangular displacement cycles are applied to the damper considering five different constant velocities (3, 75, 150, 225 and 300mm/s) and two different displacement amplitudes (10 and 20mm), for a total of 10 dynamic tests. In damping efficiency tests, harmonic displacement cycles are to be imposed (see table 7.3). Five constant–amplitude sinusoidal displacement cycles ($x(t) = A\sin(2\pi ft)$) are imposed to the specimen assuming five different frequencies f (0.5, 1.5, 2.0, 3.0 and 4.0Hz) and three different displacement amplitudes A (10, 15 and 20mm), for a total number of tests equal to 10.
It is worth to note that tests at higher velocities and frequencies and larger displacement amplitude are not considered because of the intrinsic limits of the actuator. Furthermore, 20 tests were considered sufficient to characterize the mechanical behaviour of the viscous dampers. More details about who the test were selected in accord with the normative can be found in [Spizzuoco et al., 2008].

	Test	Amplitude (mm)	Velocity (mm/sec)	Number of cycles
Constant Velocity Tests	1	10	3	4
	2	10	75	4
	3	10	150	4
	4	10	225	4
	5	10	300	4
	6	20	3	4
	7	20	75	4
	8	20	150	4
	9	20	225	4
	10	20	300	4

Table 7.2: Dynamic constitutive law tests.

Tests results

The effective force vs. displacement cycles obtained during some of the imposed constant velocity tests are given in Figure 7.11. Besides, in Figure 7.12 the temperature recorded in the damper at two locations of the main body, one towards the moving end of the device and the other one towards the fixed end, is plotted for 1200sec, i.e. approximately 5min before and 15min after the imposed constant

	Test	Amplitude (mm)	Frequency (Hz)	Number of cycles
Harmonic Velocity Tests	11	10	0.5	5
	12	10	1.5	5
	13	10	2.0	5
	14	10	3.0	5
	15	10	4.0	5
	16	15	0.5	5
	17	15	1.5	5
	18	15	2.0	5
	19	20	0.5	5
	20	20	1.5	5

Table 7.3: Dynamic damping efficient tests.

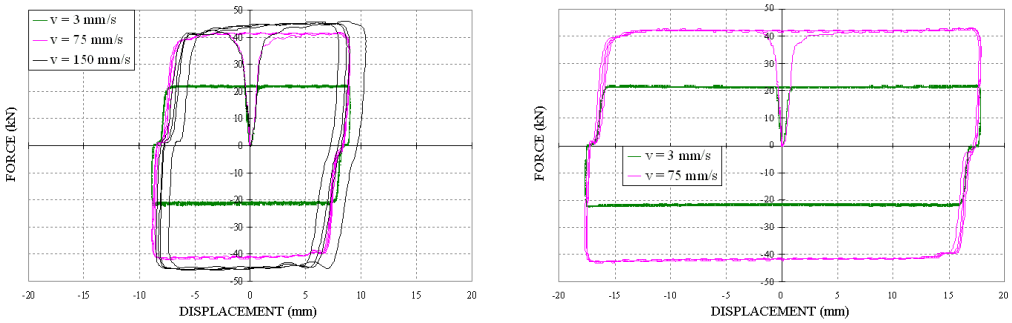

Figure 7.11: Force–displacement cycles from constant velocity tests at 10mm amplitude on the left, 20mm amplitude on the right.

velocity test at 75mm/sec and 20mm amplitude. Figure 7.13 presents the effective force vs. displacement cycles relative to the imposed harmonic displacement tests: the shape of the loops are those typical of a nearly–friction force–velocity viscous damper constitutive equation.

Now, in order to characterize the damper from the tests data, we looked for the coefficients which satisfy equation (7.2). The experimental values of c_α and α have been derived through a simple procedure using the maximum force and velocity achieved during all the tests. Figure 7.14 shows on a logarithmic diagram, the maximum experimental forces F_{max} developed during the imposed constant velocity tests as function of the constant velocities v. The red experimental points correspond to the tests at 10mm amplitude while the brown points represent the tests at 20mm amplitude. The linear regression curve of the above experimental

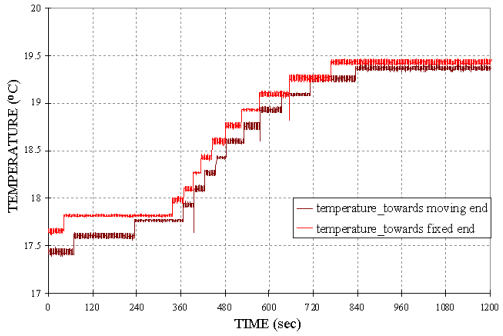

Figure 7.12: Recorded temperatures from constant velocity test at 20mm amplitude and 75 mm/s.

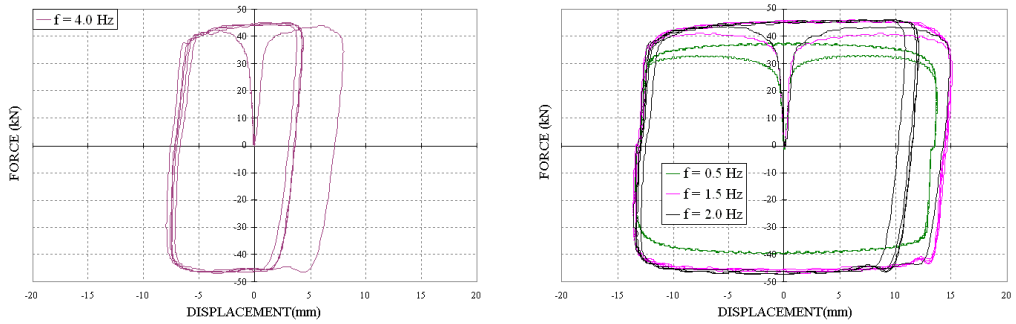

Figure 7.13: Force–displacement cycles from harmonic displacement tests at 10mm amplitude on the left, 15mm amplitude on the right.

points is drawn in black line and has the following expression:

$$\log(F_{max}) = 1.2645 + 0.190 \log(v) \tag{7.3}$$

As well, Figure 7.14 shows on a second logarithmic diagram the maximum experimental forces F_{max} developed during the imposed harmonic displacement tests as function of the maximum velocities ($v_{max} = 2\pi f A$), the red experimental points correspond to the tests at 10mm amplitude while the pink and brown points represent the tests at 15mm and 20mm amplitude, respectively. The linear regression curve of the these experimental points is drawn in black line on the respective picture and can be written as:

$$\log(F_{max}) = 1.4171 + 0.118 \log(v) \tag{7.4}$$

A mean linear regression curve, shown in both sides of Figures 7.14 in blue color,

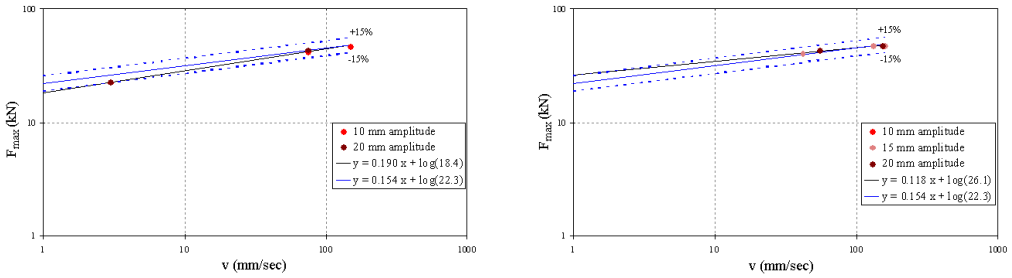

Figure 7.14: Constitutive law of the viscous damper from constant velocity tests on the left and harmonic displacement on the right.

can be obtained by taking mean values of the slopes and intersections point from the linear regression curves derived above. This mean curve is given in equation 7.5:

$$\log(F_{max}) = 1.3475 + 0.154 \log(v) \tag{7.5}$$

The mean slope represents the mean value for the exponent in expression 7.2 being α=0.154, while the mean value of the intersection with the ordinate–axis provides a mean value of the damping coefficient of the damper: $c_\alpha = 10^{1.3475} = 22.3kN/(\frac{sec}{mm})^{0.154} = 62.7kN/(\frac{sec}{m})^{0.154}$.

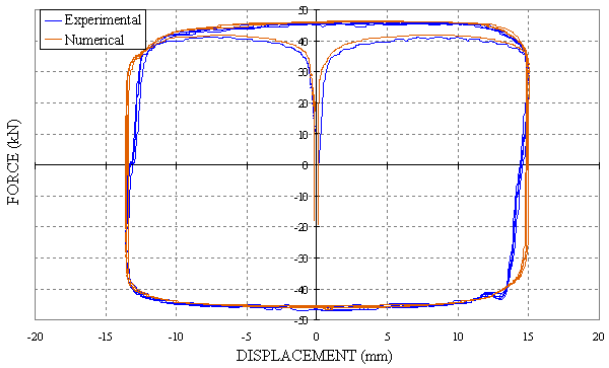

Figure 7.15: Experimental vs. numerical force–displacement cycles from harmonic displacement test at 1.5Hz×15mm.

Therefore, the experimental values closely match those declared by the man-

ufacturer, that is, the mean linear regression curve practically corresponds to the design constitutive law provided by the manufacturer. Such experimental coefficients have been assumed to obtain the numerical force vs. displacement cycles able to nearly fit the experimental data as shown in Figure 7.15 for the harmonic displacement test at 1.5Hz×15mm. Finally, Figure 7.14 also shows that all the experimental points are included between two blue dashed lines representing the tolerance limits defined by the Codes, that is the differences between the experimental values of the maximum output force F_{max} and the design values (that is to say the constitutive law) are less than the tolerance limit of $\pm 15\%$.

In this manner, the tested devices demonstrate to satisfy both the European Standard and the new Italian Technical Regulations for Constructions, for all the types of experimental tests required by them.

Non–linear viscous damper numerical model.

In order to get a more realistic numerical model of the non–linear viscous damper in terms of velocity–force behaviour, we change the model in (7.2) provided by the damper's manufacturer into the Dahl model in formula (7.6), which is able to capture the actual velocity–force dependence more accurately.

$$\begin{aligned} F(t) &= \kappa_x \dot{x}(t) + \kappa_w w(t) \\ \dot{w}(t) &= \rho \left(\dot{x}(t) - |\dot{x}(t)| \, w(t) \right) \end{aligned} \tag{7.6}$$

where:

$F(t)$: is the damper force;
$\dot{x}(t)$: is the relative damper velocity;
$w(t)$: is the hysteretic variable;
κ_x: is the viscous coefficient = 128098.06 ($\mathrm{N}\frac{\mathrm{s}}{\mathrm{m}}$);
κ_w: is the friction coefficient = 27900.5 (N); and
ρ: is the parametric constant = 811.99 ($\frac{1}{\mathrm{m}}$).

The parameters κ_x, κ_w and ρ were tuned according to the methodology presented in [Aguirre et al., 2008] in such a way that the model matches closely the damper behaviour recorded for the sinusoidal tests. To evaluate the correctness of these parameters and the effectiveness of this model, Figure 7.16 shows some time histories and force velocity cycles comparing the measured response against both the old and new numerical models.

In spite of the tuned Dahl model behaves better than the model in (7.2), more accurateness was not possible due to the strong perturbation in the force–velocity cycles caused by the backlash phenomenon, i.e, the loose in both damper ends when linking it with the transfer system.

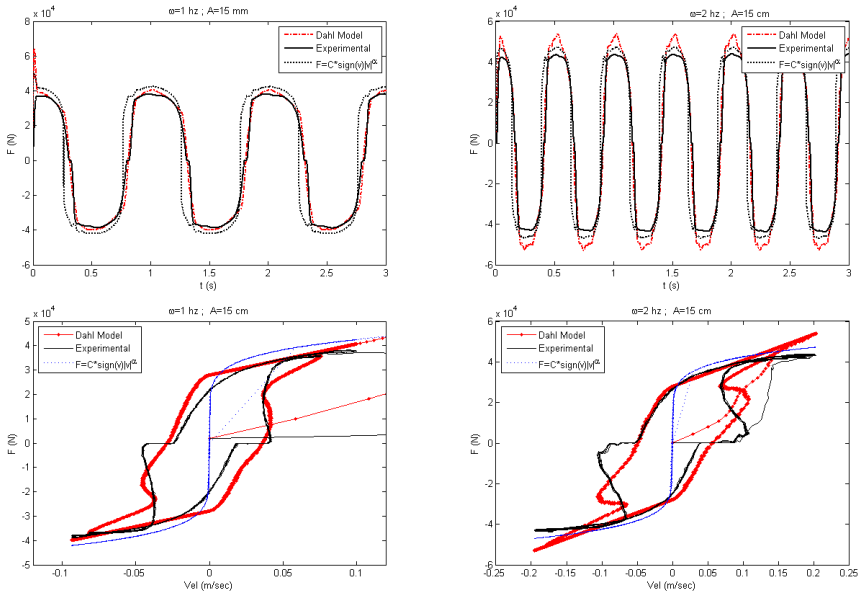

Figure 7.16: Damper's Dahl model approximation.

7.3.2 Prediction scheme

Keeping real–time behaviour is one of the principal issues to be managed while a real–time substructuring test is being carried out. It is essential to take care of the command signals' delays to prevent the overall instability caused by them.

Delay estimation.

Once the experimental rig was set up (see figure 7.25), several tests were accomplished to measure the delay by considering different kind of signals. The delay between the actual command signal (target displacement to be follow for the actuator) and the current displacement signal (measured displacement) was estimated by using two different methodologies. Namely, *zero crossing*, in which the acting delay is estimated by taking the median over all the instantaneous delays measured along the whole signal when trajectory crosses zero; and *cross correlation function* which is a measure of similarity between two signals as a function of a time–lag applied to one of them, so it provides a overall delay estimation at the time–lag where the two signals are maximally correlated. Figure 7.17 shows the test time history, the synchronization plot and the force–displacement cycles when the command signal is a 2Hz sine wave with amplitude equals to 15mm. The delays estimated for all sinusoidal tests are presented in table 7.4.

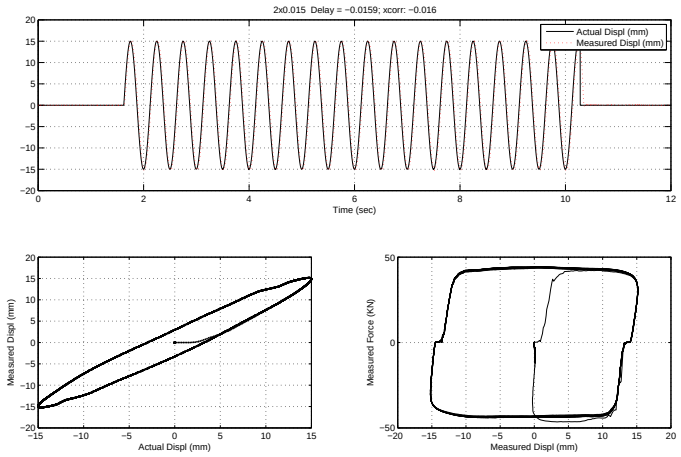

Figure 7.17: Sine wave test 2Hz at ±15mm: time history, synchronization plot and force-displacement cycles.

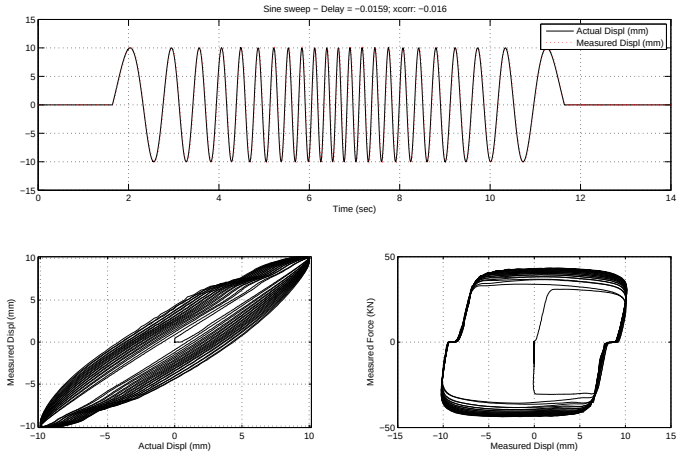

Figure 7.18: Sine sweep test from 0.5Hz to 4.0Hz at ±10mm: time history, synchronization plot and force-displacement cycles.

In light of the frequency range evaluated, the delays were estimated encircling 15∼16msec. Some sinusoidal sweep test were evaluated too. A wave at ±10mm which speeds from 0.5Hz up to 4.0Hz in 5sec and goes back to 0.5Hz in 5sec more, was considered too. Figures 7.18 and 7.19 show the test time history,

Amplitude (mm)	**Frequency** (Hz)	**Measured delay (msec)**	
		(X–corr)	(zero–X)
1.0	0.5	-14	-18.90
5.0		-16	-15.27
10.0		-15	-13.76
15.0		-16	-16.83
20.0		-13	-14.19
1.0	1.0	-16	-15.02
5.0		-15	-15.01
10.0		-15	-14.52
15.0		-15	-14.91
20.0		-15	-15.23
1.0	2.0	-16	-14.01
5.0		-15	-14.49
10.0		-15	-14.99
15.0		-16	-15.98
20.0		-18	-19.63
5.0	3.0	-16	-15.75
10.0		-16	-16.32
15.0		-20	-20.47

(X-corr) Cross correlation function ; (zero-X) Zero crossing

Table 7.4: Delays estimated for sinusoidal wave form tests.

the synchronization plot, the force–displacement cycles, the zero crossing delay measurements and its corresponding histogram. As it was expected, the higher frequency the larger delay, furthermore, it is worthy noticing that there exist different delays for the load and unload branches (which is more evident for higher frequencies), it may be due to the connection loose (backlash behaviour) which incorporates an additional damper reaction delay.

Additionally, several tests were performed predicting the displacement of the first floor in the structural model described in §7.1 under seismic load. Figure 7.20 shows time history and coherence plot for the whole system tracking a displacement signal, the picture includes measurement of the actuator displacement as well as the damper ends' relative displacement. Here is much clearer the delay effect in the damper's response caused by the connection loose. The zero crossing delay measurements and its corresponding histogram are shown in figure 7.21.

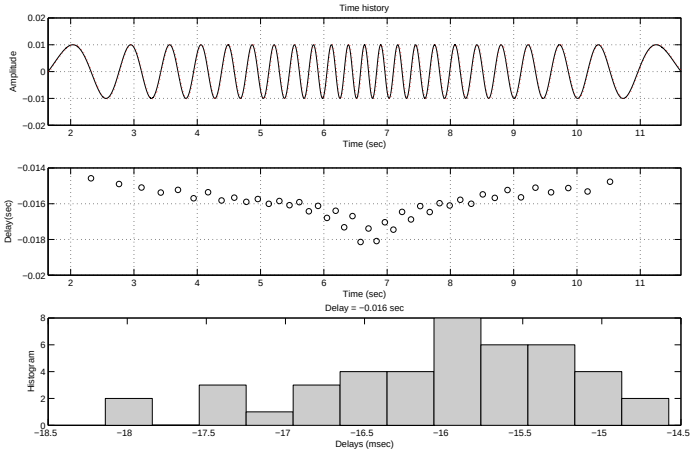

Figure 7.19: Delay estimation by zero crossing of the sinusoidal sweep test.

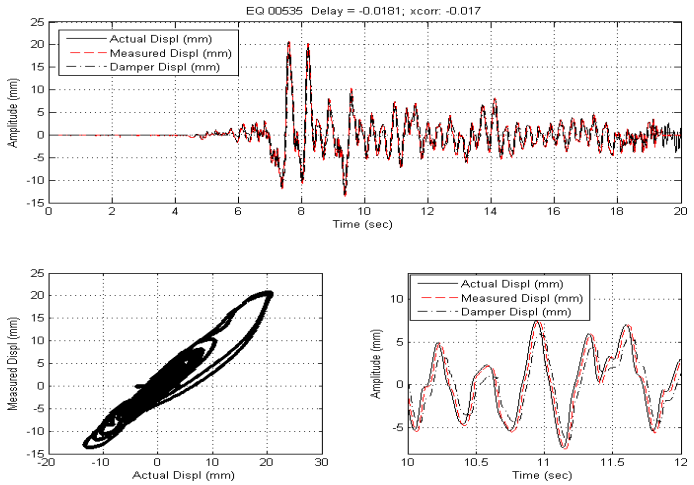

Figure 7.20: Test of tracking the first floor displacements of the structural model described in §7.1 under seismic load.

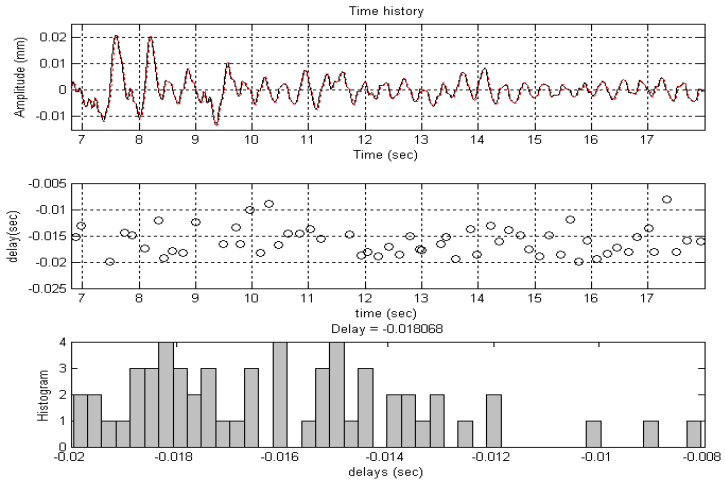

Figure 7.21: Delay estimation by zero crossing of the structural response of model in §7.1 under seismic load.

Evaluation of prediction scheme.

In order to test the time delay compensation scheme based on NNET, a predictor to estimate the command signal 16ms forward has been trained. Seeking for completeness, some noise was added to the command signals to be predicted. The SNR ratio was selected as 30dB for all the cases. Figure 7.22 contains the results from a tests run on the experimental rig at University of Bristol after using the time delay compensation scheme proposed. The coherence plot shows good delay compensation even when noise is added. As by numerical simulations was shown before in §3.4.3, the methodology based on NNETs is more accurate and faster than other common methodologies when working with noisy signals.

Considering constant delay, the prediction scheme looks pretty good. Besides, Figure 7.23 shows the results from the sine sweep test after using the prediction scheme based on NNET. In spite of the delay is no longer constant along the signal, a neural network which predict forward a constant delay (by using a average delay) works very well. All prediction tests were carried out considering two different approaches, one as it was proposed originally by using a purely forward prediction and another which adds to the predicted value an supplemental term proportional to the current instantaneous error by way of proportional control (P–control) [Ogata, 1990]. After an exhaustive search the value 0.7 was found as the best proportional constant (kp) for this basic scheme. From the experimental

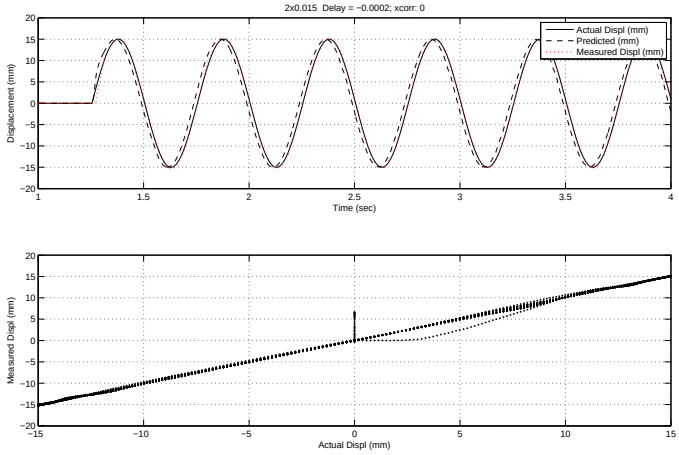

Figure 7.22: Sine wave test 2Hz at ±15mm after using time delay compensation based on NNET: time history and synchronization plot.

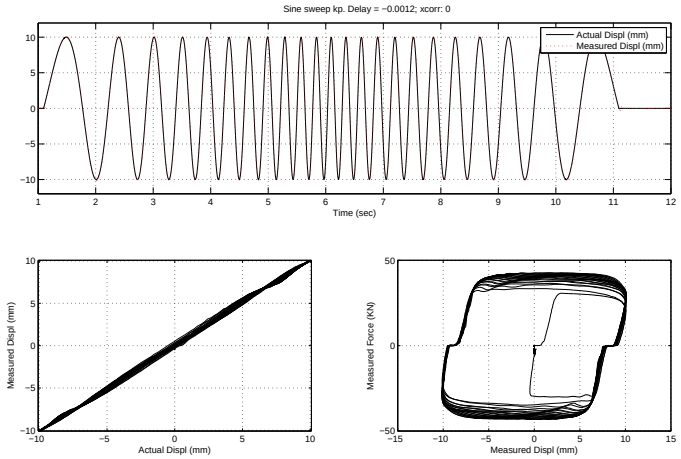

Figure 7.23: Sine sweep test after using time delay compensation.

test, kp=0.7 gives better results than the original scheme[5]. From now on, when we refer the time delay compensation scheme base on neural networks, we mean

[5]The original scheme is equivalent to kp=0

the scheme which adds the supplemental term ($-kp\times$error) with $kp = 0.7$.

Some problems predicting signals, comparison among common strategies.

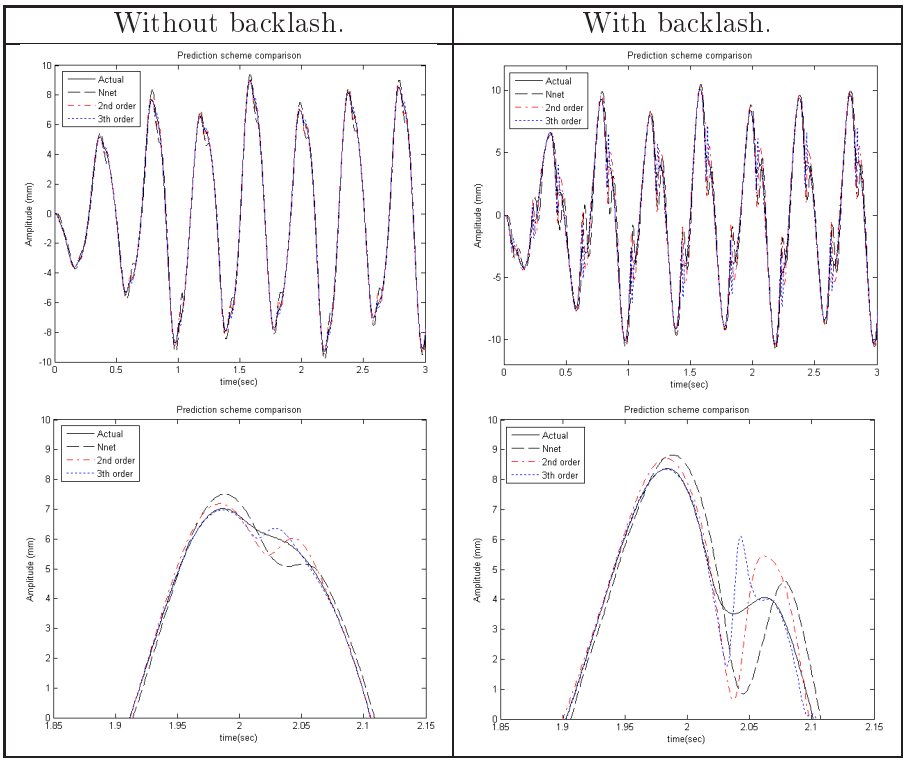

Figure 7.24: Predicting the first floor displacement of the model in 7.1 under periodic load. Comparison among polynomial 2nd–order, 3th–order and neural networks scheme.

From purely numerical simulation, it is possible to identify some troublesome issues associated with the lack of accuracy in prediction. Figure 7.24 exhibits some signals predicted by different methodologies against the original one. Two cases has been evaluated: (i) considering a perfect connection (no loose) between damper's ends and its supports, and (ii) a more realistic situation in which the backlash effect is included. From these simulations some facts come out. Considering our particular case where we are compensating signal for a RTDST simulation, we can assert that.

- No significant noise is present in the signal to be predicted, as this signal is

the outcome of the numerical substructure, in particular the displacement of the first floor[6]. Therefore, there is not great advantage in utilizing the neural network methodology because it requires additional attendance and could also present lack of training occasionally.

- The presence of such a strong damper in a structural system together with the delays, generate a sudden change of slope in the structure response. It comes just after the system velocity crosses zero (See detailed plots in Figure 7.24).

- In consequence of the connection loose, an additional delay in the damper response occurs. It intensifies the aforementioned change of slope somewhat after the peak of the signal and can cause even a reversing in this wave form.

- All prediction schemes exhibit serious problems when attempting to predict the signal in these critical zones where the system changes its behaviour.

Since without noise there are not significant benefits in utilizing a neural networks methodology, a second–order polynomial approximation was chosen as the predictor scheme. This also because polynomial–based methods have an additional advantage, the possibility of changing on–line the time forward you want to predict.

7.3.3 Real–time substructuring test results

For these experiments both the software and the experimental rig, were carefully set up to emulate the structural system presented in §7.1. The tests were set up as a typical displacement–controlled real–time substructuring simulation. That means, the displacements computed by the numerical substructure are applied through an actuator to the physical specimen (the damper), and in turn, the resisting force is measured and fed back into the numerical substructure.
A ©Matlab/simulink model of the whole substructured system was built. Figure 7.26 shows the model's outside loop in which the measured damper's force is fed back into the equations of state of the numerical substructure (representing the controlled structure).

A Dspace DS1104 board was used as platform on which the simulink–built model runs in real–time. Additionally, to control, manage and monitor the experiments, an user–interface able to download applications to the DS1104 board was developed in ControlDesk[7] (See Figure 7.27).

[6] In some way, the structural system works like a filter, cutting off the highest frequencies from the input signal.

[7] ControlDesk is an experiment software for developing working environment with Dspace© boards (http://www.dspace.com/)

Figure 7.25: Experimental rig set–up of substructured model.

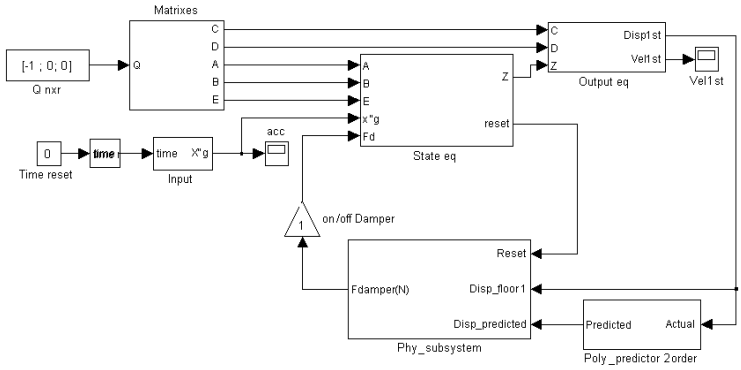

Figure 7.26: ©Simulink model of the substructured system.

As known, the instability in RTDST comes form the presence of delay in the feedback signal. So, an usual strategy to keep under control the simulation is to start with a full numerical substructuring test (i.e., where the physical substructure is replaced by a numerical approximation) and change progressively to a full hybrid simulation. Thus, attempting to prevent unforeseen and dangerous

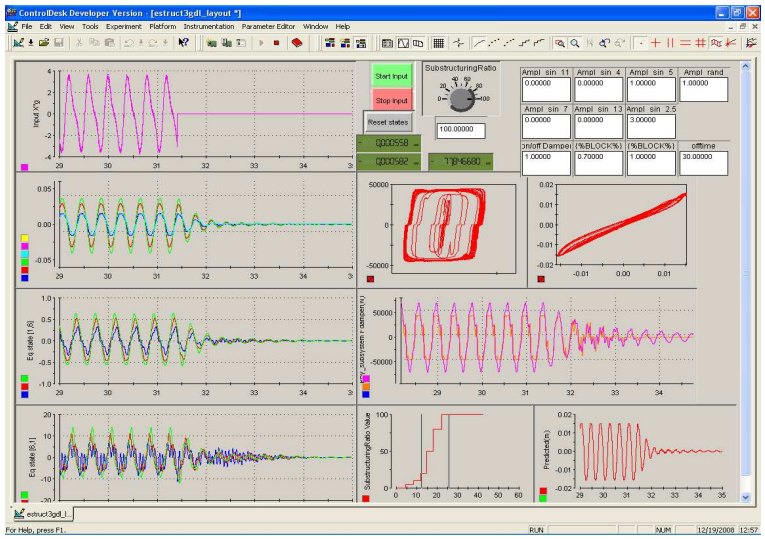

Figure 7.27: User–interface for managing and monitoring the experiments in real–time.

system behaviour because of the feedback of the delayed damper's force, some full numerical tests were completed before a realtime hybrid test were performed. The first test was accomplished feeding back the numerical approximation of the damper's force, in accord with the model presented in §7.3.1. Figure 7.28 shows results from this test including a zoom of the time history, the synchronization plot and the estimation of the delay. Therein and from now on, the parameter so–called *substructuring ratio* will indicate how much of the actual measured force is used to feedback the numerical substructure, in accord with formula (7.7).

$$F_{feedback} = (1 - SR) \cdot F_n + SR \cdot F_m \tag{7.7}$$

where: SR is the substructuring ration; $F_{feedback}$ is the effective feedback force, F_n is the damper force numerical approximation and F_m is the measured damper force. Thus e.g., $SR = 1$ means that the simulation is running in full hybrid scheme, or that, 100% of the measured damper force is used in the feedback loop.

Feeding back the numerical approximation of the damper force and considering a periodical load exciting the numerical substructure, the full–numerical RTDST simulation looks stable and the prediction scheme appears able to compensate the delay in the actuator's command signal. Besides, Figure 7.29 presents results from a real–time substructuring test which takes into account a periodical load applied to the numerical substructure. This test was started by considering full

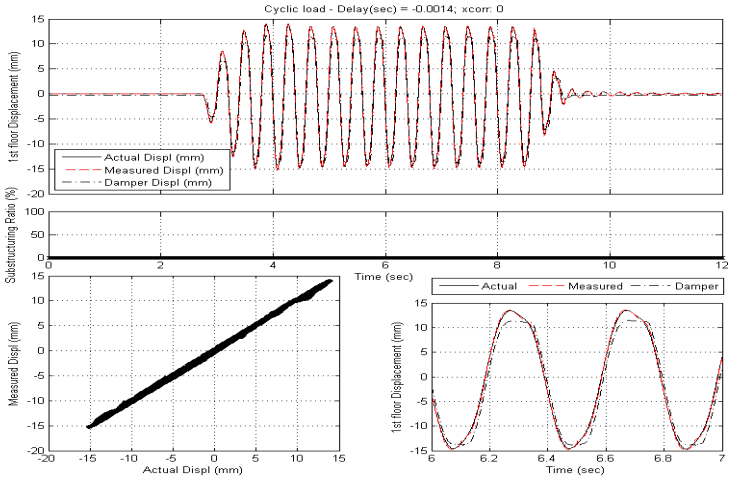

Figure 7.28: Full numerical substructuring test considering periodic load.

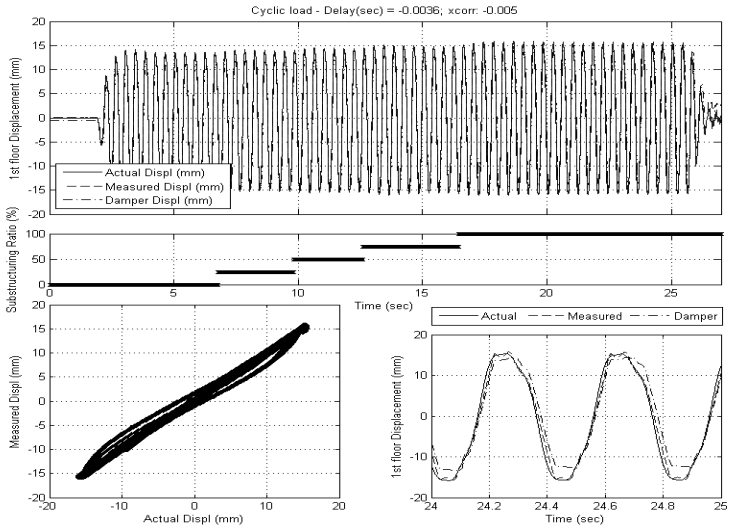

Figure 7.29: Real–time substructuring test considering periodic load.

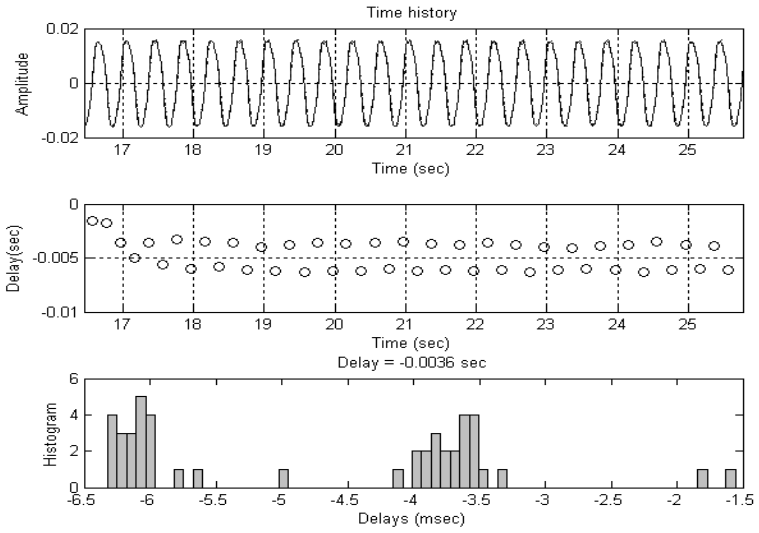

Figure 7.30: Zero crossing delay estimation for the substructuring test considering periodic load.

numerical feedback as before, but now, the substructuring ratio was gradually increased until achieving the whole measured damper's force on the feedback loop (above 17 seconds in the figure).
As well, Figure 7.30 shows the delay estimation by zero–crossing over the segment corresponding to the substructuring ratio equals to 100%.

The stability is achieved even when working with the actual measured force, nonetheless and despite the backlash phenomenon was considered in the numerical damper model, the delay seems to be increased when passing from the numerical to the full real–time substructuring test. It is worthy to note that, an important difference between the delay measured on the load and unload branches still holds.

By using earthquake load

In the following tests, properly scaled seismic accelerations were applied to the numerical substructure as the external excitation. The same as before, the fist tests were carried out by considering a full–numerical feedback of the damper force into the numerical substructure. Figures 7.31 and 7.32 shows the results by feeding back 100% and 50% of the damper's force numerical approximation respectively. In both cases the synchronization plots show a good delay compensation because of the prediction and the experiments show to be stable.

However, when running the full real–time substructuring test, that is, when all the measured damper force is being fed back, the instability arises since very earlier stages. (See Figure 7.33).

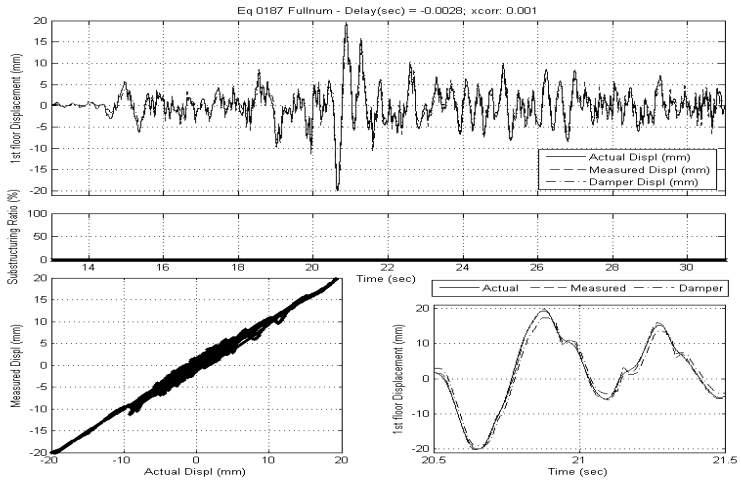

Figure 7.31: Full numerical substructuring test with earthquake 0187.

Several tests were accomplished by trying excitations with different frequency–band contents, all of them getting more or less the same results. Figures 7.34 and 7.35 show the outcomes under different earthquakes. As before, after switching from partial to full hybrid real–time substructuring test, the experiment became instable due to the propagation of the delay error through the external feedback loop.

Figure 7.36 shows what happens in terms of force when the simulation becomes inaccurate in consequence of the self–sustained oscillations. Even when those oscillations are small, the sudden change of velocity causes a stronger variation in terms of force. It is large enough to produce the structural response rises. Those oscillations together with the characteristics of such a stiff nonlinear damper, cause a continuous switching between the extreme maximum loads for the damper (both of opposite signs), a sort of chain reaction which leads the simulation to instability. As well, as it was found from the stability analysis in §6.3, the self–sustained oscillations come at small displacements under a certain velocity range. For some tests, the simulation became unstable even when the external load were vanished, that is, when the system was supposed to be arrested as consequence of non external load being applied to the system.

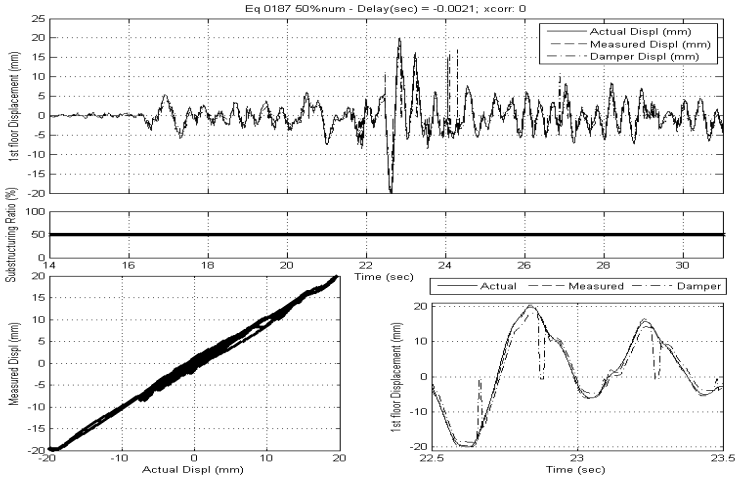

Figure 7.32: Partial real–time substructuring test with earthquake 0187.

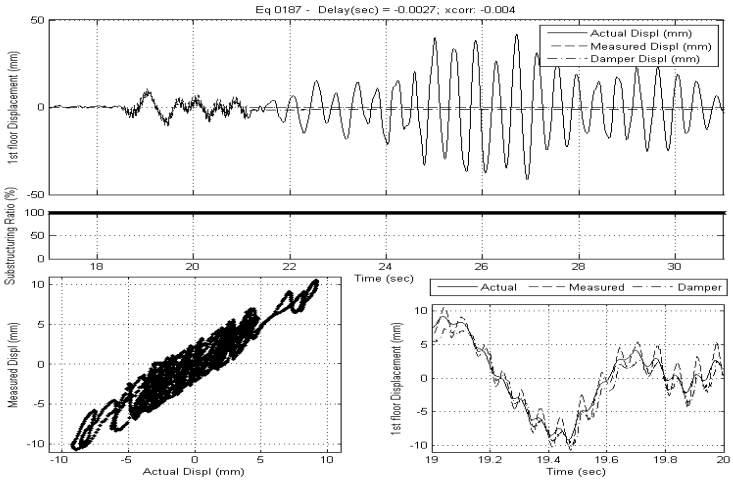

Figure 7.33: Real–time substructuring test with earthquake 0187.

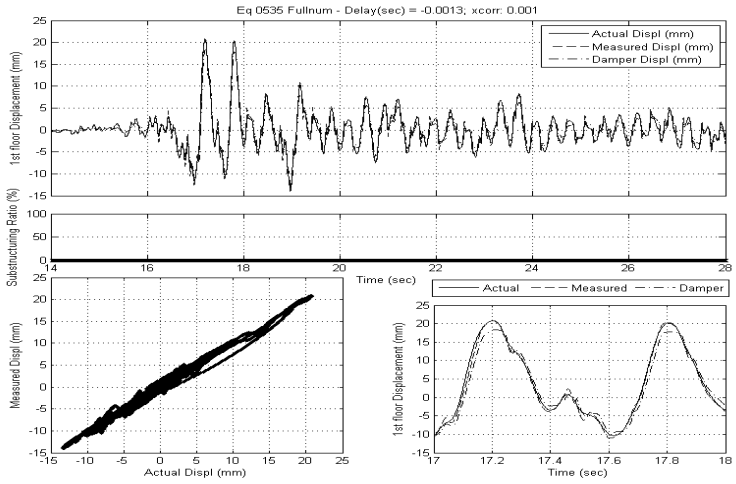

Figure 7.34: Full numerical substructuring test with earthquake 0535.

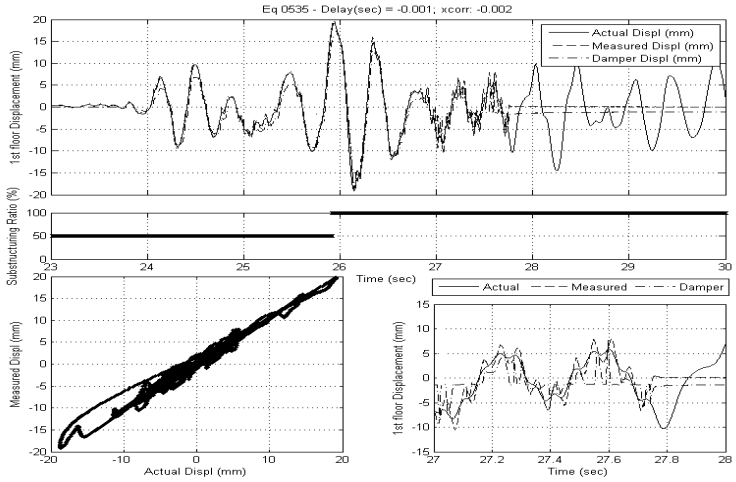

Figure 7.35: Real–time substructuring test with earthquake 0535.

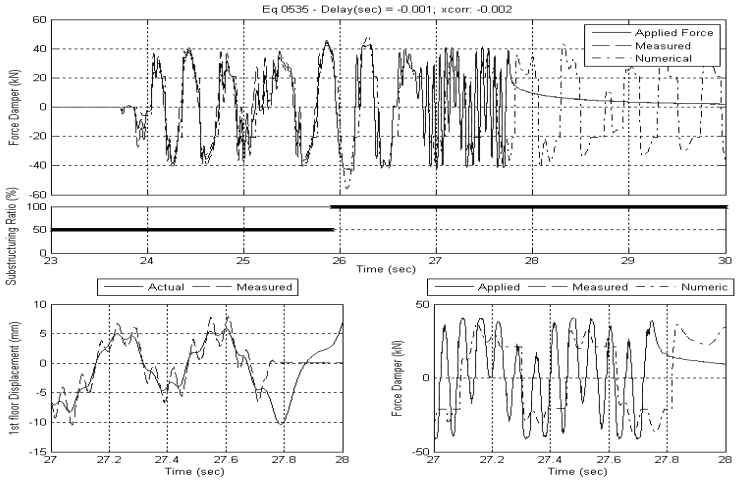

Figure 7.36: Real–time substructuring test with earthquake 0535. Force comparison

A main practical issue concerning to stability was the backlash phenomenon. Unfortunately, It was not possible to get perfect connection between the transfer system and the specimen tested. This lost motion due to clearance when movement is reversed and contact is re–established, increased the delay effect. Backlash may severely affect the stability conditions in a Real Time Dynamic Substructuring simulation when testing systems which are exceptionally sensible to delay. So that, backlash became a crucial disappointment in this simulation.

We understood the phenomenon which generates self–sustained oscillations and verified their existence experimentally. However, we are still not able to design a complementary system which prevents such high frequency oscillations. We need to include a subsystem in the RTDST–chain to counteract and take away them. Thus, our current effort is being mainly focused on thinking up in a virtual system able to absorb such high frequency oscillation, keeping the system free from the harmful effects of delay in the feedback loop in RTDST.

Chapter 8

Conclusions and final remarks

Contents

8.1 Main contributions

The contributions of this thesis have been concerned with several aspects. The work explores the use of a new testing methodology for earthquake engineering incorporating time delay compensation schemes and stability analysis. Both of them open problems that are currently matter of research in the community studying nonlinear dynamical systems. The work have been focused on the definition of conditions to guarantee reliable results when running experimental testing of nonlinear systems for structural control at real scale.

The following summarize the main contributions of this thesis:

1. Development of numerical routines.
    - Neural network training for on–line time series prediction with application to time delay compensation.
    - Numerical stability analysis of linear and nonlinear delayed systems.
    - Numerical approximation of vector field for nonlinear delayed systems.
2. Analytical investigations.
    - Stability analysis of linear delayed systems.
    - Explicit stability analysis of systems with non–linear delayed dampers.

- Existence analysis of limite cycles in systems with delayed dry friction dampers.

3. Experimental testing on RTDST for large–scale non–linear dampers.
   - Simulink model of substructured systems able to run in real–time.
   - User–interface able to run and control experiments in real–time.

8.2 Final remarks

More realistic tests of seismic protection devices allow better understanding of the overall controlled system dynamics and enable the engineer to improve its performance. Real–Time Dynamic Substructuring Test (RTDST) have enormous potential in assessing protection systems for earthquake engineering, as it allows testing components of the structure at full–scale under realistic extreme loading conditions. So, we can separate just the structural control device from the system, bring it to the lab and test it physically, taking into account its dynamic interaction with the hosting structure. Moreover, the versatility of the RTDST was certainly evidenced by the possibility of performing repeatable tests. We could not only assess the response of the control device under different load condition, but also it is possible to change the hosting structure itself and evaluate, for instance, the most well–behaved structural configuration for a particular seismic protection device. So, several structural systems could be evaluated under a wide range of load conditions by using the same experimental rig set up.

However, as it was shown along this thesis, to guarantee the success of a RTDST simulation, a very efficient time delay compensation scheme is not enough. A complete stability analysis is also required to determine how sensible the substructured system may be under small delays.

This work is focused on testing a passive control system provided with large–scale non linear fluid viscous dampers. We proposed, implemented and tested a new time delay compensation scheme for RTDST based on Neural Networks. Even if this compensation worked properly, it became impossible to reduce the delay error in the feedback signal to zero. When carrying out the experimental campaign on the case study system, unexpected self–sustained oscillations were detected. This was caused by very small delays in the feedback loop, which unavoidably lead the system to oscillations at high frequency. We completed a explicit stability analysis and achieved a comprehensive dynamic characterization of the non–linear phenomena in the system. In this thesis we presented a complete set of closed–form expression to describe the dynamics of the main complex delay–induced behaviours exhibited for the delayed system. We could identify both the region where self–sustained high frequency oscillations arise and the

limit cycle induced by the delay.

Regarding to the prediction methodology, neural network scheme demonstrates much more capacity and robustness than the other methods when predicting noisy signals. This advantageous behaviour is due to the inherent generalization capacity of neural networks and their high tolerance to noisy data. Besides, unlike other methodologies, neural network provides a smoother signal when moving from one time step to the other, so that, slight discontinuities in the predicted command signal are avoided. Because of the adaptive training, the network shows behavior improvements as long as the simulation time passes. Once the training process becomes well–balanced, the proposed compensator was able to adapt quickly to the change in the target signal. The scheme is well suitable for being used within systems whose properties do not change very rapidly and is able to smooth out the effects of noise and experimental errors.

Although more complex than used networks are expected to have higher capacity in prediction, due to the dimensional and complexity increment in the network's weight space, the optimization of the error function becomes more expensive computationally. As a result, the network becomes very slow when training and is no longer suitable for prediction in real–time.

Nevertheless, for RTDST applications this compensation scheme may not be suitable all the times. In our particular case for instance, due to the signal to be predicted was the outcome of a numerical model (namely the displacement of the first floor), no substantial noise is present on this signal. So that, there is not great advantages in utilizing the neural network methodology because it requires additional attendance and could also present lack of training occasionally.

An additional care should be taken with relation to the prediction scheme. Note that if delay is considered to be equivalent to adding negative damping in the system, then over compensating (predicting too far forward in time) will have the opposite effect of increasing the damping. Both cases may reduce the accuracy of the simulation results. Note that delay might change along the RTDST simulation, so, to avoid wrong time delay compensations, it should be done base on an accurate on–line estimation of the current delay in the system.

The case studied in this thesis is mainly characterized for having a strong nonlinearity (by way of discontinuity) when the velocity in the dissipation device changes of sign. Many others dissipation devices for seismic hazard mitigation present a similar force–velocity dependence. Our results can be easily extended to different systems in engineering which are provided with devices exhibiting such a behaviour. Additionally, the achieved results are also useful for other kind of mechanical systems different from RTDST applications. Systems where the

response of some components is arriving with delay and may cause a harmful effects on the system behaviour. Semi–active control by MR dampers are examples of such a systems. In fact, it is a work derived from this thesis which is already being carried out. Large–scale MR dampers also suffer from mechanical delayed response. That is why, we are studying the reduction on the semi–active control system efficacy caused by delays in the MR dampers response.

In order to get the close–form expressions for describing the delayed system dynamics, a mathematical trick was used in this thesis. We substituted the original non–linear system by one dynamically equivalent. When passing to the equivalent system, that one which uses dry friction instead of viscous damping, some complex phenomena exhibit in the original system can not be represented any more. From numerical simulations, we identified a sliding phenomenon just before the high frequency oscillations (induced by delay) arise. Such phenomenon do not cause any important problem in terms of dynamic stability, but its analysis may be very interesting from a mathematical point of view. Readers interested in catching such phenomenon could try a piecewise dynamical system by using a Fillipov's systems approach, which can reproduce such a behaviour.

Another practical issue to take care about when setting up the experimental rig for RTDST, is the backlash phenomenon. When perfect connection between the transfer system and the specimen is not assured, this lost motion due to clearance when movement is reversed and contact is re–established, can increase even more the delay effect. In spite of the fact that such phenomenon may be present in the emulated system without any significant drawback, backlash may severely affect the stability conditions in a Real Time Dynamic Substructuring simulation when testing systems which are exceptionally sensible to delay. So that, if the system proves to be highly sensitive to delay, backlash becomes crucial in the simulation.

Finally, although we got a complete mathematical description of systems with delayed non–linear dampers and we could assert that any small delay causes self–sustained oscillations, the problem is still far from solved. We have understood the phenomenon, unexplained before, which generates self–sustained oscillations. But to carry out reliable and accurate RTDST simulations on the large–scale nonlinear dampers, we still have to find a complementary system which prevents such high frequency oscillations. We need to include a subsystem in the RTDST–chain to counteract and take away them. Our guess is that a system which is tuned according to the frequency of the undesirable oscillations can be useful. A sort of virtual tuned mass damper able to absorb the high frequency oscillation, keeping the system free from the harmful delay effects.

Bibliography

[Eur, 2007] (2007). *European Standard prEN 15129: Anti-Seismic Devices*. European Committee for Standardization.

[Ita, 2008] (2008). *New Technical Standards for Constructions*. Ministry of Infrastructures. Ministerial Decree of 14 January 2008. Official Gazette No. 29 of 4 February 2008 – Ordinary Supplement No. 30. (In Italian).

[Abrams, 1996] Abrams, D. (1996). Effects of scale and loading rate with test of concrete and mansory structures. *Earthquake Spectra*, 12(1):2–28.

[Aguirre et al., 2008] Aguirre, N., Ikhouane, F., Rodellar, J., and Christenson, R. (2008). Modeling and identification of large scale magnetorheological dampers. In *Fourth European Conference on Structural Control, St. Petersburg, Russia.*

[Ahmadizadeh et al., 2008] Ahmadizadeh, M., Mosqueda, G., and Reinhorn, A. M. (2008). Compensation of actuator delay and dynamics for real–time hybrid structural simulation. *Earthquake Engineering and Structural Dynamics*, 37:21–42. Published online 17 August 2007 in Wiley InterScience.

[Ang et al., 2005] Ang, K. H., Chong, G., and Li, Y. (2005). PDI control system analysis, design and technology. *IEEE Transactions on Control Systems Technology*, 13(4):559–576.

[Aristizabal and Clark, 1980] Aristizabal, J. D. and Clark, A. J. (1980). Large–scale earthquake simulation table. In *Proc. of 7th World Conf. on Earthquake Engineering*, volume 7, pages 157–164, Istanbul, Turkey.

[Bacic, 2006] Bacic, M. (2006). Hardware–in–the–loop simulation: Taxonomic framework, survey and new research directions. Report No.2290/06, University of Oxford.

[Bathe and Wilson, 1976] Bathe, K. J. and Wilson, E. L. (1976). *Numerical Methods in Finite Element Analysis*. Prentice–Hall, New Jersey.

[Bayer et al., 2005] Bayer, V., Dorka, U. E., Füllekrug, U., and Gschwilm, J. (2005). On real-time pseudo-dynamic sub-structure testing: algorithm, numerical and experimental results. *Aerospace Science and Technology*, 9(3):223 – 232.

[Bonnet et al., 2007] Bonnet, P. A., Williams, M. S., and Blakeborough, A. (2007). Compensation of actuator dynamics in real–time hybrid tests. In Publishing, P. E., editor, *Proceedings of the Institution of Mechanical Engineers. Part I: Journal of Systems and Control Engineering*, volume 221, pages 251–264.

[Bouwkamp et al., 1971] Bouwkamp, J. G., Penzien, J., and D, R. (1971). Earthquake engineering facilities at university of california, berkeley. In *Proc. of 3rd European Symposium on Eartquake Engineering*, Sofia, Bulgaria.

[Bursi and Shing, 1996] Bursi, O. and Shing, P. (1996). Evaluation of some implicit time–stepping algorithms for pseudodynamic tests. *Earthquake Engineering & Structural Dynamics*, 25(4):333–355.

[Butcher, 2003] Butcher, J. C. (2003). *Numerical Methods for Ordinary Differential Equations*. John Wiley & Sons, Chichester, UK.

[Cahis et al., 2000] Cahis, X., Bozzo, L., and Torres, L. (2000). An innovative elasto–plastic energy dissipator for the structural and non–structural building protection. In *Proceedings of 12th World Conference on Earthquake Engineering*, Auckland.

[Cao et al., 1998] Cao, H., Reinhorn, A. M., and Soong, T. T. (1998). Design of an active mass damper for a tall tv tower in nanjing, china. *Engineering Structures*, 2(3):134–143.

[Casciati et al., 2006] Casciati, F., Magonette, G., and Marazzi, F. (2006). *Technology of semiactive devices and applications in vibration mitigation*. John Wiley & Sons Inc.

[Chen et al., 2003] Chen, Z. Q., Wang, X. Y., Ko, J. M., Ni, Y. Q., Spencer, B. F., and Yang, G. (2003). MR damping system on Dongting lake cable–stayed bridge. In *Proc. of Smart Structures and Materials 2003: Smart Systems and Nondestructive Evaluation for Civil Infrastructures*, San Diego, CA, USA.

[Christenson et al., 2008] Christenson, R., Lin, Y. Z., Emmons, A., and Bass, B. (2008). Large–scale experimental verification of semiactive control through real–time hybrid simulation. *Structural Engineering*, 134(4):522–534.

[Colombo et al., 2007] Colombo, A., di Bernardo, M., Hogan, S. J., and Kowalczyk, P. (2007). Complex dynamics in a hysteretic relay feedback system with delay. *Nonlinear Science*, 17:85–108.

[Combescure and Pegon, 1997] Combescure, D. and Pegon, P. (1997). α–operator splitting time integration technique for pseudodynamic testing error propagation analysis. *Soil Dynamics and Earthquake Engineering*, 16(7-8):427–443.

[Constantinou and Symans, 1992] Constantinou, M. C. and Symans, M. D. (1992). Experimental and analytical investigation of seismic response of structures with supplemental fluid viscous dampers. Technical Report NCEER-92-0032, National Center for Earthquake Engineering Research, Buffalo, New York.

[Constantinou and Symans, 1993] Constantinou, M. C. and Symans, M. D. (1993). Seismic response of buildings with supplemental damping. *Journal of Structural Design of Tall Buildings*, 2(77):92–103.

[Dallard et al., 2001] Dallard, P., Fitzpatrick, A. J., Flint, A., Bourva, S. L., Low, A., Ridsdill, R. M., and Willford, M. (2001). The london millennium footbridge. *The Structural Engineer*, 79(22):17–33.

[Darby et al., 1999] Darby, A. P., Blakeborough, A., and Williams, M. S. (1999). Real–time substructure tests using hydraulic actuator. *J. Engrg. Mech*, 125(10):1133–1139.

[Darby et al., 2002] Darby, A. P., Williams, M. S., and Blakeborough, A. (2002). Stability and delay compensation for real–time substructure testing. *J. Engrg. Mech*, 128(12):1276–1284.

[di Bernardo et al., 2007] di Bernardo, M., Budd, C., Champneys, A., and Kowalczyk, P. (2007). *Piecewise–smooth Dynamical Systems: Theory and Applications*. Number 163 in Applied mathematical Science. Springer.

[Dimig et al., 1999] Dimig, J., Shield, C., French, C., Bailey, F., and Clark, A. (1999). Effective force testing: A method of seismic simulation for structural testing. *Structural Engineering – ASCE*, 125(9):1028–1037.

[Donea et al., 1996] Donea, J., Magonette, P., Negro, P., Pegon, P., Pinto, P., and Verzeletti, A. (1996). Pseudodynamic capabilities of the ELSA laboratory for earthquake testing of large structures. *Earthquake Spectra*, 12(1):163–180.

[Dowdell and Cherry, 1994] Dowdell, D. J. and Cherry, S. (1994). Semiactive friction dampers for seismic response control of structures. In *Proceedings of the Fifth US National Conference on Earthquake Engineering*, volume 1, pages 819–828.

[Dullerud and Paganini, 1999] Dullerud, G. E. and Paganini, F. (1999). *A Course in Robust Control Theory: A Convex Approach*. Springer-Verlag, New York.

[Dyke, 2005] Dyke, S. J. (2005). Current directions in structural control in the US. In *Proceedings of the 9th World Seminar on Seismic Isolation, Energy Dissipation and Active Vibration Control of Structures*, Kobe, Japan.

[Dyke et al., 1997a] Dyke, S. J., Spencer, B. F., Sain, M. K., and Carlson, J. D. (1997a). An experimental study of MR dampers for seismic protection. *Smart Materials and Structures*, 7:693–703. Special Issue on Large Civil Structures.

[Dyke et al., 1997b] Dyke, S. J., Spencer, B. F., Sain, M. K., and Carlson, J. D. (1997b). On the efficacy of magnetorheological dampers for seismic response reduction. In *Proceedings of DECTC'97. ASME Design Engineering Technical Conferences*, Sacramento, USA.

[Dyke et al., 1996] Dyke, S. J., Spencer, J. B. F., Sain, M. K., and Carlson, J. D. (1996). Modeling and control of magnetorheological dampers for seismic response reduction. *Journal of Smart Materials and Structures*, 5:565–575.

[Erkus and Johnson, 2006] Erkus, B. and Johnson, E. A. (2006). Smart base isolated benchmark building part III: A simple controller for bilinear isolation. *Structural Control and Health Monitoring*, 13:605–625.

[Faithfull et al., 2001] Faithfull, P. T., Ball, R. J., and Jones, R. P. (2001). An investigation into the use of hardware–in–the–loop simulation with a scaled physical prototype as an aid to design. *Engineering Design*, 12(3):231–243.

[Feng et al., 1993] Feng, M. Q., Shinozuka, M., and Fujii, S. (1993). Friction-controllable sliding isolation system. *Engineering Mechanics ASCE*, 119(9):1845–1864.

[Gavin, 2001] Gavin, H. P. (2001). Control of seismically excited vibration using electrorheological materials and lyapunov function. *IEEE Transactions on Control Systems Technology*, 9(1):27–36.

[Gawthrop et al., 2007] Gawthrop, P. J., Wallace, M. I., Neild, S. A., and Wagg, D. J. (2007). Robust real–time substructuring techniques for under–damped systems. *Structural Control and Health Monitoring*, 14:591–608. Published online 19 May 2006 in Wiley InterScience.

[Gilsinn, 2002] Gilsinn, D. (2002). Estimating critical hopf bifurcation parameters for a second-order delay differential equation with application to machine tool chatter. *Nonlinear Dynamics*, 30:103–154. Kluwer Academic Publishers.

[Gökçek et al., 2000] Gökçek, C., Kabamba, P. T., and Meerkov, S. M. (2000). An LQR/LQG theory for systems with saturating actuators. *CGR-00-03, EECS, University of Michigan, Ann Arbor*, 46:1529–1542.

[Gravatt, 2003] Gravatt, J. W. (2003). *Magnetorheological dampers for super-sport motorcycle applications*. PhD thesis, Virginia Polytechnic Institute and State University.

[Hanson and Soong, 2001] Hanson, R. D. and Soong, T. T. (2001). *Seismic Design with Supplemental Energy Dissipation Devices*. MNO–8. EERI Monograph.

[Horiuchi et al., 1999] Horiuchi, T., Inoue, M., Konno, T., and Namita, Y. (1999). Real–time hybrid experimental system with actuator delay compensation and its application to a piping system with energy absorber. *Earthquake Engineering and Structural Dynamics*, 28(10):1121–1141.

[Housner et al., 1997] Housner, G. W., Bergman, L. A., Caughey, T. K., Chassiakos, A. G., Claus, R. O., Masri, S. F., Skelton, R. E., Soong, T. T., Spencer, B. F., and Yao, T. P. (1997). Structural control: Past, present and future. *Journal of Engineering Mechanics ASCE.*, 123(9):897–923.

[Ikhouane and Rodellar, 2007] Ikhouane, F. and Rodellar, J. (2007). *Systems with Hysteresis: Analysis, Identification and Control Using the Bouc-Wen Model*. Chichester, UK: Wiley.

[Jang et al., 1997] Jang, J. S., Sun, C. T., and Mizutani, E. (1997). *Neuro–Fuzzy and Soft Computing: A Computational Approach to Learning and Machine Intelligence*. Prentice Hall, USA, us ed edition.

[Jansen and Dyke, 2000] Jansen, L. M. and Dyke, S. J. (2000). Semi-active control strategies for the MR damper: comparative study. *Journal of Engineering Mechanics, ASCE*, 126:795–803.

[Ji et al., 2009] Ji, X., Kajiwara, K., Nagae, T., Enokida, R., and Nakashima, M. (2009). A substructure shaking table test for reproduction of earthquake responses of high–rise buildings. *Earthquake Engineering and Structural Dynamics*, 38:1381–1399.

[Jung and Lee, 2002] Jung, H. and Lee, W. (2002). State of the art of MR damper–based control systems in civil engineering applications. In *US-Korea Workshop on Smart Infra-Structural systems, Busan, Korea*.

[Jung and Shing, 2006] Jung, R. Y. and Shing, P. B. (2006). Performance evaluation of a real–time pseudodynamic test system. *Earthquake Engineering and Structural Dynamics*, 35:789–810. Published online 10 February 2006 in Wiley InterScience.

[Jung et al., 2006] Jung, R. Y., Shing, P. B., Stauffer, E., and Thoen, B. (2006). Performance of a real–time pseudodynamic test system considering nonlinear structural response. Technical report, Network for Earthquake Engineering Simulation Program of the National Science Foundation and the University of Colorado.

[Kalmár-Nagy et al., 2001] Kalmár-Nagy, T., Stépán, G., and Moon, F. (2001). Subcritical hopf bifurcation in the delay equation model for machine tool vibrations. *Nonlinear Dynamics*, 26:121–142. Kluwer Academic Publishers.

[Kamagata and Kobori, 1994] Kamagata, S. and Kobori, T. (1994). Autonomous adaptive control of active variable stiffness system for seismic ground motion. In *Proceedings of the First World Conference on Structural Control*, volume TA4, pages 33–42, Los Angeles, California.

[Kelly, 1996] Kelly, J. (1996). *Earthquake–Resistant Design with Rubber*. Springer, Berlin, 2nd edition.

[Khalil, 2000] Khalil, H. (2000). *Nonlinear Sistems*. Prentice–Hall, Inc., Upper Saddle River, NJ, USA, third edition.

[Kobori et al., 1991] Kobori, T., Koshika, N., Yamada, K., and Ikeda, Y. (1991). Seismic-response-controlled structure with active mass driver system. part I: Design. *Earthquake Engineering and Structural Dynamics*, 20:133–149.

[Krasovskii, 1959] Krasovskii, N. (1959). *Some problems of the motion stability theory*. Fizmatgiz, Moscow. English traduction for Stanford University Press, 1963.

[Kucera, 2007] Kucera, V. (2007). The h_2 control problem: a general transfer–function solution. *International Journal of Control*, 80(5):800–815.

[Kurata et al., 2000] Kurata, N., Kobori, T., Takahashi, M., Ishibashi, T., Niwa, N., Tagami, J., and Midorikawa, H. (2000). Forced vibration test of a building with semiactive damper system. *Earthquake Engineering and Structures Dynamics*, 29:629–645.

[Kuznetsov, 2004] Kuznetsov, Y. (2004). *Elements of Applied Bifurcation Theory*, volume 112 of *Applied Mathematical Science*. Springer–Verlag, New York, second edition.

[Kwok and Samali, 1995] Kwok, K. and Samali, B. (1995). Performance of tuned mass dampers under wind loads. *Engineering Structures*, 17(9):655–667.

[Kyrychko et al., 2007] Kyrychko, Y. N., Hogan, S. J., Gonzalez-Buelga, A., and Wagg, D. J. (2007). Modelling real–time dynamic substructuring using partial delay differential equations. In *Proceedings of the Royal Society of London*, volume 463, pages 1509–1523.

[Lee and Taylor, 2001] Lee, D. and Taylor, D. P. (2001). Viscous damper development and future trends. *The Structural Design of Tall Buildings*, 10:311–320.

[Lee et al., 2007] Lee, S. K., Park, E. C., Min, K. W., and Park, J. H. (2007). Real–time substructuring technique for the shaking table test of upper substructures. *Engineering Structures*, 29:2219–2232.

[Leitmann and Reithmeier, 2002] Leitmann, G. and Reithmeier, E. (2002). Semiactive control of a vibrating system by means of electrorheological fluids. *Dynamics and Control*, 3(1):7–33.

[Londoño and Serino, 2008] Londoño, J. M. and Serino, G. (2008). Using computational intelligence strategies in delay compensation for real-time systems. In *Proceedings of the Fourth European Conference of Structural Control*, volume 2, pages 1250–1258, St.Petersburg, Russia. ISBN: 978-5-904045-10-4.

[Looney, 1997] Looney, C. G. (1997). *Pattern recognition using Neural Networks: Theory and Algorithms for Engineers and Scientists*. Oxford University Press, USA.

[Lyapunov, 1992] Lyapunov, A. M. (1992). *The general problem of the stability of motion*, volume 55 of *International Journal of Control*. Lyapunov Centenary Issue. English translation of PhD dissertation in 1892.

[Magonette et al., 1998] Magonette, G., Pegon, P., Molina, F., and Buchet, P. (1998). Development of fast continuous pseudodynamic substructuring tests. In *Proc. of Second World Conference on Structural Control*, Kyoto, Japan.

[Mahin et al., 1989] Mahin, S. A., Shing, P. B., Thewalt, C. R., and Hanson, R. D. (1989). Pseudo dynamic test method: Current status and future directions. *Structural Engineering*, 115(8):2113–2128.

[Marazzi and Magonette, 2001] Marazzi, F. and Magonette, G. (2001). Active and semiactive control of structures. In *European Meeting on Intelligent Structures*, Ischia, Italy.

[Masri et al., 1994] Masri, S. F., Chavakula, S., and Caughey, T. K. (1994). Control of intelligent nonlinear adaptive structures under earthquake excitation. *Structural Control*, 1(1):23–38.

[May, 1976] May, R. M. (1976). Simple mathematical models with very complicated dynamics. *Nature*, 261(4):459–467.

[McCulloch and Pitts, 1943] McCulloch, W. W. and Pitts, W. (1943). A logical calculus of ideas imminent in nervous activity. *Bull. Math. Biophys*, 5:115–133.

[Miyamoto and Hanson, 2004] Miyamoto, H. K. and Hanson, R. D. (2004). Structural practices. seismic dampers: State of the applications. *Structure Magazine*, pages 16–18.

[Moon et al., 2003] Moon, S. J., Bergman, L. A., and Voulgaris, P. G. (2003). Sliding mode control of cable–stayed bridge subjected to seismic excitation. *Journal of Engineering Mechanics, ASCE*, 129:71–78.

[Nakashima et al., 1992] Nakashima, M., Kato, H., and Takaoka, E. (1992). Development of real–time pseudo dynamic testing. *Earthquake Engineering and Structural Dynamics*, 21:79–92. John Wiley & Sons, Ltd.

[Nakashima and Masaoka, 1999] Nakashima, M. and Masaoka, N. (1999). Real–time on-line test for MDOF systems. *Earthquake Engineering and Structural Dynamics*, 28:393–420.

[Nakata et al., 2006] Nakata, N., Spencer, B. F., and Elnashai, A. S. (2006). Mixed load/displacement control strategy for hybrid simulation. In *Proc. on 4th International Conference on Earthquake Engineering*, Taipei, Taiwan. Paper No. 94.

[Neild et al., 2005] Neild, S. A., Stoten, D. P., Drury, D., and Wagg, D. J. (2005). Control issues relating to real–time substructuring experiments using a shaking table. *Earthquake Engineering and Structural Dynamics*, 34:1171–1192. Published online 3 March 2005 in Wiley InterScience.

[Newmark, 1959] Newmark, N. M. (1959). A method of computation for structural dynamics. *Engineering Mechanics*, 85:67–94.

[Nishimura and Shidomaira, 2003] Nishimura, H. and Shidomaira, S. (2003). Vibration isolation control for a structure taking account of actuator saturation. In *Proceedings of the Third World Conference on Structural Control*, volume 3, pages 275–282, Como, Italy.

[Nishitani and Inoue, 2001] Nishitani, A. and Inoue, Y. (2001). Overview of the application of active/semiactive control to building structures in japan. *Earthquake Engineering and Structural Dynamics*, 30:1565–1574.

[Ogata, 1990] Ogata, K. (1990). *Modern control engineering*. Prentice–Hall, Inc., Upper Saddle River, NJ, USA, second edition.

[Osorio, 2007] Osorio, G. (2007). *Complex Behavior in Impacting Systems*. PhD thesis, Department of Computer and Systems Engineering. University of Naples Federico II, Naples; Italy.

[Pegon, 2001] Pegon, P. (2001). Alternative characterization of time integration schemes. *Computer Methods in Applied Mechanics and Engineering*, 190(20-21):2707–2727.

[Pegon and Pinto, 2000] Pegon, P. and Pinto, A. V. (2000). Pseudo–dynamic testing with substructuring at the ELSA laboratory. *Earthquake Engineering and Structural Dynamics*, 29:905–925.

[Piiroinen and Kuznetsov, 2008] Piiroinen, P. T. and Kuznetsov, Y. A. (2008). An event-driven method to simulate filippov systems with accurate computing of sliding motions. *ACM Transactions on Mathematical Software*, 3(34).

[Pinto et al., 2004] Pinto, A. V., Pegon, P., Magonette, G., and Tsionis, G. (2004). Pseudo–dynamic testing of bridges using non–linear substructuring. *Earthquake Engineering and Structural Dynamics*, 33:1125–1146.

[Ponzo et al., 2008] Ponzo, F., diCesare, A., Moroni, C., Nigro, D., Dolce, M., and Marnetto, R. (2008). Jet-pacs project: dynamic test on steel frame equipped with hysteretic energy dissipating bracing system. In *Proceedings of the 14th World Conference on Earthquake Engineering*, Beijing, China.

[Poynor, 2001] Poynor, J. (2001). Innovative designs for magnetorheological dampers. Master's thesis, Virginia Polytechnic Institute and State University.

[Press et al., 1992] Press, W. H., Teukolsky, S. A., Vettering, W. T., and Flannery, B. R. (1992). *Numerical recipes in C: the art of scientific computing.* Cambridge University Press, Cambridge UK, 2nd edition.

[Preumont, 1997] Preumont, A. (1997). *Vibration Control of Active Structures. An Introduction.*, volume 50 of *Solid Mechanics and its Applications.* Kluwer Academic Publishers, The Netherlands.

[Renzi and Serino, 2004] Renzi, E. and Serino, G. (2004). Testing and modelling a semi–actively controlled steel frame structure equipped with MR dampers. *Structural Control and Health Monitoring*, 11(3):189–221. John Wiley and Sons, Ltd.

[Ricciardelli et al., 2003] Ricciardelli, F., Mattei, M., and Pizzimenti, A. D. (2003). Effectiveness of passive and active mass dampers for the control of the wind excited motion of tall buildings. In *Proceedings of the Third World Conference on Structural Control*, pages 283–290, Como, Italy.

[Rodellar et al., 1987] Rodellar, J., Barbat, A. H., and Sanchez, J. M. (1987). Predictive control of structures. *Journal of Engineering Mechanics (ASCE)*, 113(6):797–812.

[Rosenblatt, 1961] Rosenblatt, F. (1961). Principles of neurodynamics. Technical report, Spartan Press, Washington, DC.

[Sakamoto et al., 1994] Sakamoto, M., Kobori, T., Yamada, T., and Takahashi, M. (1994). Practical applications of active and hybrid response control systems and their verification by earthquake and strong winds observations. In *Proceedings of the First World Conference on Structural Control*, volume 2, pages 90–99.

[Sanz, 2005] Sanz, M. (2005). Control robusto cuantitativo QFT: Historia de una idea (robust QFT control: A history of an idea). *Iberoamerican Automatic and Industrial Computation*, 2:25–38.

[Serino and Georgakis, 1999] Serino, G. and Georgakis, C. T. (1999). Response prediction methods for semi–active control of structures. In *Structural Dynamics-EURODYN'99*, ISBN 90 5809 0566, pages 109–118, Balkema, Rotterdam.

[Serino and Occhiuzzi, 2003] Serino, G. and Occhiuzzi, A. (2003). A semi–active oleodynamic damper for earthquake control. part 1: Design, manufacturing and experimental analysis of the device. *Earthquake Engineering*, 1(2):275–302.

[Serino et al., 2008] Serino, G., Spizzuoco, M., and Chandrasekaran, S. (2008). Seismic isolation and modelling of a worship structure. In *Proceedings of Fourth European Conference on Structural Control*, pages 711–718, St.Petersburg, Russia. ISBN: 978-5-904045-10-4.

[Shampine and Thompson, 2001] Shampine, L. F. and Thompson, S. (2001). Solving ddes in matlab. *Appl. Numer. Math.*, 37(3):441–458.

[Shield et al., 2001] Shield, C. K., French, C. W., and Timm, J. (2001). Development and implementation of the effective force testing method for seismic simulation of large–scale structures. *Philosophical Transaction of the Royal Society*, A. 359:1911–1929. Theme Issue on Dynamic Testing of Structures.

[Shing, 2006] Shing, P. B. (2006). Recent advances in hybrid testing for earthquake performance evaluation. Technical report, Dept. of Structural Engineering, Universiy of California at San Diego.

[Shing and Mahin, 1983] Shing, P. B. and Mahin, S. A. (1983). Experimental error propagation in pseudodynamic testing. Report UCB/EERC-83/12, Earthquake Engineering Research Center–University of California, Berkeley, CA.

[Shing et al., 1996a] Shing, P. B., Nakashima, M., and Bursi, O. (1996a). Application of pseudodynamic test method to structural research. *Earthquake Spectra*, 12(1):29–56.

[Shing et al., 1996b] Shing, P. B., Nakashima, M., and Bursi, O. S. (1996b). Application of pseudodynamic test method to structural research. *Earthquake Spectra*, 12(1):29–56.

[Sivaselvan et al., 2004] Sivaselvan, M. V., Reinhorn, A., Liang, Z., and Shao, X. (2004). Real–time dynamic hybrid testing of structural systems. In *Proc. 13th World Conf. Earthquake Engineering*.

[Skinner et al., 1993] Skinner, R. I., Robinson, W. H., and Verry, G. H. M. (1993). *An introduction to seismic isolation*. Wiley, Chichester.

[Slotine and Li, 1991] Slotine, J.-J. E. and Li, W. (1991). *Applied nonlinear control*. Prentice–Hall, Inc., Englewood Cliffs, NJ, USA.

[Soong, 1990] Soong, T. T. (1990). *Active structural control: theory and practice*. John Wiley & Sons.

[Soong et al., 1991] Soong, T. T., Reinhorn, A. M., Wang, Y. P., and Lin, R. C. (1991). Full–scale implementation of active control. I: Design and simulation. *Journal of Structural Engineering*, 117:3516–3536.

[Soong and Spencer, 2002] Soong, T. T. and Spencer, B. F. (2002). Supplemental energy dissipation: State–of–the–art and state–of–the–practice. *Engineering Structures*, 24(3):243–259.

[Sorace and Terenzi, 2008] Sorace, S. and Terenzi, G. (2008). Seismic protection of frame structures by fluid viscous damped braces. *Journal of Structural Engineering (ASCE)*, 134(1):45–55.

[Sozen et al., 1969] Sozen, M. A., Otani, S., Gulkan, P., and Nielsen, N. N. (1969). The universiy of illinois earthquake simulator. In *Proc. of 4th World Conf. on Earthquake Engineering*, volume 3, Santiago, Chile.

[Spencer et al., 1997a] Spencer, B. F., Dyke, S. J., and Deoskar, H. S. (1997a). Benchmark problems in structural control–part I: Active mass driver system. In *Proceedings of the ASCE Structural Congress XV*, Oregon, USA.

[Spencer et al., 1997b] Spencer, B. F., Dyke, S. J., Sain, M. K., and Carlson, J. D. (1997b). Phenomenological model for a magnetorheological damper. *Journal of Engineering Mechanics, ASCE*, 123:230–238.

[Spencer and Nagarajaiah, 2003] Spencer, B. F. and Nagarajaiah, S. (2003). State of the art in structural control. *ASCE Journal of Structural Engineering*, 129(7):845–856.

[Spizzuoco et al., 2008] Spizzuoco, M., Serino, G., and Londoño, J. M. (2008). Design and experimental characterization of non-linear viscous dampers for steel braced frame structure. In *Atti del Seminario di fine Progetto ReLUIS Linea 7 Tecnologie per lisolamento ed il controllo di strutture ed infrastrutture*, page In press, Naples, Italy.

[Symans and Constantinou, 1999] Symans, M. and Constantinou, M. (1999). Semi-active control systems for seismic protection of structures: a state-of-the-art review. *Engineering Structures*, 21:469–487.

[Takanashi and Nakashima, 1987] Takanashi, K. and Nakashima, M. (1987). Japanese activities on on–line testing. *Engineering Mechanics*, 113(7):1014–1032.

[Vidyasagar, 1992] Vidyasagar, M. (1992). *Nonlinear Systems Analysis*. Number 42 in Classics in Applied Mathematics. Prentice–Hall, Inc., Upper Saddle River, NJ, USA, second edition.

[Wagg and Stoten, 2001] Wagg, D. J. and Stoten, D. P. (2001). Substructuring of dynamical systems via the adaptive minimal control synthesis algorithm. *Earthquake Engineering and Structural Dynamics*, 30:865–877.

[Wallace et al., 2005a] Wallace, M. I., Sieber, J., Neild, S. A., Wagg, D. J., and Krauskopf, B. (2005a). Stability analysis of real–time dynamic substructuring using delay differential equation models. *Earthquake Engineering and Structural Dynamics*, 34:1817–1832.

[Wallace et al., 2005b] Wallace, M. I., Wagg, D. J., and Neild, S. A. (2005b). An adaptive polynomial based forward prediction algorithm for multi–actuator real–time dynamic substructuring. In *Proc. of the Royal Society Series A*, number 461, pages 3807–3826.

[Wallace et al., 2007] Wallace, M. I., Wagg, D. J., Neild, S. A., Bunniss, P., Lieven, N. A., and Crewe, A. J. (2007). Testing coupled rotor blade–lag damper vibration using real-time dynamic substructuring. *Journal of Sound and Vibration*, 307:737–754.

[Williams and Blakeborough, 2001] Williams, M. S. and Blakeborough, A. (2001). Laboratory testing of structures under dynamic loads: an introductory review. *Philosophical Transactions of The Royal Society*, 359:1651–1670. Series A, London.

[Yamamoto et al., 2001] Yamamoto, M., Aizawa, S., Higashino, M., and Toyama, K. (2001). Practical applications of active mass dampers with hydraulic actuator. *Earthquake Engineering and Structural Dynamics*, 30:1697–1717.

[Yang et al., 2004] Yang, G., Spencer, B. F., Jung, H. J., and Carlson, J. D. (2004). Dynamic modeling of large-scale magnetorheological damper systems for civil engineering applications. *Journal of Engineering Mechanics*, 130:1107–1114.

[Yang et al., 2002] Yang, J. N., Lin, S., Kim, J. H., and Agrawal, A. K. (2002). Optimal design of passive energy dissipation systems based on h_∞ a and h_2 performances. *Earthquake Engineering and Structural Dynamics*, 31(921–936).

[Yoshida et al., 1995] Yoshida, I., Kurose, H., Fukui, S., and Iemura, H. (1995). Parameter identification on active control of a structural model. *Smart Materials and Structures*, 4(1):A82–A92.

[Zapateiro et al., 2009] Zapateiro, M., Karimi, H. R., Luo, N., and Spencer, B. F. (2009). Real–time hybrid testing of semiactive control strategies for vibration reduction in a structure with MR damper. *Structural Control and Health Monitoring*, page In press.

[Zhao et al., 2003] Zhao, J., French, C., Shield, C., and Posbergh, T. (2003). Considerations for the development of real–time dynamic testing using servo-hydraulic actuation. *Earthquake Engineering and Structural Dynamics*, 32:1773–1794.